Faculty of Science and Engineering
Department of Physics and Astronomy

Windfield Investigations at Lake Turkana Wind Farm, Kenya

Victor Savatia Indasi

This Thesis is presented for the degree of
Doctor of Philosophy
of
Curtin University

August 2015

Declaration

To the best of my knowledge and belief this thesis contains no material previously published by any other person except where due acknowledgment has been made.

This thesis contains no material which has been accepted for the award of any other degree or diploma in any university.

Signature: .....

Date: 27/8/2015

Abstract

Kenya has relied on petroleum imports and hydropower to meet its ever increasing domestic and commercial energy requirements. Only 28% of Kenya has access to electricity, the situation is aggravated by over reliance on hydropower which has often been unreliable, especially in the dry seasons. Alternate power generation is therefore fundamental in order to reach a greater percentage of the population and support economic growth. Fortunately, wind energy generation provides a real opportunity for the country to meet its energy demands and reduce environmental impacts associated with fossil fuel use.

For a wind project to have sustainability there's a need to apply meteorological and climatic information into its economic strategy both during the assessment phase and projected through the project's lifetime. Of particular interest are wind speeds and their spatial and temporal variability. The lack of comprehensive and accurate wind measurements has rendered numerical modelling a key component of wind farm assessment and operation. This, in turn, has required a focus on the selection and performance of the numerical models coupled with reliable validation methods. The main aim of this study was therefore to make a detailed assessment of the local wind field at the Lake Turkana wind energy site using Doppler LIDAR data, anemometer datasets from 3 installed masts, and numerical modelling techniques.

The methods used to achieve this objective include the Advanced LIDAR data volume processing technique (ALVPT), time series analysis, error estimation and skill score analysis. Data was collected at 3 masts, Kalkumpei, Nyiru and Sirima using cup anemometers and wind vanes for the entire 2009 calendar year. The Doppler LIDAR collected data for 2 weeks from 11th to 24th July 2009. The annual average wind speed at the 3 masts was, 10.44 m/s, 10.75 m/s and 11.10 m/s respectively while the predominant wind direction was from the south east.

Comparison between mast and LIDAR measurements was undertaken for the period when the LIDAR data was available. The differences between Doppler LIDAR measurements and mast wind speed were small, the mean standard deviations were - 0.33 m/s, 0.05 m/s and 0.47 m/s and the correlation coefficients were 0.9, 0.6 and 0.73 for the 3 masts, Kalkumpei, Nyiru and Sirima respectively. Wind speeds derived from

LIDAR observations were output onto a 20 km by 20 km gridded domain and overlaid on a digital terrain model to create a wind atlas. This map provides a useful product that was used to evaluate Wind Atlas Analysis and Application Program (WAsP) generated wind atlases.

Weather Research and Forecast (WRF) model was used to simulate near-surface winds using six different planetary boundary layer (PBL) and surface layer parameterizations. The model runs were for the entire 2009 calendar year and the results were compared to measurements from 3 meteorological mast locations. WRF simulation using the Yonsei State University PBL scheme produced the best annual results at both Kalkumpei and Nyiru with a mean difference of 0.01 m/s and 0.15 m/s and Index of Agreement (IOA) of 0.66 and 0.61 at Kalkumpei and Nyiru respectively. The predominant south east wind direction was correctly captured by the model at these locations.

WRF simulation using the Mellor-Yamada-Janjic PBL scheme produced the best annual results at Sirima with a mean difference of 0.56 m/s and IOA of 0.61. Observed data at Sirima had 2 dominant wind directions: east and south east whereas WRF predicts wind direction to be predominantly south east. Possible explanations for the poorer model performance at Sirima may be linked to its physical location. The Sirima meteorological mast was atop a very exposed ridgeline that could be subject to sporadic wind gusts and rapidly changing wind directions which could be difficult to model.

Evaluating WAsP mean wind speed map using LIDAR data showed that Nyiru station provides the best data to model mean wind speed over the Lake Turkana wind farm domain with a mean difference of 0.16 m/s, RMSE of 0.85 m/s and IOA of 0.61. Based on the analysis and results presented in this work, it was concluded that WRF model may be used to generate wind data that can be used directly in wind resource assessment. Construction of a 310 Megawatts Lake Turkana wind farm comprising 365 Vestas V52-850kW turbines has commenced at this site.

To my family

Acknowledgements

In more than one way, the completion of this study was due to the support from many individuals and organizations. I am indeed grateful to them all and will mention a few below.

I wish to recognize with profound appreciation, the Advanced Coherent Doppler LIDAR project group comprising Prof. Lynch, Dr. McGann, Dr. Yu, Dr. Jeanneret, Dr. Rye and John Sutton, our manager for their academic and social impact on my life as a student at Curtin University. I am particularly grateful for the invaluable academic mentoring I received from my dear supervisors Prof. Mervyn Lynch, Dr. Brendan McGann and Mr. John Sutton. Their personal character made working with them not only fulfilling academically, but also enriched my personality.

Many thanks to the support I received from iVEC through the use of advanced computing resources located at Pawsey Centre. The special training extended to me particularly by Dr. Chris Harris was a great input to achieving some of my study objectives. Thanks to DTU for providing a free WAsP student license and to Heidi, their sales assistant for responding promptly to our correspondences.

My heartfelt appreciation goes to my sponsors CRC CARE for providing a postgraduate scholarship and Curtin university for providing a fee waiver through Curtin International Postgraduate scholarship.

There are many friends and colleagues who spent their time with me and kept on encouraging me. I thank them all especially Joseph Karianjahi, for his remote tutelage in programming language R.

Finally, it's my parents Mr. and Mrs. Indasi, for their care, encouragement and constant prayers that have brought me this far. To my sisters and brothers, thanks for all those encouraging messages. Love you all.

The completion of this study is as much their achievement as it is mine. To them all I say Bravo!

Above all, I thank Almighty God for giving me strength, good health, courage and wisdom to make it through to the end.

Table of Contents

Acronyms

ACM2	Asymmetrical Convective Model version 2 PBL scheme
AEP	Annual Energy Production
AGL	Above Ground Level
ASL	Above sea level
ALVPT	Advanced LIDAR data volume processing technique
ASAL	Arid and Semi-Arid Lands
CRC CARE	Cooperative Research Centre for Contamination Assessment and Remediation of the Environment
CSIRO	Commonwealth Scientific and Industrial Research Organisation
DEC	Western Australian Department of Environment and Conservation
ECMWF	European Centre for Medium-Range Weather Forecasts
GDAS	Global Data Assimilation System
GFS	Global Forecast System
IOA	Index of Agreement
IEC	International Electrotechnical Commission
iVEC	unincorporated joint venture between CSIRO, Curtin University, Edith Cowan University, Murdoch University and The University of Western Australia and is supported by the Western Australian and Federal Governments.
KAMM	Karlsruhe Atmospheric Mesoscale Model
LIDAR	Light Detection and Ranging
LTWPC	Lake Turkana Wind Power Project Consortium
MAE	mean absolute error
MCP	Measure-Correlate-Predict
MM5	Fifth-Generation Penn State/NCAR Mesoscale Model
MRF	Medium Range Forecast Model PBL scheme
MW	Megawatt
MYJ	Mellor-Yamada-Janjic PBL scheme
NCAR	National Center for Atmospheric Research
NCEP	National Centre for Environmental Prediction Remediation of the Environment
NOAA	National Oceanic and Atmospheric Administration
NWP	Numerical Weather Prediction

PBL	Planetary boundary layer
Pbias	Percentage bias
R	Programming language and software environment for statistical computing and graphics
RIX	Ruggedness index
RMSE	Root mean square error
SAGA GIS	(System for Automated Geoscientific Analyses) is a free and open source geographic information system used for editing spatial data.
SODAR	Sonic Detection and Ranging
SRTM	Shuttle Radar Topography Mission
TKE	Total Kinetic Energy
USGS	United State Geological Survey
UTM	Universal Transverse Mercator coordinates system
WAsP	Wind Atlas Analysis and Application Program
WMO	World Meteorological Organization
WPS	WRF Pre-processing System
WRF	Weather Research and Forecast (WRF) Model
YSU	Yonsei University PBL scheme

List of figures

List of tables

1. CHAPTER 1

1.1 Background to the Research

Kenya has experienced a steady increase in energy demand over the past decade which is linked to both the rising population and the expanding economy. According to 2009 national census, the Kenyan population is about 38 million and only 28% has access to electricity (Kirai, 2009). Over the years, Kenya has relied on petroleum imports and hydropower to meets ever increasing domestic and commercial energy requirements (Oludhe, 2008), but the frequent droughts thought to be caused by climate change have led to critical power shortages particularly in years when the droughts are more pronounced like 1999 – 2002 (Oludhe, 2008, Kirai, 2009, Muthuri et al., 2009). Further electricity generation is necessary in order to meet the demands of a greater percentage of the population and support economic growth (LTWP, 2013).

Renewable energy resources, particularly wind energy, are progressively being investigated for electricity generation with negligible emissions of greenhouse gases (Theuri and Hamlin, 2008). Wind energy resource is naturally a function of the climate system because electricity is generated by the wind turbines which are moved by the winds. Therefore, the prospect of wind energy power generation will increase the resilience of Kenya's power generation vis-à-vis potential climate risk variations. The assessment and eventual commissioning of wind power projects in Kenya, especially the 310 MW Lake Turkana Wind Power Project, will help the nation address power shortage and spur further economic growth.

The region of study is north-western Kenya where the winds are generated by a low level jet called the Turkana Channel jet. The jet stream is created by the much bigger East African low level jet. The Turkana Channel jet blows through the year from the South East through the valley between the East African and the Ethiopian Highlands extending from the Ocean to the deserts in Sudan (Kinuthia, 1992). The wind is enhanced locally between Mt. Kulal (2300 m ASL) and the Mt Nyiru Range (2750 m ASL). Due to thermal effects, the wind decreases around midday and is at full force during the night (Kinuthia, 1992).

The mesoscale meteorological models used in this study can be classified into two types, diagnostic and prognostic. Diagnostic models, such as WAsP, use interpolated

wind fields (from a given wind database) that are then adjusted to satisfy the laws of mass conservation when forced by topography or other physical constraints. Prognostic models provide an evolving state of mesoscale features of the atmosphere through the integration of conservation equations for mass, momentum, heat and water. They are initialised by meteorological data available at a coarse resolution, but can provide simulations at much higher resolutions in areas where limited data currently exists. This thesis combines the use of both model types to provide a detailed wind resource assessment at Lake Turkana and investigate whether reliable wind and energy simulations can be made in the absence of actual wind data.

The prognostic modelling using Weather Research and Forecasting (WRF) model addresses two primary goals of this study. First, by simulating the airflow over a region for a period of one year, the spatial variation of mean wind speed was obtained. Areas of higher mean wind speed can be identified and quantified through this process. Second, in the absence of reliable actual wind data, it is possible to obtain hourly wind data from the prognostic model for anywhere within the modelled area.

Atmospheric modelling by the wind energy industry has tended to be dominated by the use of Wind Atlas Analysis and Application Program (WAsP). WAsP model was developed at the Riso National Laboratory, Denmark as a result of economic and environmental interest in wind energy in Europe, and a desire for reliable wind resource information (Troen and Petersen, 1989). The WAsP model is based on using wind data from one site (reference site) and then applying this to a predicted site or region. It is a reliable method for making wind and energy simulations, but sometimes there are limitations, particularly if the observed and predicted sites are located in different climate and topographic environments.

WAsP model was used to make wind and energy simulations at Lake Turkana wind farm site. WAsP model is able to resolve the speed-up and slow-down effects that result from the interaction of airflow with small-scale terrain and roughness features. These effects are not fully accounted for in the relatively low resolution prognostic WRF model. The main goal in this part of the study was to model local winds using both anemometer and WRF simulated data.

Due to some of the simplifications made to the numerical models used within WAsP, the program can produce somewhat inaccurate results when used outside its recommended operational envelope, such as when a site has complex, rugged terrain or very complex atmospheric conditions (Bowen and Mortensen, 2004). This problem can be solved by using several reference sites and cross-referencing sites where wind observations are available. There is also the option for some user corrections at problematic sites which can significantly improve the accuracy of the model in complex terrain (Wagner R. et al., 2009). However, in this study, the accuracy of the WAsP model in complex terrain was evaluated using high spatial resolution LIDAR data. To achieve this, WAsP was executed using wind datasets from 3 instrumented meteorological masts. The resulting mean wind speeds were compared to mean wind speeds retrieved from LIDAR.

To be able to predict the wind at a site without erecting a meteorological mast for a long period of time could save wind farm developers significant time and money. Model validation against observation data will still likely be required, but this could be for a shortened period merely to confirm the reliability of the prognostic model results.

Lake Turkana Wind Power Project consortium (LTWPC) involves the construction and operation of a 310 MW wind power farm in Marsabit District, near Lake Turkana. The wind farm will comprise 365 turbines of 850 kW capacity each (Muthuri et al., 2009). In October 2008, LTWPC approached the Cooperative Research Centre for Contamination Assessment and Remediation of the environment (CRC CARE) through its participant Organisation; Western Australian Department of Environment and Conservation (DEC), which has now become the Department of Environmental Regulation to assist in the measurement of wind fields using WindTracer Doppler LIDAR. This involved field monitoring program in mid and late 2009 to map the wind field on site and support validating the accuracy of wind modelling (CRC-CARE., 2010).

1.2 Objectives

The main purpose of this research project was to make a detailed assessment of the local wind field at Lake Turkana wind farm in North Western Kenya. To achieve this, the following specific objectives were undertaken:

1. Investigate the temporal and spatial wind characteristics of the Lake Turkana region.
2. Evaluate the application of a mesoscale WRF model for the identification of high potential wind energy generating areas in complex terrain.
3. Develop a methodology that uses WRF wind output data to drive industry standard wind energy model WAsP, so that the wind and energy generation potential can be identified and quantified.
4. Develop a methodology that uses high spatial resolution LIDAR data to evaluate WAsP mean wind speeds.

1.3 Significance

The amount of power in the wind is directly proportional to the cube of the wind speed, consequently a small difference in the wind speed make a significant difference in the power harnessed from the wind. A 10% difference in wind speed causes a 33% change in electric power harnessed.

Dissimilar to other sources of energy, wind speeds fluctuate greatly with time and space, causing electricity production rates to change more strongly than other energy sources. Therefore, errors in the estimated wind speed of only 1% for a 100 MW wind farm can lead to losses around $12,000,000 over that wind farm's lifetime (Schreck et al., 2008).

In order to evaluate wind for power generation and produce a dependable, clean energy source, more precise wind estimation techniques and associated measurements are required. The primary contribution of this study to the broad wind energy sector is the provision of accurate calibrated wind measurements and accurate wind forecasts.

1.4 Thesis structure

This thesis has six main sections. The first chapter gives a brief background to the current research, outlines the objectives and significance of the study.

Chapter 2 describes the two methods used to measure wind characteristics at Lake Turkana: mast-mounted cup anemometer and wind vane measurements and 1.6 μm Doppler LIDAR. The uncertainties and limitations of both methods are discussed in detail in this chapter. Chapter 2 also covers the principles of wind energy assessment and discusses the link between wind and energy.

Chapter 3 presents a description of observational data used in this study. The performance of 1.6 μm WindTracer LIDAR deployed at the Lake Turkana site between 11th and 25th July 2009 is described and analyzed. This activity was intended to demonstrate the capabilities of LIDAR for remotely making temporally and spatially sampled measurements of wind speed and direction in the atmospheric boundary layer. A statistical assessment and error analysis was conducted on these datasets i.e. LIDAR observations versus cup anemometers. These two observed datasets are later used to validate numerical modelling results

Chapter 4 was divided into two main sections: a section describing the methodology for mesoscale numerical prognostic modelling and a section describing the methodology for a combined mesoscale and microscale diagnostic modelling approach. A discussion of the limitations of the combined modelling was also discussed. Understanding the model limitations is important when interpreting results, and also when attempting to overcome them.

Chapter 5 presents and discusses the results obtained using the methods described in Chapter four to achieve the objectives outlined in Section 1.2 of the study. First, WRF model results for 3 mast locations: Kalkumpei, Nyiru and Sirima are analyzed using standard statistical approaches followed by higher resolution WAsP modelling results for mean wind speed and energy production for the Lake Turkana wind farm. The methodology used to evaluate WAsP mean wind speeds is also discussed.

Chapter 6 presents the conclusions drawn from results presented in chapter 5 and provide recommendations for the use of WRF and WAsP models for wind resource assessment in a complex terrain environment. Recommendations for future work to advance the knowledge presented in this study are also provided.

1.5 Area of Study

The area of study is Northern Kenya which is an Arid and Semi-Arid Lands (ASAL) region. The mean annual maximum temperature is 43°C while the mean minimum annual temperature is 14°C. The mean annual rainfall is 230 mm. Nomadic pastoralism is the major economic activity in the area. Figure 1.1 shows the region of study.

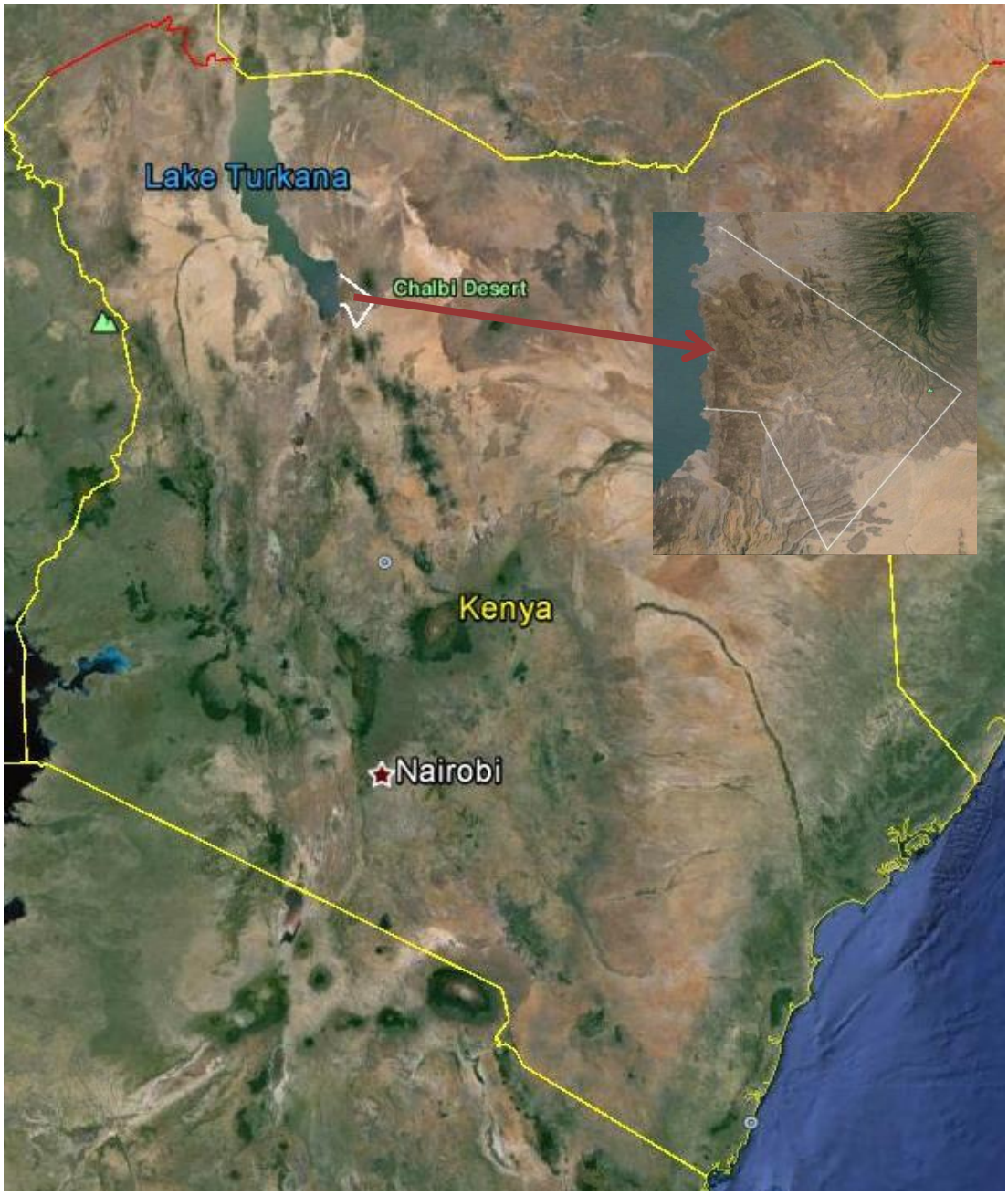

Figure 1.1: Map of Kenya showing the area of study

1.5.1 Wind Climatology of Lake Turkana Region

Lake Turkana region has various topographic features that include the Ethiopian highlands to the northeast and East African highlands to the southwest (Figure 1.2). In between the Ethiopian highlands and the East African highlands lies a low-level region. This valley is referred to as the Turkana channel (Kinuthia and Asnani, 1982). It is above 500 m from the mean sea level and has a depth that varies between 610 and 1524 m, and a width that varies about 140 to 700 km. The channel is approximately 700 km long and oriented from southeast to northwest (Kinuthia, 1992).

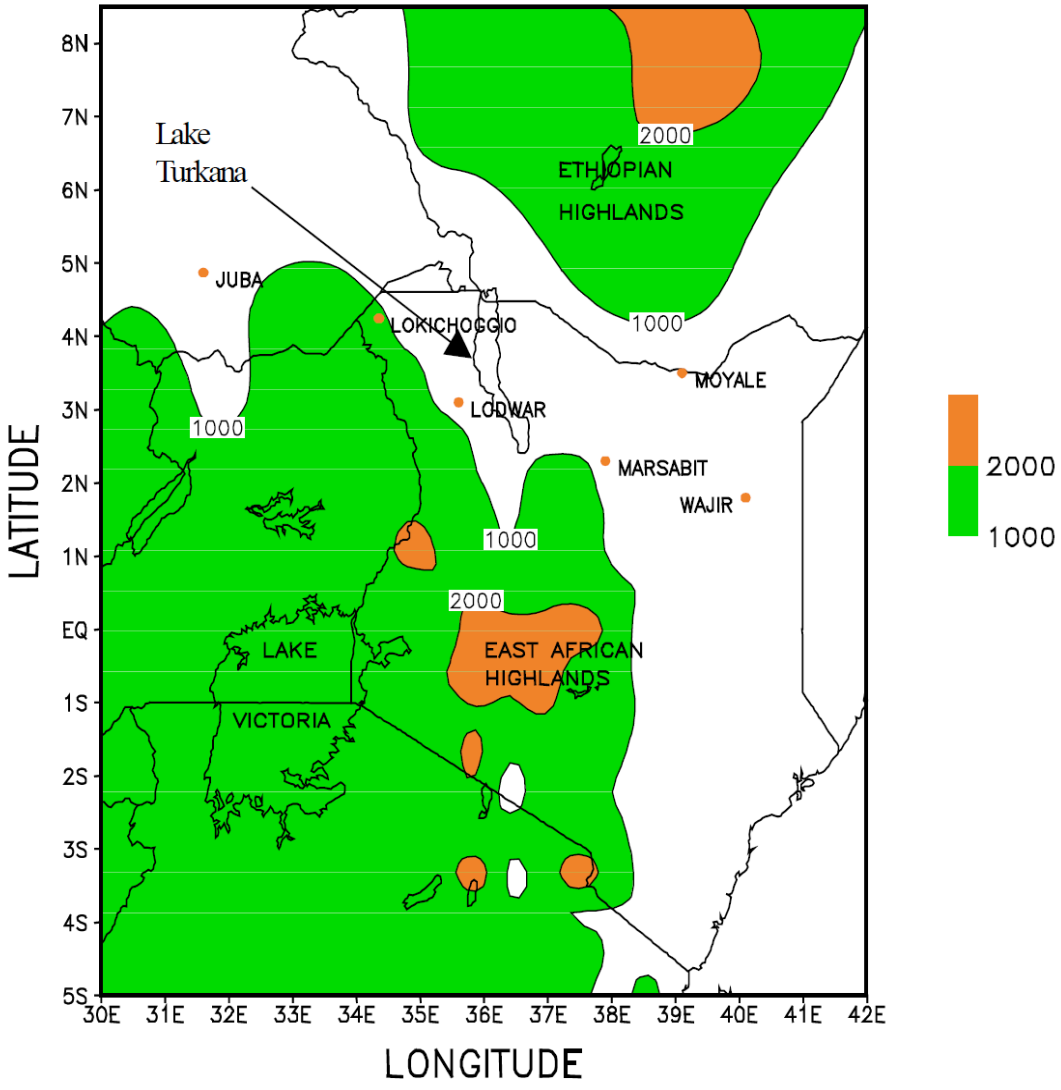

Figure 1.2: Topography over the Turkana Channel. Terrain height values greater than 1000 m are shaded (Indeje, 2000).

Both Kinuthia and Asnani (1982) and Kinuthia (1992) observed that, throughout the year, the NE and SE monsoon near the equator branches off from the Indian Ocean, enters the Turkana channel and intensifies, maintaining an average speed around 10 ms^{-1} (Figure 1.3). Their observations showed quite distinct low-level jet in the channel (Turkana easterly low-level jet) that persists throughout the year. They further hypothesized that the configuration of the Ethiopian highlands and the East African highlands could be playing a critical role in the development and maintenance of the Turkana low-level jet through the orographic channeling effect.

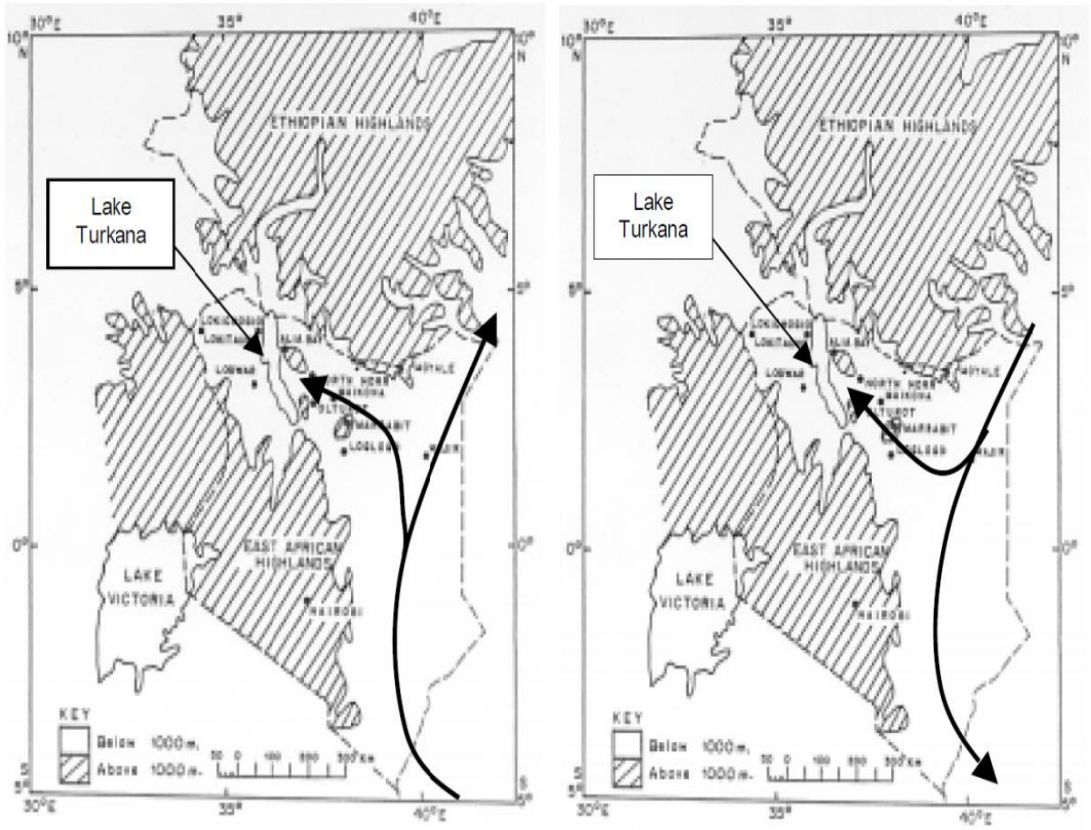

Figure 1.3: A simplified model showing the cross-equatorial monsoon flow diverting into the Turkana channel during (a) northern summer, and (b) northern winter (Indeje, 2000).

2. CHAPTER 2

This chapter describes traditional wind resource assessment using cup anemometers and remote sensing techniques using scanning coherent Doppler LIDAR, hereafter simply referred to as LIDAR, and the links between wind and energy. Sections provide the research context and background information from which the methodology and results of this research have developed.

2.1 Traditional Wind Resource Assessment

Traditional site assessment process relies on the use of masts with wind speed and direction sensors in order to evaluate the wind resource at a site. The most common wind speed and direction sensors are cup anemometers and wind vanes. The Wind Resource Assessment Handbook (Baily, 1997) provides a detailed description of many aspects of the site assessment process, especially a method of evaluating the wind resource.

Wind resource varies inter-seasonally and inter-annually thus an estimate of the long-term characteristics is critical to accurately estimate the energy production over the lifetime of the turbine (McCaa, 2006, Oliver, 2006). Wind resource measurement campaigns last at least one year in the traditional site assessment process, this is uniformly recommended in reputable manuals of site assessment (Baily, 1997, Gardner et al., 2004). This practice is accepted primarily because of seasonal variations in the wind resource.

Most meteorological masts used for wind resource assessment are typically between 40 m and 60 m tall, masts of this height (including labor and sensors) cost on the order of $20,000-30,000 (Gardner et al., 2004). Masts in excess of 80 m are significantly more expensive, and are potentially much more difficult to permit and install. The result is that the use of a standard mast for site assessment necessitates a shear extrapolation model to estimate the hub height wind resource.

This process is highly uncertain as shear profiles are extremely site dependent (Elkinton et al., 2006). Furthermore, without hub height measurements of the wind resource there is no way to tell if the shear model that is employed is appropriate. Consequently, the use of shear extrapolation introduces a great deal of uncertainty

into the estimate of the wind resource at the turbine hub height (Feuquay et al., 2005).

Meteorological masts are the most well-known methods for evaluating the wind resource at an area that is under consideration for wind energy development. Most meteorological masts used in wind resource assessment are tall tubular steel masts. Figure 2.1 shows meteorological masts at the Lake Turkana site.

Figure 2.1: Meteorological masts at Sirima (left), Nyiru (center), and Kalkumpei (right) at the Lake Turkana site. The measurement heights are 38 m and 20 m for Sirima, 46 m and 20 m for Nyiru, and 38.5 m and 20 m for Kalkumpei (DEWI, 2010).

2.1.1 Cup Anemometers and Wind Vanes

Anemometers and wind vanes are usually positioned at two or three heights on the mast, with two anemometers and one vane at each height. The redundant anemometers help combat mast shadow, which occurs when the wake of the mast affects the measurement of an anemometer. At each height, booms are attached to the mast extending horizontally. These booms are generally 2-3 m in length, and the wind monitoring sensors are secured to the end of the booms. By situating the sensors far from the mast, the impacts of the mast wake are minimized. The sensors normally deliver information that give the average wind speed and wind direction over 10-minute or 1 hour intervals. These datasets are recorded and stored by a logger box at the bottom of the mast.

The most common type of anemometer used for wind energy site assessment is the cup anemometer (Manwell et al., 2010). The performance of a cup anemometer is determined by a variety of factors, including its size and weight, bearing friction, and cup design (Manwell et al., 2010, Pedersen and Paulson, 1999). The accuracy of a cup anemometer is generally assumed to be approximately 0.1 m/s (1-2% of the mean wind speed), based on wind tunnel tests (Pedersen, 2004, Westermann, 2003, RISØ., 2004).

Cup anemometers are often characterized by their distance constant, which indicates how rapidly the anemometer responds to changes in the wind speed. Formally, the distance constant is equal to the length of fluid flow past the anemometer required to cause it to respond to 63.2% of a step change in speed (Manwell et al., 2010). Most cup anemometers used for wind resource assessment, have distance constants less than 5 m. In general, cup anemometers with small distance constants can be classified as "point measurements" of the wind speed, are said to measure the instantaneous wind speed at a given point in space and time (Gardner et al., 2004).

2.1.2 Traditional Wind Assessment Uncertainty

There are several factors which influence the accuracy of a power estimates using traditional assessment methods. These factors are broadly classified into six categories and are discussed below:

2.1.2.1 Wind Speed Measurement Uncertainty

Uncertainty emerges when measuring the real wind speed at a site. The wind speed at a site is generally measured by taking 10-minute means (sometimes 1-hour averages). Wind data at a site are then presented as a time series of these 10-minute averages (Baily, 1997). Numerous factors can contribute to errors in the measurement of the wind speed as detailed in the following subsections.

2.1.2.1.1Anemometer Uncertainty I (Calibration Uncertainty)

While anemometers are the preferred means of measuring wind speed, they also have the potential for measurement error. The uncertainty due to this measurement error arises from variations between anemometers of a given model, and is referred to as a "calibration uncertainty." While a general transfer function may exist for a particular

model of anemometer, this transfer function may not exactly represent a specific anemometer, and therefore unknown bias may be present. Alternatively, if a specific anemometer is calibrated in a wind tunnel, measurement errors in the calibration process can again lead to an inaccurate transfer function, and so unknown bias is again present.

Lockhart and Bailey 1998, investigate the accuracy of the maximum 40 anemometer. They conclude that the maximum 40 anemometer is accurate to within 0.1 m/s for the wind speed range 5 m/s to 25 m/s. This uncertainty therefore ranges between 0.4% and 2% depending on the wind speed. Likewise, the Risø P2546 model anemometer has an approximate uncertainty of 0.1 m/s (RISØ., 2004). Similarly the Thies First Class 4.3350.10.000 has an uncertainty of approximately 1% (Westermann, 2003).

2.1.2.1.2 Anemometer Uncertainty II (Dynamic Overspeeding)

Overspeeding is a well-known source of error in cup anemometers, as their inherent physical design causes them to speed up more rapidly than they slow down, thereby causing an overestimation of the wind speed. Overspeeding is more prevalent in turbulent wind, where the wind speed changes rapidly. Overspeeding is inextricably linked to turbulence in the wind and therefore is a function of the turbulence intensity (as well as other factors). The turbulence intensity is standard deviation of the wind speed measurements over a certain period, normalized by mean wind speed over the same period.

Turbulence intensity is a non-dimensional term that quantifies the degree of turbulence in the wind during a certain time period. The effect of turbulence on the measurements of cup anemometers is an extremely complicated phenomenon, and it is still not fully understood (Pedersen, 2004, Pedersen et al., 2002).

Kristensen (1999) identifies four sources of error due to turbulence in the wind. However, for purposes of site assessment using cup anemometry, only two error sources are relevant (Papadopoulos et al., 2001). These are longitudinal overspeeding and vertical turbulence effects, also called the *u*-bias and the *w*-bias. Longitudinal overspeeding is considered to consist of the effect of fluctuations in the direction of mean wind speed. However, the vertical component of turbulence can also cause

error in the anemometer readings, and under some conditions it is much larger than the effect of overspeeding.

Kristensen shows that the error due to longitudinal overspeeding is proportional to the square of the longitudinal turbulence intensity (Kristensen, 1999). The longitudinal overspeeding is also proportional to the distance constant of the anemometer. Longitudinal overspeeding always produces a positive bias, so that the measured wind speed is larger than the true wind speed (Kristensen, 1996). Overspeeding for modern cup anemometers with small distance constants is a fairly small effect. Several sources indicate that it is almost certainly less than 1% (Kristensen, 1999, Papadopoulos et al., 2001, Petersen Erik L. et al., 1997).

2.1.2.1.3 Anemometer Uncertainty III (Vertical Flow Effects)

When the power curve of a wind turbine is calculated, the IEC standards require that the measured wind speed is the horizontal component (lateral and longitudinal, but not vertical) of the wind velocity vector. The standards state that the wind speed to be measured is defined as the average magnitude of the horizontal component of the instantaneous wind velocity vector, including only the longitudinal and lateral, but not the vertical, turbulence components (Quarton, 2004.). Therefore, when the wind speed is measured during site assessment, the goal should likewise be to measure the horizontal component of the wind speed. In this way, the measured wind speed and the wind speed measured during power curve calibration are defined consistently, and so a power curve of a particular turbine satisfactorily predicts the power output for a given measured wind resource.

In practice, the vertical component of the wind speed vector can affect the measurement of an anemometer. Different anemometers have different angular response characteristics, so they respond differently to flow that is not purely horizontal. At some sites, the terrain causes a consistent flow inclination that can affect the measured wind speed of an anemometer.

Currently, only three models of anemometer are approved by the IEC and MEASNET for power curve calculation – the Risø P2546A, Thies First Class 4.3350.10.000 (used in this study) and a Vector A100 model anemometer. These

three anemometers are approved in part because they are fairly insensitive to vertical flow, and so the wind speed measurement approximates the horizontal wind speed.

2.1.2.1.4 Anemometer Uncertainty IV (Vertical Turbulence Effects)

Even at sites with no flow inclination, turbulence in the vertical direction can cause an over-estimation of the mean wind speed. Like overspeeding, vertical turbulence effects depend on the physical characteristics of the cup anemometer. In the case of overspeeding, this characteristic is the distance constant in the case of vertical turbulence effects, the angular response curve is the relevant parameter. These effects are explored in detail by (Kristensen, 1999, Papadopoulos et al., 2001). However, one of the major finding in these studies is that vertical turbulence effects can produce either positive or negative biases, which is not the case for overspeeding.

2.1.2.1.5 Tower Effects

Masts used in wind resource measurement can significantly affect the flow of air near the anemometers. This effect is often referred to as “tower shadow”, and it is especially pronounced when the anemometer is in the wake of the mast. Work by Kline was used to evaluate the uncertainty due to tower effects (Kline, 2002), he recommends the selection of the higher reading of two anemometers at each height as the value of the measured wind speed, for each averaging period.

2.1.2.1.6 Boom Effects

The boom that supports the anemometer and connects it to the mast can also affect the reading of the anemometer. Pedersen et al., 1992 looked at the influence of the boom on anemometer measurements. They conclude that the boom could have a significant effect on the anemometer measurement if they are not adequately separated vertically. However, if the anemometer is positioned 12-15 boom diameters from boom, there is a fairly small effect.

2.1.2.2 Wind Resource Estimation Uncertainty

These uncertainty sources emerge when the measured wind resource information are utilized to gauge the long-term wind resource at a site. While wind resource measurement normally goes on for one year, the measured resource for this specific year may not be illustrative of the actual long-term resource at the site (Gardner et al., 2004, McCaa, 2006, Oliver, 2006, Moon and Miler, 2005). The long-term

resource is characterized by the mean wind speed and wind speed distribution that exists at a site over a much longer period of time. Normally, twenty years is thought to be a long enough time period to describe the long-term wind resource. Since a twenty year measurement campaign is far too long for practical purposes, the long-term resource must be assessed from the measured data. The measured data, alongside long-term data from a nearby site (the "reference site"), are usually used in a methodology called Measure-Correlate-Predict (MCP) to estimate the long-term wind resource at a site (Oliver, 2006). Global climate change, whether anthropogenic or naturally caused, may cause additional uncertainty (Moon and Miler, 2005).

2.1.2.3 Site Assessment Uncertainty

Wind speed measurements ordinarily happen at heights significantly lower than the hub height of a typical modern wind turbine. Because wind speeds generally increase with height, a wind shear model is used to extrapolate the estimated long-term wind resource to the hub height (Feuquay et al., 2005). The wind shear model is created using the measured wind speed data. The use of a wind shear extrapolation introduces uncertainty (Livingston and Anderson, 2004). Additionally, the mast used to measure the winds is regularly not at the precise area of the wind turbine(s). Topographic impacts can mean that wind speeds at separate areas at a site vary. When multiple wind turbines are installed at a site, the wind resource may vary between each turbine due to topography (Oliver, 2006, Brower, 2006). In complex terrain, this effect can be significant.

2.1.2.4 Wind Shear Model Uncertainty

Meteorological masts that measure wind speeds at potential sites typically have heights significantly shorter than the hub heights of modern wind turbines (Livingston and Anderson, 2004). Consequently, the measured wind resource has to be extrapolated up to the hub height to get an estimate of the wind resource at the hub. This extrapolation is a significant source of error. The accuracy of the shear extrapolation is highly dependent on the particular shear model that is used. However, one does not know beforehand which shear model provides the most accurate extrapolation.

2.2 Wind Resource Assessment using Remote Sensing Devices

Wind monitoring for wind energy development purposes has, to date, depended on the cup anemometer as the accepted standard (Baily, 1997), basically because the technology and its measurement uncertainties is well understood (Elliot et al., 1986, Gardner et al., 2004). A cup anemometer requires mounting on a mast that must be at or close to the hub height of the wind turbine for which the site is to be developed, this mast must be situated in an area that represents the wind flow over the site and which is not compromised by obstacles or terrain features that distort the flow at the point location of the cup anemometer.

However, with the ever-increasing development of physically larger wind turbines (both in hub height and rotor diameter), the need for taller and taller masts (and multiple masts for the larger sites now being developed) is adding both significant cost and risk to projects, particularly those in the early stages, prior to financing. Planning impacts, cost and the physical limitations of masts have led to decreasing rewards for continuing higher than about 80–100 m. This necessitates the need for more flexible methods of monitoring wind.

At the same time, the current practice of basing power performance measurements on a solitary, hub-height wind speed measurement gets to be instinctively more suspect for such huge rotor swept areas. Recent numerical studies (Wagner et al., 2007) indicate that the correlation between measured electrical power and wind speed increases if the wind speed is based on a weighted average of the wind speed profile over the entire rotor rather than on a single point measurement. Here, remote sensing is well suited to play a major role.

LIDAR systems are ground-based wind speed measurement devices that utilize electromagnetic radiation to measure the wind speed. The use of LIDARs for wind resource assessment is a more recent development (Albers, 2006). Until recently, making wind speed measurement using LIDARs was comparatively expensive and basically restricted to the aerospace domain (Huffaker R. M. et al., 1970). Suitable lasers were costly, large and required elaborate cooling systems. The optical systems were built on traditional optical-benches and were inherently difficult to keep

aligned. These limitations were swept aside by the emergence of sufficiently coherent lasers.

2.2.1 LIDAR and Wind Resource Assessment

LIDAR systems are potentially useful devices for wind energy site assessment, as they are portable and capable of measuring at the hub height of a wind turbine. LIDAR is a volume averaging device, as opposed to cup anemometers which are point measurements.

The performance of LIDARs for wind resource assessment appears to be very promising. While there is not a great deal of experience with the use of LIDARs, preliminary evaluations of the ZephIR LIDAR show a high level of performance (Smith et al., 2006). The evaluations of the ZephIR from three separate institutions compare the LIDAR wind speed measurements to cup anemometer wind speed measurements from a mast, and the results indicate very high correlation coefficients (~0.99) between the measurements, with average errors less than 1% (Albers, 2006, Smith et al., 2006, Jaynes et al., 2007). The evaluations indicate that a LIDAR system has the potential to be utilized for wind resource assessment in lieu of cup anemometry.

In 2004, a comparison between a newly developed continuous wave LIDAR ZephIR and cup anemometry up to 100 m was carried out (Smith et al., 2006). This study explained the offset observed between LIDAR and cup anemometer measurements as due to laser calibration at too short a range and beam focusing due to curvature on "flat" optical surfaces. While they contended that each measurement of velocity with LIDAR was accurate and reliable, errors arose because of the uncertainty of what is actually moving at that velocity. They questioned the assumption that the backscattered signal always only originates from aerosols moving at the wind speed close to beam focus. Non-uniform backscatter can occur, e.g., from cloud or mist, as contributions from the Doppler signal from the cloud or mist layer base can contaminate that from aerosols at the height being measured. In the worst case, the return signals from a cloud base could dominate those from aerosols at the desired height, leading, in many instances to an overestimation of wind speed. Hence a cloud correction algorithm is necessary.

In 2007, an on-shore comparison of the QinetiQ ZephIR LIDAR beside a 120 m instrumented mast, followed by a 3-month campaign on the FINO-1 research platform in the North Sea off the German coast was described in (Pedersen et al., 2002). The FINO-1 platform is 20 m above sea level (a.s.l.), on which is mounted an 80 m instrumented mast, with top-mounted cup anemometry at 103 m a.s.l. LIDAR *versus* mast regression slopes were shown to decrease with height, although most correlation coefficients were close to 1. These results were considered anomalous (Rogers et al., 2007), in which it was noted that LIDAR performs similarly to SODAR and with comparable uncertainty, particularly if the LIDAR results are normalized to the results from a cup anemometer at a fixed height. It was contended that the main limitation to the accuracy of the ZephIR in flat terrain was probably the leveling of the instrument, and that even though its large beam (zenith) angle results in lower tilt errors, these were still likely to be the cause of the systematic deviations evident in the data of (Pedersen et al., 2002).

A pulsed LIDAR intended for wind energy applications ('Windcube') was introduced to the wind energy industry in 2007. Albers, 2006 provided details regarding a measurement campaign including both the ZephIR and Windcube, in flat terrain at a northern German test Centre. Both LIDARs performed well, with data availabilities more than 96% at 124 m elevation and LIDAR-cup standard deviation errors of 0.24 m/s (Windcube) and 0.3 m/s (ZephIR).

Remote sensing instrumentation for wind energy purposes has grown quickly in the recent years, with continuous changes being made to equipment and software components. The 2009 performance (against cup anemometers) of the two kinds of LIDAR then available commercially (ZephIR and Windcube) was described for flat landscape (Addison et al., 2000) and for complex terrain (Bechrakis et al., 2004). The previous study reported broad testing of the LIDARs at the Høvsøre Test Station in Denmark. Testing uncovered critical shortcomings, which were to be addressed by the manufactures. The principle issue with the ZephIR was the sensitivity to backscatter from clouds and mist, and the authors noticed an enhanced cloud-correction algorithm had been implemented since their study. Nonetheless, the issue of backscatter from low-lying mist remained unsolved.

2.2.1.1 WindTracer LIDAR

The WindTracer LIDAR manufactured by US Defence Company Lockheed Martin Coherent Technologies is an infrared LIDAR and utilizes a 1.6 μm laser source which is eye safe. The strength of WindTracer LIDAR lies in its ability to measure winds and aerosol levels with high temporal and spatial resolution. Specifically, hemispherical volumes with radii of 8-12 km can be scanned within minutes. Single cross-sections, for example a vertical cross-section, can be completed in seconds, allowing measurement of transient atmospheric processes. The range capabilities of the LIDAR are strongly influenced by atmospheric backscatter conditions (aerosol levels), and as such they vary between locations.

2.2.1.2 Basic Principles of WindTracer Operation

The WindTracer produces a pulsed beam of laser light which passes through the air and as it does, small portions of the light are reflected back to the system by aerosols. This reflected light is detected and recorded. By analyzing the difference in time between when the pulse of light left the laser and when the reflected light returned, a distance to the particle that reflected the light can be determined. In addition, by measuring the frequency of the original pulse and the frequency of the reflected light, a shift in frequency can be measured (called a Doppler shift). The Doppler shift is induced by the component of the velocity of the particle directly towards or away from the laser. By analyzing the frequency shift, a direct measurement of the radial component of velocity of the aerosol particle is made.

Figure 2.2 highlights the basic principles of operation. The pulse length of the laser transmitted by the system can be set to approximately 90 m and pulses are transmitted around 500 times per second (a pulse repetition frequency, or PRF, of 500 Hz). This implies that the beam is considered to be a series of ‘pencils’ that are radiated every 2 milliseconds and measuring 90 m long by 10-30 cm wide, depending on the distance away from the system. However, some WindTracer systems use a PRF other than 500 Hz, like the system used in this study which uses a PRF of 600Hz.

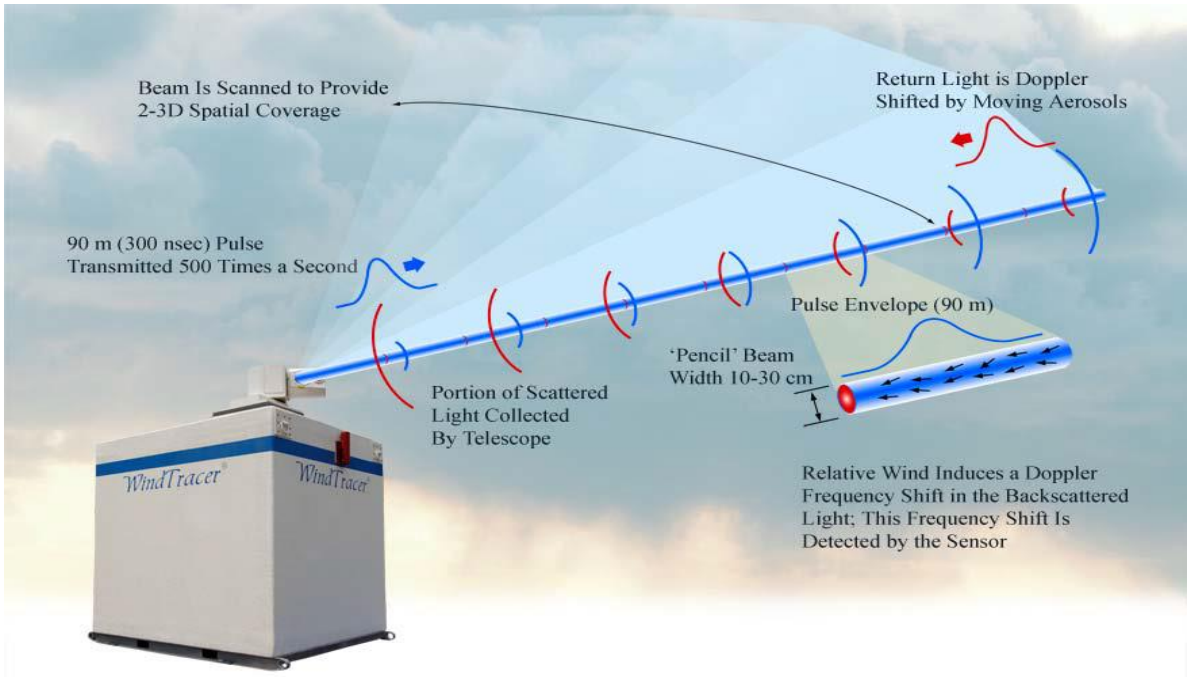

Figure 2.2: LIDAR principle of operation (CRC-CARE., 2010).

The Doppler frequency shift is $\Delta v=-2v_r/\lambda$, where v_r is the radial velocity and λ is the operating wavelength. For a 1.6 μm operating wavelength, the frequency shift is roughly 1.25 MHz per meter/second of particle velocity.

2.2.1.3 Data acquisition

A trigger signal (T=0) is received by the data acquisition system from the laser slightly before the laser pulse is transmitted to the atmosphere. As it is transmitted, a "copy" is recorded to analyze and find the precise frequency and timing of the pulse as it left the system. This recorded copy is called the Monitor pulse, because it "monitors" the frequency of the laser. After a small time period, atmospheric returns are recorded in what is called the Signal Block. This data can be analyzed to determine the speed and distance of a group of aerosol particles.

The receiver system samples every 4 nanoseconds (corresponding to a 250 megasample per second rate). In spatial coordinates, the 4 nanoseconds correspond to 0.6 m of round-trip distance (sample spacing). The signal block is divided in range gates of a chosen number of samples for velocity retrieval.

The velocity algorithm utilizes the Fast Fourier Transform (FFT) algorithm to transpose the temporal return signal to the frequency domain for each gate to produce

range-resolved estimates of the radial wind velocity. The highest peak of the FFT spectrum gives the predominant signal frequency, and therefore the prevailing radial wind speed, in each gate. A Graphical User Interface (GUI) enables selection of the number of range gates and the size (number of samples) of each gate. A typical range gate size of 256 samples results in a range resolution of 153.6m (256 * 0.6 m = 153.6 m). The dilemma in the LIDAR signal FFT processing is that the frequency resolution (and accuracy in wind speed retrieval) is proportional to the length of the signal while the range resolution is inversely proportional: the longer the gate, the better the wind speed accuracy and the worse the range resolution. Coherent LIDAR wind speed measurement is a compromise between spatial resolution and velocity accuracy.

Various retrieval techniques have been developed to obtain two dimensional (2D) and three dimensional (3D) wind field estimates based on radial velocity measurements. These include the Velocity Azimuth Display (VAD), Modified Velocity Azimuth Display (MVAD), Volume Velocity Processing (VVP) and Radial Velocity Feature Tracking (RVFT). These techniques are potentially suitable for many applications including vertical wind profiling at airports and wind farms, atmospheric and pollution transport studies.

2.2.2 Factors influencing the accuracy of wind sensing LIDARs:

There are several factors which influence the accuracy of using LIDAR for wind resource assessment. Some can be tied to uncertainties in the hardware, for example uncertainties in the cone angle, while others are spurred by atmospheric effects, like rain or clouds. The influence of each factor is qualitatively discussed below:

2.2.2.1 Uncertainties connected to errors in LIDAR hardware

Coherent LIDAR systems are based on heterodyne detection and their wind speed accuracy is therefore practically independent of drifting laser quantities such as power and wavelength which are extremely sensitive parameters in direct detecting LIDAR. However, there is more to a wind sensing LIDAR than heterodyne detection. A list of uncertainty sources due to errors in the LIDAR hardware include:

2. 2.2.1.1 Sensing range error (Range gate trigger, Focusing, Range gate distortion)

One inherent problem with remote sensing is to accurately know the distance you are sensing at. Since the wind on average increases significantly with height an error in sensing distance introduces a measurement bias. An average error of 5 m in the sensing height can easily introduce a bias of 0.2 m/s in typical shear conditions (Lindelöw P., 2009).

2. 2.2.1.2 Cone angle and Tilted mounting

LIDAR only can measure the wind speed in the beam direction, i.e. the radial wind speed. To construct the horizontal wind velocity it is important to know the cone angle with high accuracy. A likely source of uncertainty in conically scanning LIDARs is uncertainty in the intended cone angle, φ, (figure 2.3). An error in cone angle, Δφ, is transferred to an error in the sensed horizontal wind speed, which is linearly proportional to the wind velocity. An error in cone angle likewise presents a small error in sensing (Lindelöw P., 2009).

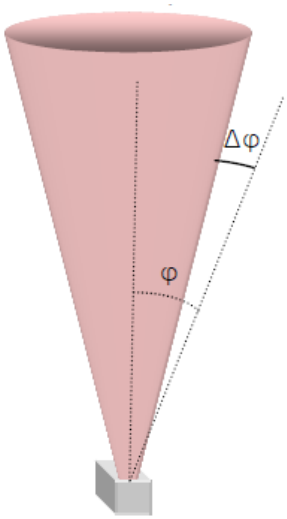

Figure 2.3: Illustration of the cone angle error. The intended cone angle is shown as a dotted line, the actual cone angle is illustrated by the pink cone.

2. 2.2.1.3 Tilted mounting

The mounting of a LIDAR is equally important as mounting of cup anemometers and wind vanes. A tilted LIDAR experiences significant cone angle and limited sensing range errors which are different for the different sensing directions. The errors

introduced leads to direction dependent biases both on speed and direction (Lindelöw P., 2009).

2.2.2.2 Uncertainties connected to atmospheric phenomena

The uncertainty in the wind sensed by a coherent LIDAR also depends on the atmospheric conditions, for example to what degree the assumptions on a horizontally uniform flow and homogeneity of the aerosol distribution are fulfilled. The magnitude of the errors in the LIDAR hardware also depends on for example wind speed and shear. The influence of each factor is qualitatively discussed below:

2.2.2.2.1 Turbulence over the scan perimeter

The differences of the wind sensed over the scan perimeter are both due to spatial turbulence and that the radial measurements are taken at different times. In flat terrain the turbulence is nominally random and only introduces a standard deviation on the measurement. In complex terrain veer, flow angles, speed up/down effects can introduce significant biases. LIDAR can to some degree evaluate the turbulence at a flat site by studying the variability of the wind velocity sensed in different, for example opposing, directions. In complex terrain, more advanced flow models can be used in combination with the radial velocities to estimate three dimensional flows (Lindelöw P., 2009).

2.2.2.2.2 Inhomogeneous aerosol scatter distribution

The weighting function of the sample volume, which is used to set the sensing range, is calculated for a homogeneous aerosol distribution. This is probably unlikely in a real atmosphere especially since the number of collected photons is limited. However, in a clear atmosphere, i.e. one without clouds or fog, the atmosphere can be considered as homogeneous over ten minutes (Petter Lindelöw-Marsden., 2009).

2.2.2.2.3 Clouds and rain

LIDAR systems are influenced by clouds since the weighting function of the sample volume is erroneous in the presence of significantly non-homogeneous backscatter distributions. A significant part of the measured wind distribution is usually taken at the cloud height and not at the intended measurement height. Positive biases on the wind horizontal wind speed are introduced in cloudy weather since clouds

predominantly are above and the wind thus typically stronger at the cloud height than at the set sensing height (Lindelöw P., 2009).

2.3 The wind Power equation

The performance of a wind turbine is measured in terms of the rate of work done or energy transferred over a given period of time. With a wind turbine, kinetic energy of the wind is converted into electrical energy. Energy is usually measured in kilowatt-hours (kWh), which accumulated over a certain time period, such as an hour, day or year provides a measure of power output.

The power from the wind satisfies the equation below:

$$P = \frac{1}{2}\rho A V^3$$

This shows that the power (*P)* of the wind is a function of air density (ρ), the area swept by the turbine blades (*A*), and the velocity of the wind (*V).* As any one of these factors increase, so does the power available from the wind. Each variable in the power of the wind equation are described below.

2.3.1 Mean wind speed

In the long term, the mean annual wind speed at a particular site provides a good indication of the amount of energy likely to be captured by the wind. In general, it is said that the energy content of the wind is directly proportional to the cube of the wind speed, as indicated in equation above. However, the ability of a wind turbine to capture this energy is not perfect. For low wind speed sites, the relationship between energy capture and wind speed is nearer to being squared.

For example, in New Zealand, locations with mean annual wind speed above 7 m/s have been considered as potential wind farm sites. As a rough guide, wind farm developments on sites with mean annual wind speeds of 8 m/s yields electricity at a third of the cost for a 5 m/s site (Milborrow, 2002).

2.3.2 Air density

Air density varies with temperature and air pressure, so that air density is higher for cold temperatures and low elevations. Increasing the air density increases the resistance of the wind turbine blades in the air, hence increasing the turbine's ability to generate power.

2.3.3 Area swept

The final variable in the 'power from the wind' equation is the area swept by the turbine blades. As this increases, so the energy captured increases by the same proportion.

2.3.4 The power coefficient

For any wind turbine, the power output must also incorporate another term in the power of the wind equation, called the power coefficient (c_p). Therefore, the power from a turbine can be given as:

$$P = C_p \frac{1}{2} \rho A V^3$$

The power coefficient is the ratio of net generated power to the available power of the undisturbed flow through the wind swept area. The power coefficient can be seen as a measure of the turbine's efficiency.

2.4 Calculating the energy capture from the wind

Below are some important factors to consider when energy conversion calculations are performed. These factors are used in the Wind Atlas and Analysis Application Program (WAsP) (Troen and Petersen, 1989) to predict the energy conversion at a given site from an observed wind climate.

2.4.1 The power curve

Power curves are used directly in energy conversion estimates. Power curves are empirically derived by using wind measurements, air density, and other characteristics of the turbine such as the generator, blade diameter and the power coefficient. The Vestas turbines which will be installed at the proposed site have established themselves as a premier brand within the wind energy industry. The Vestas V52 turbines have a rotor diameter of 52 metres and have a hub height of 45 metres at the Lake Turkana. It has a nominal power output of 850kW, cut in wind speed of 4 m/s, a cut out wind speed of 25 m/s and reaches its maximum output at 16 m/s. Figure 2.3 shows the power curve for vestas V52 turbines.

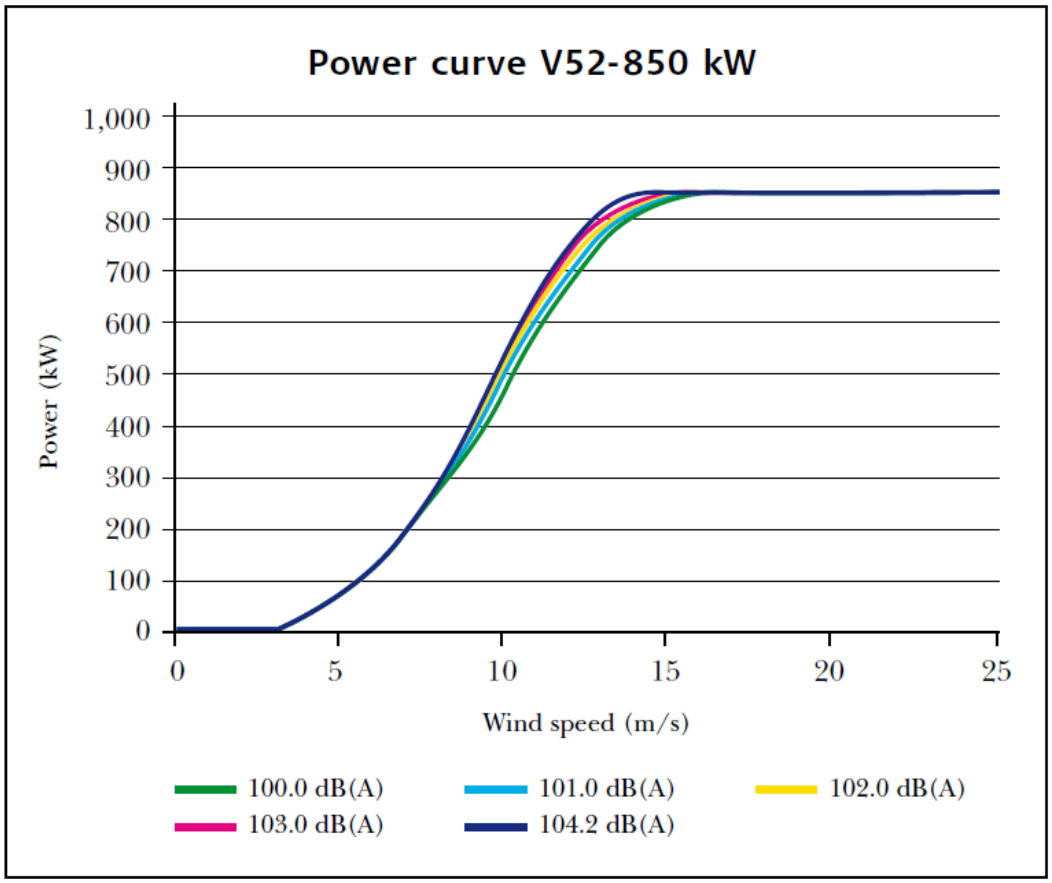

Figure 2.4: Power curves at different sound levels for the V52-850 kW turbine.

An innovative feature of the V52 turbines is the OptiSpeed generator which allows the turbine rotor speed to vary between 14 and 31 rpm depending on the conditions at any given time. It also reduces wear and tear on the gearbox, blades and tower on account of lower peak loading. Moreover, as turbine sound is a function of wind speed, the lower rotation speeds made possible by OptiSpeed naturally reduce sound levels. The sound output level can be adjusted by varying the revolution speed of the turbine (Vestas, 2016).

2.4.2 The Weibull distribution

The Weibull distribution is a two-parameter probability density function that best models the observed or forecast frequency distribution of wind speeds at a specific site (Seguro and Lambert, 2000). It approximates wind speed data given initially as a histogram, to a smooth curve described by a specific formula. The formula for this function is:

$$P(v) = \frac{k}{A}[\frac{v}{A}]^{k-1}\exp[-\left[\frac{v}{A}\right]]^{k}$$

Where: P(v) is the probability of the occurrence of a given wind speed,
k is the shape parameter, where $k > 1$,
A is the 'scale' parameter, where $A^3 > 0$.

In general, k specifies how steep the peak of the curve is, while A is a value close to the mean wind speed. The Weibull parameters k and A are empirically derived by statistical calculations based on the wind data.

2.4.3 Annual energy production

By convention, Annual Energy Production (AEP) is the total amount of energy produced by the wind turbine over the period of one year. Although it may be more suitable to call AEP annual electrical energy conversion, since energy is converted from one form to another. The power curve for a turbine and the Weibull curve for the wind climate of a particular site are combined by multiplying the probability that small increments of wind speeds occur, with corresponding values from the power curve. The result is then multiplied by the number of hours in a year (8760) to get the resulting annual energy production estimate. AEP is measured in terms of giga-Watt hours (GWh) (note that 1 GWh is equal to 1,000,000,000 Wh).

2.5 Predicting the wind

In the previous section, it was shown that to optimise the energy production from the wind, it is essential to find and utilise the 'windiest' locations. The cubic relationship between mean wind speed and energy output means that a relatively small increase in the mean wind speed can make a significant difference in energy output. Therefore, subtle differences in the mean wind speed might determine whether a wind energy conversion project is viable or not. For example, if the wind speed at a site is increased by 10%, the energy output will be approximately 30% higher.

The interaction between topographic features and airflow patterns is complex and difficult to model, although there is significant interest in undertaking research in this area. Ultimately, the wind energy industry needs reliable tools for estimating mean wind speeds at selected heights for locations and extensive sites where data are sparse. This would allow wind farm developments to proceed in less time, without the need to collect years of actual wind data for specific sites under investigation. However, such methods are required to be accurate enough to ensure confidence that

power generation will be consistent with the simulations. One of those methods considered in this study is the use of computer modelling techniques briefly described below.

2.5.1 Diagnostic modelling

Diagnostic models are also referred to as mass-consistent models. These model types contain no time derivative and therefore specify the balance of quantities at a particular moment in time. Starting with some upper level and surface wind data, mass-consistent models firstly reconstruct the three dimensional wind fields by interpolation. The interpolated wind fields are then adjusted to satisfy the laws of mass conservation caused by forcing by topography or by other physical constraints. Mass consistent models are therefore specifically designed to predict the effects of orography on steady mean wind flow (Ratto, 1996). One advantage of diagnostic models, especially in the past, is their lower computational demand. The Wind Atlas and Analysis Program (WAsP) is an example of a diagnostic model.

2.5.2 Prognostic modelling

Prognostic modelling is the method used by weather forecasting models. Prognostic model (also known as 'predictive' or dynamic models) are utilized to forecast the time evolution of atmospheric systems through the integration of conservation equations for mass, momentum, heat and water, and if necessary, other substances like gases and aerosols (Finardi et al., 1998).

Prognostic models can be used for a range of scales of motion from microscale, up to 2 km (cumulus cloud structure or pollution dispersion), to mesoscale, 2-2000 km (thunderstorm or urban pollution), to synoptic scale, 500-10000 km (for weather fronts and hurricanes), to planetary scale, greater than 10000 km (global wind patterns and ozone) (Jacobson, 2005).

Prognostic models can be used to investigate the effects of synoptic scale weather systems on local scale airflow and provide the ability to simulate such events. While synoptic scale weather systems are driven primarily by large-scale dynamic and thermal processes, mesoscale processes are governed more by orography and irregularities of the surface energy balance (Lalas and Ratto, 1996). Therefore,

computer codes or models can be constructed so that atmospheric phenomena can be simulated at the scale at which they occur.

Prognostic mesoscale models are frequently used with nested grids, which range from a coarse to a finer scale. The outer grid can obtain boundary or initial conditions from global scale models (low resolution grid data). In the nesting procedure, output of the larger domain is used as the boundary conditions for the next inner grid, until the required resolution is gained. Output from global models is usually computed six hourly, so that the boundary conditions can be 'nudged' at these times to maintain the accuracy of the simulation. Most prognostic mesoscale models now use terrain following co-ordinate systems. This allows for easy reconstruction and analysis of the wind field features at a local scale. Weather Research and Forecasting model (WRF) is an example of a prognostic model.

2.6 Model Selection

There has been much research into the best ways of simulating the airflow close to the Earth's surface, especially in complex terrain, and many issues still remain unresolved. Diagnostic models, such as WAsP, have been most commonly used in the past, but they have recognised limitations. These models types are likely to be able to improve their calculations in complex terrain by using non-linearised equations in the model calculations (Walmsley, 1986). Prognostic models also have limitations with simulating airflow near the Earth's surface, but with increased computing power, these limitations should diminish. Some hybrid modelling techniques combine both prognostic and diagnostic techniques.

Non-hydrostatic source codes are considered to be the new generation models. In computer modelling, the hydrostatic approximation has resulted in significant reductions in computing time and expense. Effectively, this approximation neglects hydrostatic effects, and thus localized dynamical vertical accelerations. Models adopting this approach should not be applied for horizontal scales less than 10 km, because in this case non-hydrostatic effects should not be neglected (Lalas and Ratto, 1996). In non-hydrostatic diagnostic and prognostic models, mesoscale pressure differences can be computed, and hence wind fields can be evaluated at a higher resolution. With greater computing capabilities, non-hydrostatic models are not only

accessible to the research field, but also for more practical applications, such as in the wind energy field.

2.7 Chapter Summary

The first part of this chapter discussed the two methodologies that can be utilized to measure wind at a specific area: use of mast-mounted anemometer and vanes and use of remote sensing devices i.e. LIDAR. The wind farm under current study lies in a region of complex terrain. Accurately modelling wind flow patterns in such regions are important for both locating and assessing this wind energy potential. Understanding airflow patterns in complex landscape is vital for the identification of high mean wind sites, and to acknowledge and perceive confinements of the models utilized.

The mean wind speed and distribution of wind speeds is a fundamental factor in assessing the wind energy potential for a location. Section 2.3 and 2.4 described the relationship between wind speed and energy.

Finally, there are many models used to predict wind flow patterns, from simpler diagnostic models to complicated prognostic numerical models. Chapter 3 present the analysis of observed data used in this study, and in the chapters that follow; the use of prognostic and diagnostic modelling techniques is described and used in a case study to assess the wind energy potential in the Lake Turkana region.

3. CHAPTER 3

Chapter 3 provides a description of observational data utilized in this study. Two sources of observational datasets are used to validate numerical modeling results, wind speed and direction measured by cup anemometers and windvanes at Kalkumpei, Nyiru and Sirima mast locations within Lake Turkana wind farm, and measurements by LIDAR deployed at the site between 11th July and 25th July 2009. The statistical analysis of these datasets is also presented in this chapter.

3.1 Meteorological mast measurements

Three masts equipped with cup anemometers and wind vanes have been positioned at Kalkumpei, Nyiru and Sirima in Lake Turkana wind farm region to carry out high quality wind measurements (figure 2.1). The stations provide 10-minute average measurements throughout the day. Table 3.1 shows the location of meteorological masts while table 3.2 gives more detail about the measured wind data at the mast locations. The wind speed measurements were recorded with four decimal place precision but the results are presented to one decimal place.

At all masts, the anemometers are mounted on horizontal booms approximately 7.5 mast face widths long, and the cups of the anemometers are at least 15 boom diameters above the booms in each case. These mounting arrangements are consistent with the recommendations provided by IEC (Standard 2005)

Table 3.1: Table giving the details about the sites location

Site name	Latitude (°N)	Longitude (°E)	UTM Zone	Easting	Northing	Height ASL (m)
Kalkumpei	2.5314	36.8569	37	261707	279998	804
Nyiru	2.4607	36.8033	37	255724	272182	872
Sirima	2.4743	36.8380	37	259589	273686	832

Table 3.2: Table summarizing the masts data used

Site name	Start	End	Anemometer heights (m)	Wind vane heights (m)
Kalkumpei	1/1/2009	31/12/2009	38.5, 20	39, 21
Nyiru	1/1/2009	31/12/2009	46, 20	49, 20
Sirima	1/1/2009	31/12/2009	38, 20	40, 20

3.2 Data Quality Control

Prior to data analysis, there was a need to examine data quality. This is necessary if correct statistical inferences are to be made from the data. The quality of data may be compromised by inconsistencies in records and data gaps. Inconsistent data can occur for several reasons such as change of location of observing stations and/or in instruments, or human error. World Meteorological Organization (WMO) standard recommends that a climate dataset for which more than 10% is missing, is not good. The wind data was subject to a quality checking procedures to identify records which were affected by equipment malfunction and other anomalies. The main periods for which valid wind data were suspicious are summarized below, together with details of the errors identified.

Kalkumpei mast

Erroneous data from 9th November to 23 November 2009 at 38.5 m anemometer.

Nyiru mast

Erroneous data from 14th November to 31st December 2009 at 49 m wind vane due to sensor setup fault.

Sirima mast

Erroneous data from 17th April to 31st December 2009 at 40 m wind vane

Missing and erroneous wind speed and direction data at the 38.5 m, 49 m and 40 m for Kalkumpei, Nyiru and Sirima masts respectively were synthesized from wind speed and direction data at the 20 m and 21m measurements.

3.3 Measured Wind Statistics

The measured wind statistics for Kalkumpei, Nyiru and Sirima are presented and discussed in the following sections.

3.3.1 Kalkumpei mast data.

Wind speed data recorded between 9th November 2009 and 23st November 2009 at 38.5 m was below 1 m/s and hence declared erroneous. During this period wind speed data at 20 m anemometer was used to replace the suspicious data at 38.5 m height. The measured mean annual wind speed for Kalkumpei at 38.5 m was 10.44

m/s while the mean wind direction at 39 m was 117.25° respectively. The mean annual temperature was 28.3°C.

Table 3.3: Mean monthly wind speed, wind direction and temperature at Kalkumpei mast.

Month	Mean wind speed at 38.5 m (m/s)	Mean wind direction at 39 m (°)	Mean temperature (°C)
Jan	10.3	119.9	28.6
Feb	11.3	120.7	29.2
Mar	10.5	120.1	30.3
Apr	9.2	116.3	29.3
May	9.3	117.2	28.8
Jun	10.6	112.2	28.1
Jul	11.5	112.9	26.7
Aug	11.8	113.8	26.9
Sept	11.2	113.7	28.4
Oct	10.3	119.0	27.9
Nov	10.1	116.4	28.4
Dec	8.7	124.2	27.8

3.3.2 Nyiru mast data.

Wind direction data recorded between 14th November and 31st December 2009 at 49 m was erroneous due to wind vane setup fault. During this period wind direction data recorded by 20 m wind vane was used to replace the suspicious data at 49 m height. The measured mean annual wind speed for Nyiru at 46 m was 10.75 m/s while the mean wind direction at 49 m was 121.21°. The mean annual temperature was not computed because 4 months data (June, July, August and September) was missing.

Table 3.4: Mean monthly wind speed, wind direction and temperature at Nyiru mast.

Month	Mean wind speed at 46 m (m/s)	Mean wind direction at 49 m (°)	Mean temperature (°C)
Jan	10.5	127.8	29.1
Feb	11.3	127.3	29.7
Mar	10.9	124.3	30.9

April	9.7	121.7	30.0
May	9.7	121.7	29.3
Jun	10.8	115.5	28.4
Jul	11.7	112.8	missing
Aug	12.1	113.2	missing
Sept	11.6	118.5	missing
Oct	10.6	120.8	missing
Nov	10.6	122.1	28.9
Dec	8.9	133.5	28.5

3.3.3 Sirima mast data.

Wind direction data recorded between17th April to 31st December 2009 at 40 m was erroneous. During this period wind direction data recorded by 20 m wind vane was used to replace the suspicious data at 40 m height. The measured mean annual wind speed for Sirima at 38 m was 11.10 m/s while the mean wind direction at 40 m was 110.73°. The mean annual temperature was 28.0°C.

Table 3.5: Mean monthly wind speed, wind direction and temperature at Sirima mast.

Month	Mean wind speed at 38 m (m/s)	Mean wind direction at 40 m (°)	Mean temperature (°C)
Jan	10.8	118.1	28.0
Feb	11.8	117.0	28.7
Mar	11.2	115.4	30.0
Apr	10.1	119.8	29.1
May	10.1	116.8	28.5
Jun	11.2	107.2	27.7
Jul	11.9	94.4	26.3
Aug	12.4	94.9	26.6
Sept	11.9	94.9	28.1
Oct	11.1	105.7	27.6
Nov	11.1	118.4	28.0
Dec	9.3	126.0	27.6

Figure 3.1 and 3.2 shows the monthly mean wind speed variation and temperature for Kalkumpei, Nyiru and Sirima mast locations respectively. The period between June and October has the highest mean wind speed hence the best period for electricity generation. The highest mean wind speed was recorded in August with a mean of 11.86 m/s, 12.1 m/s and 12.4 m/s. The lowest wind speed was recorded in December with a mean of mean 8.79 m/s, 8.9 m/s and 9.3 m/s. Figure 3.3 shows that high wind speeds are experienced during morning hours from midnight to around 11am.

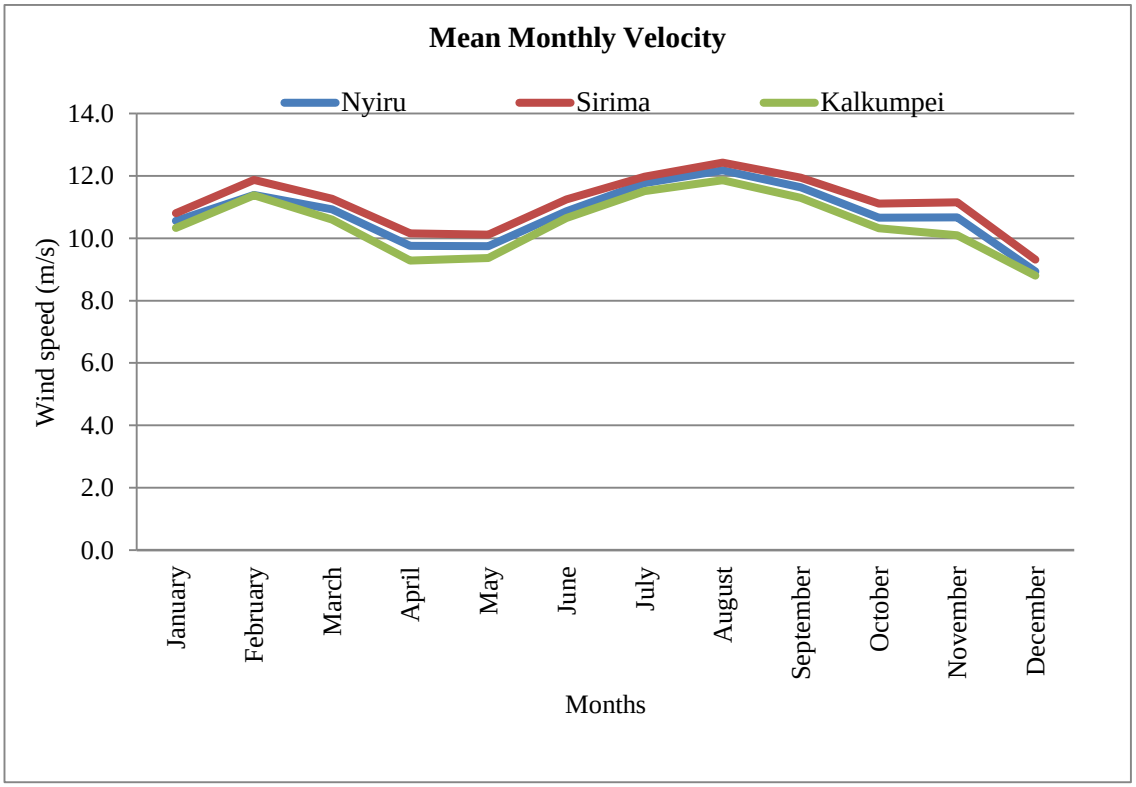

Figure 3.1: Mean monthly wind speed for Kalkumpei, Nyiru and Sirima mast locations.

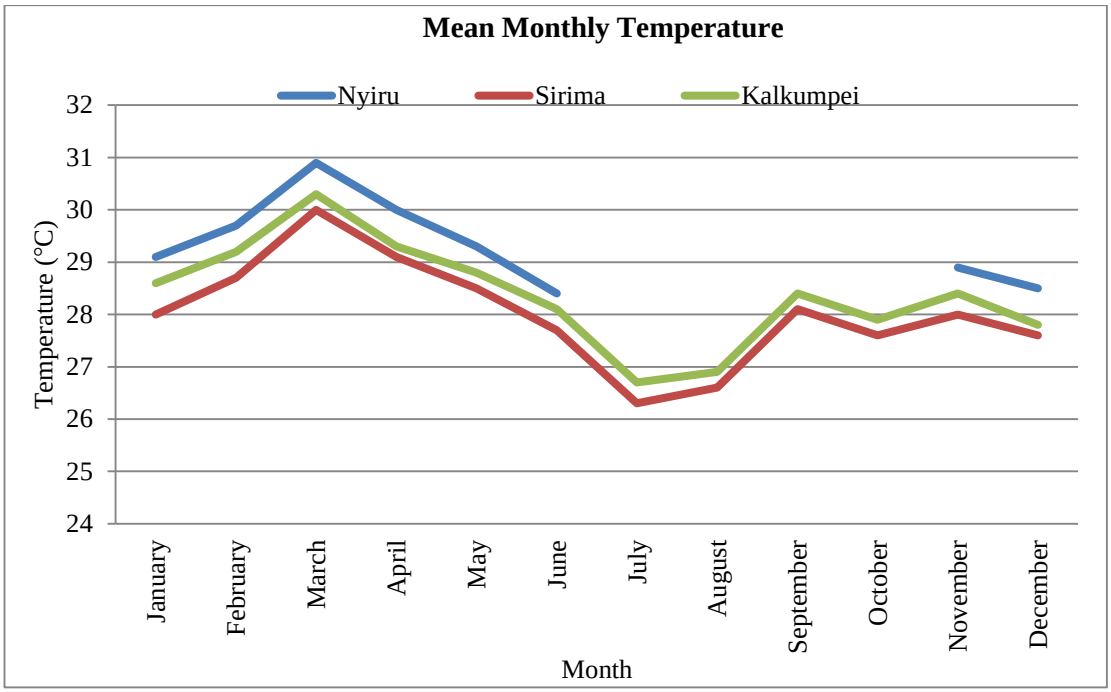

Figure 3.2: Mean monthly Temperature variation for Kalkumpei, Nyiru and Sirima mast locations.

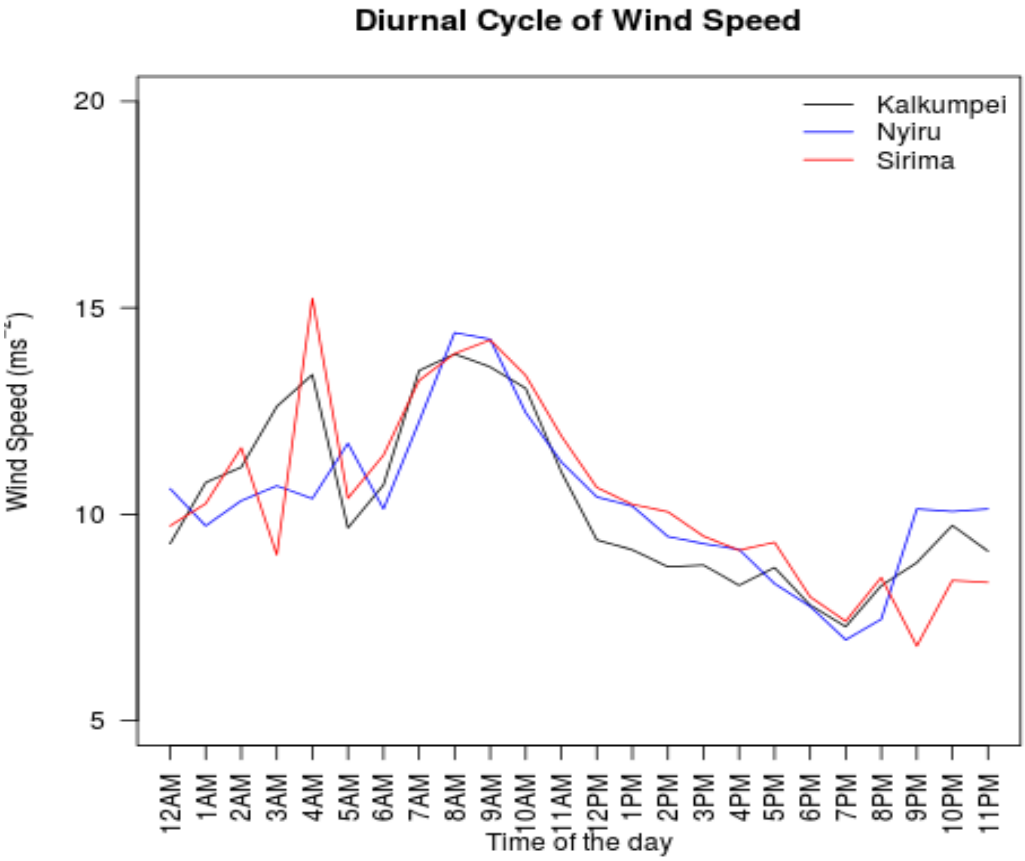

Figure 3.3: Annual Diurnal variation in wind speed for 2009 at the three mast locations

Table 3.6 shows Annual Mean Absolute Error (MAE), Correlation coefficient (r) and Root Mean Square Error (RMSE) while table 3.7 shows monthly Mean Absolute Error (MAE), Correlation coefficient (r) and Root Mean Square Error (RMSE) between the 3 masts for wind speed. The statistics presented in these two tables confirm that the 3 mast locations are within the same wind speed climatology. This further corroborates the hypothesis that the wind farm is located within an area of fairly consistent wind climatology.

Table 3.6: Annual MAE, RMSE and r for wind speed between the three mast locations. The towers are located 842.5 m, 918 m and 870 m AGL at Kalkumpei, Nyiru and Sirima respectively.

Statistics/Mast locations	Kalkumpei vs Nyiru	Kalkumpei vs Sirima	Nyiru vs Sirima
MAE (m/s)	1.09	0.97	1.01
r	0.825	0.906	0.851
RMSE	1.453	1.229	1.358

Table 3.7: Monthly MAE, RMSE and r for wind speed between the three mast locations

Month/Mast	Kalkumpei vs Nyiru 38.5 m/46 m			Kalkumpei vs Sirima 38.5 m/38 m			Nyiru vs Sirima 46 m/38 m		
	MAE	RMSE	r	MAE	RMSE	r	MAE	RMSE	r
January	1.17	1.53	0.75	0.97	1.22	0.87	1.15	1.48	0.87
February	1.32	1.77	0.72	0.98	1.26	0.89	1.34	1.74	0.89
March	1.14	1.50	0.77	1.00	1.24	0.89	1.11	1.43	0.89
April	1.16	1.50	0.85	1.08	1.34	0.92	1.00	1.34	0.92
May	1.16	1.56	0.82	1.02	1.30	0.91	0.99	1.36	0.91
June	1.05	1.41	0.82	0.90	1.15	0.89	0.96	1.35	0.89
July	0.83	1.04	0.84	0.74	0.93	0.89	0.73	0.98	0.89
August	0.87	1.10	0.79	0.78	0.98	0.87	0.78	1.02	0.87
September	0.94	1.20	0.76	0.86	1.09	0.85	0.85	1.15	0.85
October	1.14	1.48	0.79	1.02	1.28	0.89	1.02	1.35	0.89
November	1.17	1.54	0.64	1.26	1.56	0.77	1.04	1.36	0.77
December	1.18	1.61	0.84	0.98	1.24	0.92	1.13	1.53	0.92

3.5 LIDAR wind measurements

A major part of material presented in this section was initially presented in a report prepared by CRC CARE (CRC-CARE. 2010). LIDAR measured wind speed and direction from 11th July to 24th July 2009 are used in this study. The WindTracer LIDAR was transported to site by road and positioned on a high point within the landscape (latitude 2.48333°N, longitude 36.84835°E, at height 788 m above sea level). The LIDAR was positioned approximately 20 kilometers to the south east of Lake Turkana.

Figure 3.4: Google map showing LIDAR and mast locations.

3.5.1 Scanning strategy

The radial wind field to a distance of approximately 10 kilometers from the LIDAR was retrieved using a series of 360 degree horizontal scans. Each scan took approximately 10 minutes to complete providing data consistent with the averaging period of the mast anemometers. The scans were configured to scan between -1 degree and 1 degree in vertical elevation to achieve radial wind velocity data above and below the 45 m height across the landscape. Data across 10 or 11 layers were typically used to produce a terrain-following wind speed map.

Figure 3.5 shows the location of the closely spaced laser beams along the horizontal plane radiating from the LIDAR (brown lines). A laser scanning rate of 6~8 degrees per second was typically used to achieve the required data averaging period. Radial wind speed estimates were recovered from each beam at spatial resolution (range gates) of 150 m. The LIDAR is effectively "blind" for the first 500 m along the laser beams due to electro optical constraints within the receiver. The "blind" spot is indicated by the grey ring surrounding the laser measurement site.

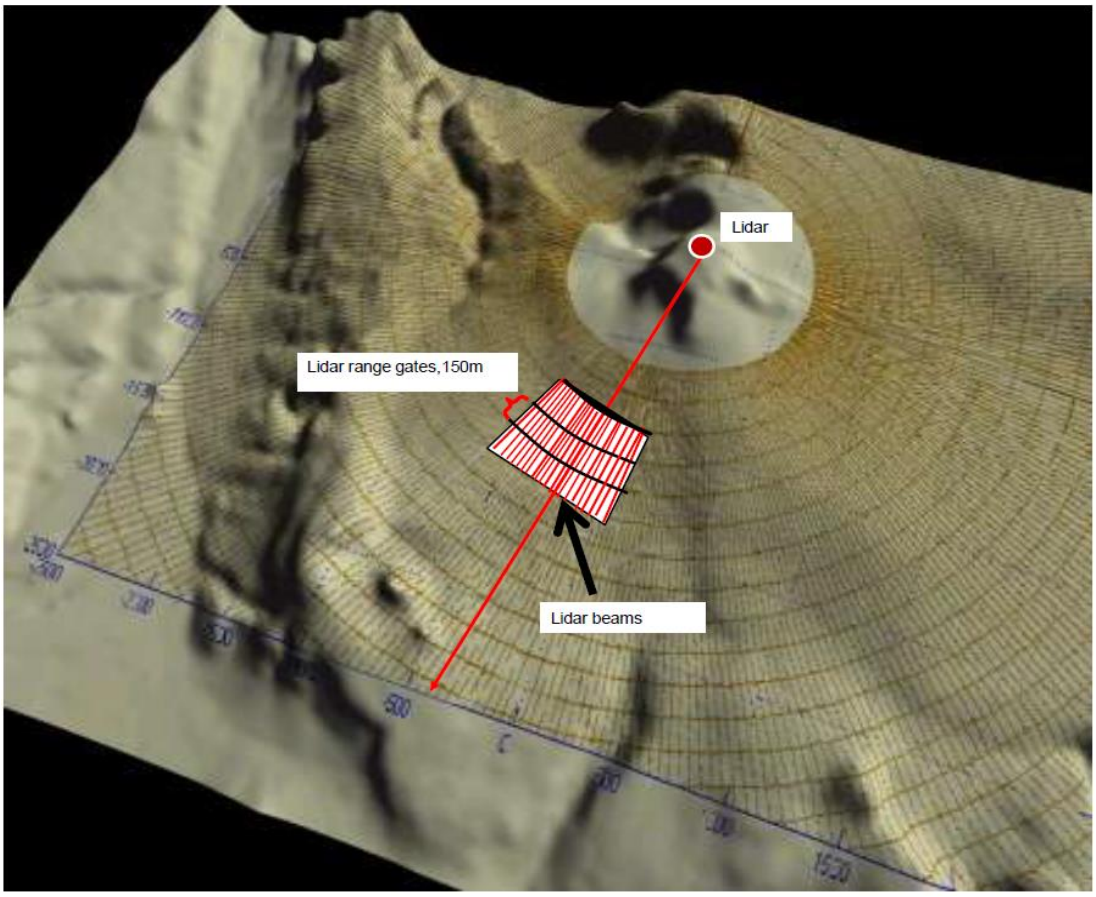

Figure 3.5: LIDAR scanning pattern in the South Western Sector of the study site (CRC-CARE., 2010).

Figure 3.6 is a 15 degree sector of the scan in the vicinity of the Sirima mast. Data collected within the 15 degrees sectors of all layers of the 360 degree horizontal scans are used to recover the full wind vector at each range gate as described in section 3.5.2. Figure 3.6 also shows two layers of the horizontal scanning planes within a 15 degree sector. It can be seen that the two horizontal scanning planes lay either side of anemometer. The positioning of the vertical scans permits the use of interpolation techniques for deriving the 45 m terrain- following wind speed maps.

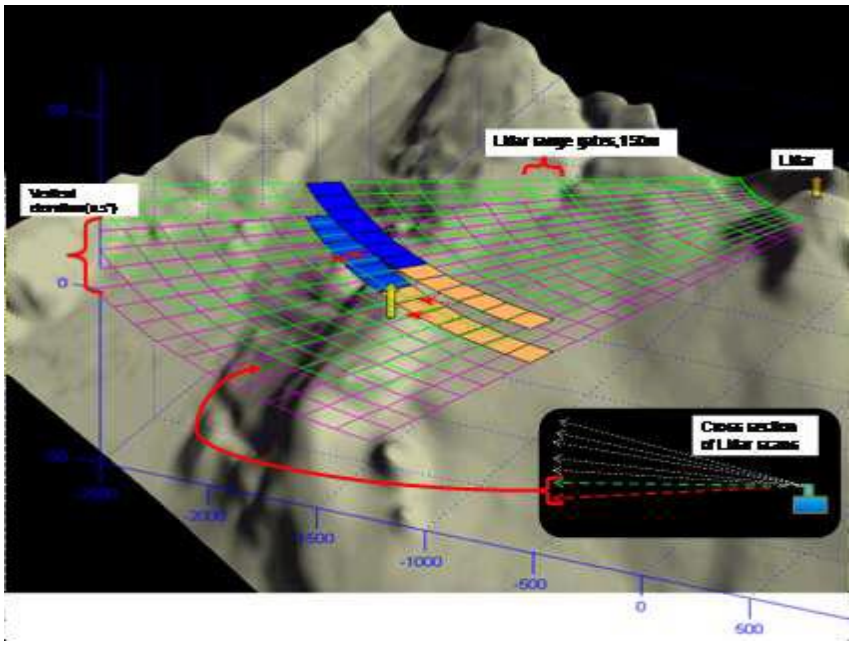

Figure 3.6: Scanning planes within a 15 degree horizontal sector (CRC-CARE., 2010).

3.5.2 Wind vector retrieval

An advanced LIDAR data volume processing technique developed by a research group based in Perth, Western Australia was used to retrieve the wind vectors. The technique categorizes the available LIDAR data into several conical layers and subsequently subdivides each layer into many small analysis volumes. The fundamental theory of this technique was derived from the general Doppler LIDAR data processing scheme called Volume Velocity Processing (VVP). This type of scheme is considered to be a more straightforward way of resolving wind velocity directly from the LIDAR radial velocity data (Boccippio, 1995, Koscielny et al., 1982, Crook N.A. et al., 2005, Hannon S. et al., 2008).

In each analysis volume, an optimized wind vector is obtained after fitting through all data points included in the volume. A constraint that uses the VAD (Velocity Azimuth Display) retrieved mean wind is applied in order to control the instability in the processing, especially at the perpendicular area (orthogonal to the mean wind direction, i.e. typically at the north-east and southwest direction from the LIDAR site). After each layer of the wind speed values is retrieved, the processing algorithm interpolates these values to 45 m above ground level.

3.5.3 Volume Velocity Processing (VVP) Algorithm

The advanced VVP algorithm developed is an improved version based on the traditional VVP. It has improvements in retrieval stability and solution quality control. The direct measurements of wind by LIDAR are restricted to the radial component of the wind. To resolve the tangential components of the wind LIDAR beam measurements of the radial component are used from other directions. In a constant wind field, radial winds measured vary at each direction, and the rate of this variation with direction can be used to estimate the tangential wind velocity. By taking adjacent or lateral radial velocity measurements at defined range gates, the VVP algorithm is then used to estimate wind vectors at the specified range gate location.

The VVP algorithm firstly clusters the measured LIDAR data from the volume of sweeps into small conical analysis volumes. Each of these volumes utilizes 10 to 20 radial velocity data points, contingent upon the size of the conical analysis volume. As more radial velocity data points are included in the analysis volume, the larger the analysis volume needs to be. This would mean a reduction in the retrieved wind field resolution. On the other hand, with less radial velocity data points, the retrieval of the wind becomes ill-conditioned and unstable, which leads to errors in the retrieved wind field. It is therefore important to understand the trade-off between these two factors in order to produce a quality controlled retrieval. Krishnamurthy et al., 2012 uses a similar approach for wind farm characterization using LIDAR.

The size of the unit analysis volume used in the field investigation of the Lake Turkana wind field is defined with $\Delta\varphi = 10°$, $\Delta r = 150$ m and $\Delta\alpha = 0.4°$ (figure 3.7). For the given unit analysis volume, the VVP algorithm automatically loops through all analysis volumes, applying a least squares minimization scheme to obtain the solution.

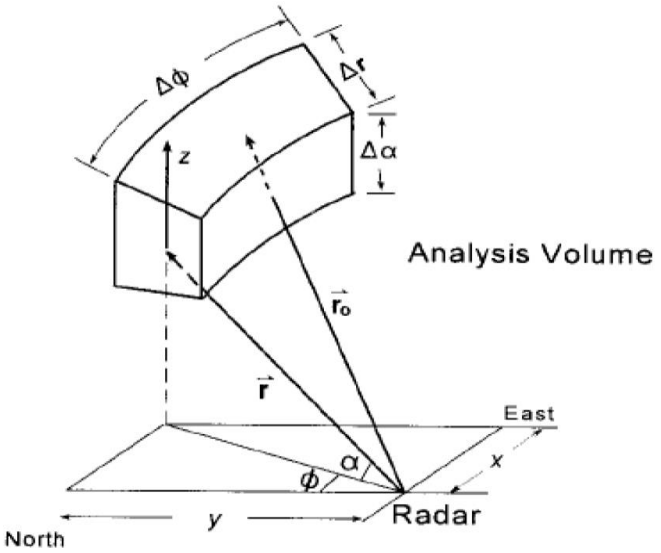

Figure 3.7: Unit conical analysis volume.

Once the solutions are obtained, a quality check is performed to filter out solutions that are not considered to be reasonable. The solutions retrieved are then registered at the center of each analysis volume and further gridded to a rectangular mesh of 150 m x 150 m resolution. While the VVP algorithm requires more processing time than the tradition Velocity Azimuth Display (VAD) approach, it produces the more detailed output required for this project.

3.5.4 Generation of wind map

With the obtained layers of rectangular meshed wind velocity solutions, it is possible to create a 45 m terrain-following wind map. At each grid point, there are usually 5 velocity values at distinctive heights that can be used to interpolate speeds to the 45 m level. However, due to the terrain-blocking at lower levels of the LIDAR scans and noise caused by atmospheric conditions, the required scan levels may not be available. To overcome this problem, three separate approaches were used to complete the interpolation:

a) Interpolation method: At the grid point where there are at least 2 available data points at different heights and the 45 m level is at the level in between these data, wind profile power law fit (with exponent value of 0.143 under neutral atmospheric condition assumption) is used to obtain the wind speed at the 45 m level.
b) At the grid point where there are at least 2 available data points at different heights but the 45m level is below these data, the linear interpolation is

implemented to a reference height (between heights of these available data). The 45m level wind speed is then obtained applying the theoretical wind power law (with the same 0.143 exponent value) under neutral atmospheric condition assumption.

c) Extrapolation method: At the grid point where there is only one available data along the vertical, the 45 m level is simply obtained by applying the wind profile power law with the same exponent number.

3.6 LIDAR Measured wind characteristics

The LIDAR retrieved wind speed was compared to mast measurements at three locations from 11th July to 24th July 2009 after removal of poor quality LIDAR data. It was shown that the differences between the two means (mast and LIDAR 45 m level wind speed) are small and the standard deviations from the mean in both instruments are in good agreement. The standard deviation is based on the time series of wind speed deviation of each instrument to its own mean. It represents the degree of variability of the time series wind speed data

Table 3.8: Mean wind speeds, mean difference and standard deviations (11th to 24th July 2009)

Mast locations	Height	Mean wind speed (m/s)	Mean difference (m/s)	Standard Deviation (m/s)
Kalkumpei	Mast (38 m)	11.03	0.33	1.90
	LIDAR (45 m)	10.70		1.65
Nyiru	Mast (46 m)	11.19	0.05	1.92
	LIDAR (45 m)	11.23		1.79
Sirima	Mast (38 m)	11.43	0.47	1.71
	LIDAR (45 m)	10.95		1.72

Table 3.9: RMSE, Correlation coefficient and MAE between LIDAR and Mast data (11th to 24th July 2009)

	RMSE	Correlation	MAE
Kalkumpei	0.94	0.90	0.42
Nyiru	1.52	0.60	0.91
Sirima	1.10	0.73	0.94

The time series plots for the three mast locations are presented in Figures 3.8, 3.9 and 3.10. It can be seen that the LIDAR and mast measurements are in close agreement with the mean wind differences between two different instruments less than 0.5 m/s. There was a significant difference between LIDAR and mast measurements for 21/7/2009. This could be associated with the presence of localized wind gusts, this can only be detected and well represented in the LIDAR dataset as opposed to anemometer datasets (CRC CARE, 2010).

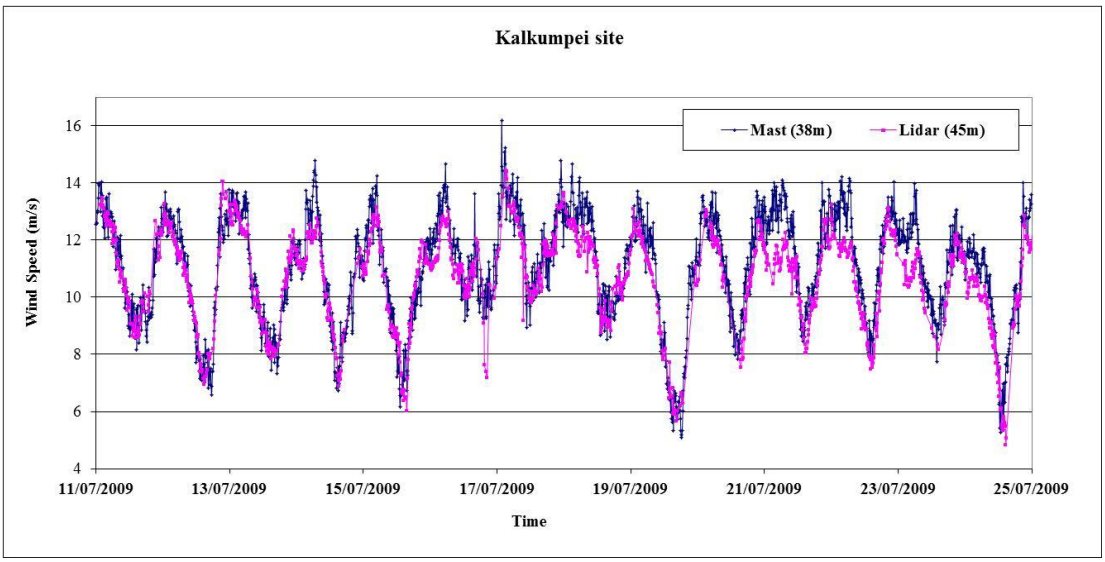

Figure 3.8: Comparison of LIDAR analyzed and Mast wind speed at Kalkumpei.

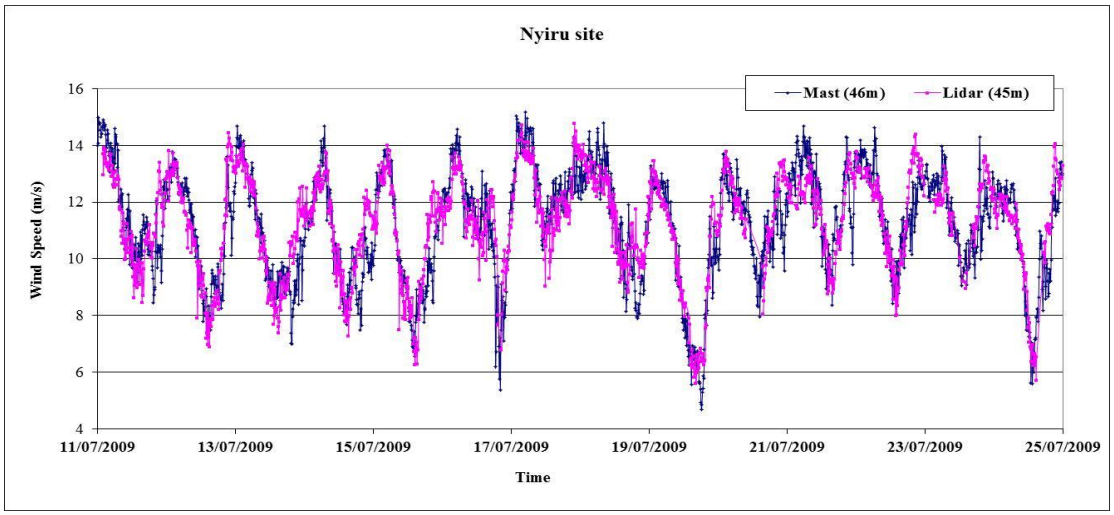

Figure 3.9: Comparison of LIDAR analyzed and Mast wind speed at Nyiru.

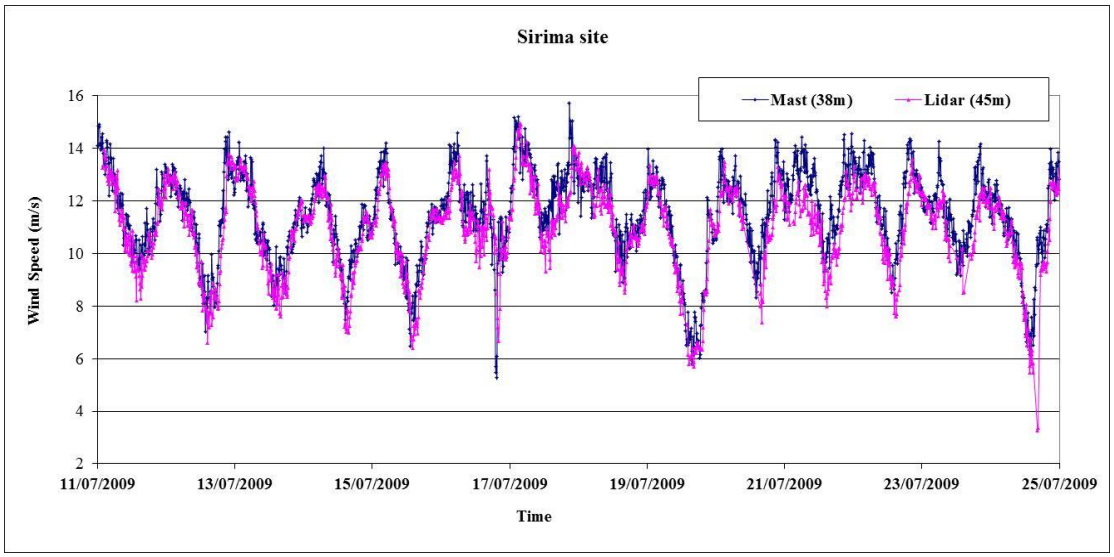

Figure 3.10: Comparison of LIDAR analyzed and Mast wind speed at Sirima.

3.6.1 Terrain-following wind speed plots

The derived wind speed data was output into a 20 km x 20 km grid domain and overlaid on a digital terrain model. The data was adjusted to remove bias arising from an uneven distribution of 10 minute sample periods within the data set caused by a difference in the number of wind speed data available for producing averaged wind speed at each hour, the number of wind speed data available for averaging is relating to the measured data (radial velocity data) density after noise filtering and the instrument down time

The resultant map covers a geographic area of 400 square kilometers and comprises approximately 18,000 data points along the 45 m terrain- following plane. Figure 3.11 and Figure 3.12 contain two plots, the first being a 3D image of the wind field, the second providing the same information in 2D, enhanced with terrain-following vector fields.

The maps show that the average wind speed gradually increases as the flow moves west to approximately 10 m/s near the LIDAR site. Maximum velocities occur on the higher ridges on the western boundary with wind speed reaching over 14 m/s. Wind shadow effects from topography are also evident in the maps.

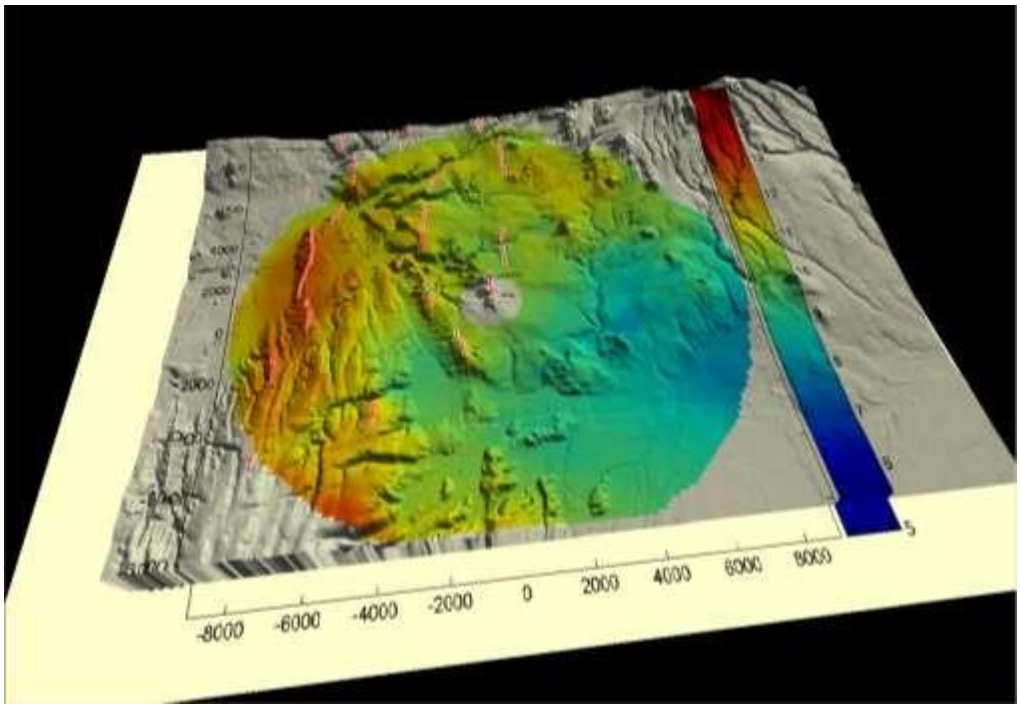

Figure 3.11: Mean three dimensional horizontal wind speeds at Lake Turkana wind farm.

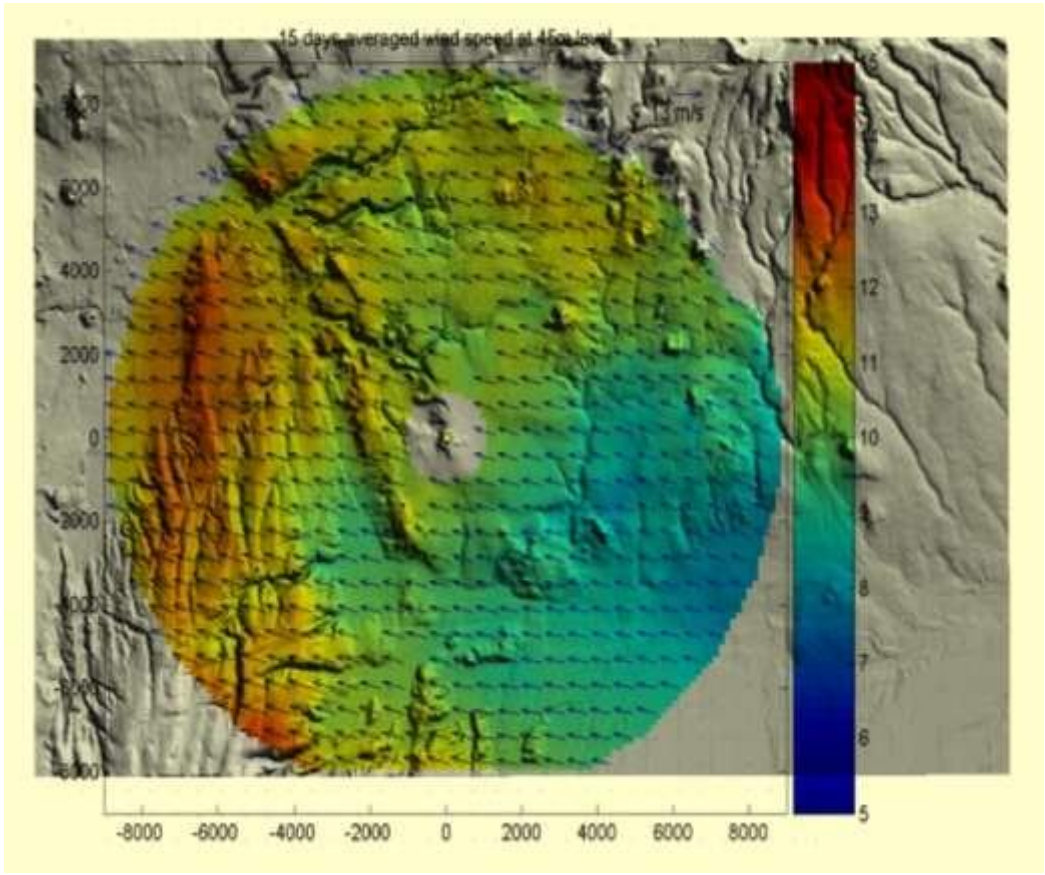

Figure 3.12: Mean two dimensional horizontal wind speeds with terrain-following vector fields at Lake Turkana wind farm.

3.7 Chapter Summary

Analysis of wind speed data collected by mast mounted cup anemometers show that the local winds are generally characterized by high annual mean wind speed with values over 10.3 m/s and relatively large diurnal variability. The mean diurnal cycle was characterized by stronger winds during night-time and early morning than during daytime.

Anemometers provide averages of point measurements of wind speed independent of wind direction ("scalar averages") while LIDAR measure average vertical, lateral and horizontal wind speeds. These are generally transformed to provide "vector averages" of wind speed. In turbulent conditions, vector averages are lower than scalar averages. These differences imply that remote sensing and anemometry may not provide the same wind speed values although each may be measuring accurately.

Results presented in section 3.6 show good agreement between the LIDAR and the anemometer wind speed measurements. Terrain-following wind speed maps discussed in section 3.6.1 will be used to validate hub height wind atlas maps produced by WAsP model in chapter 5. This is a clear indication that LIDARs can assume a significant role in supplementing traditional measurement masts or used alone to provide detailed wind speed profiles for wind resource assessments. This can significantly speed up the development of wind farms.

The use of remote sensing technologies in wind resource assessment is still maturing. Equipment configuration and software changes particularly ALVPT may influence measurement quality and accuracy of retrieved wind speed and direction. In an energy assessment, remote sensing data may be used to evaluate resource variability over the site, validate and improve wind forecast models.

4. CHAPTER 4

This chapter is divided into two main sections: one describing the methodology for mesoscale numerical prognostic modelling and the second describing the methodology for a combined mesoscale and microscale diagnostic modelling approach. Understanding the model limitations is important when interpreting results, and also when attempting to overcome them.

4.1 Mesoscale models

Numerical Weather Prediction models are computer programs that solve the fluid dynamics equations that govern the atmosphere: conservation of mass, momentum and energy on a three-dimensional grid. The models additionally incorporate numerous parameterization schemes that take into account sub-grid physical processes that cannot be resolved by the numerical model, for instance the formation of raindrops (Stensrud, 2007). Several global weather models exist. They require supercomputers, thus they are only run by national or supranational meteorological organizations, such as the European Centre for Medium-Range Weather Forecasts (ECMWF), the UK Meteorological Office, the French weather service Météo-France or the National Oceanic and Atmospheric Administration (NOAA).

A mesoscale model (like WRF) is very similar to a global model but is generally limited to an area of some thousand square kilometers. The horizontal resolution is a few kilometers (or even below a kilometer). The initial and boundary conditions necessary for input to the mesoscale model are given by a global NWP model. These models vary in physical parameterizations, numerical schemes, data assimilation and coordinate systems (Lee and Fernando, 2004). Mesoscale models are of particular importance for wind energy developers and wind prospectors, serving as the primary input for wind integration studies if measured data are not available.

Mesoscale numerical wind models have also been used frequently in the creation of wind resource atlases: in Bolivia (3TIER, 2009), in the United States, the Philippines and Mongolia (Brower et al., 2004), Montenegro (Burlando et al., 2009), Ireland (Frank and Landberg, 1997), the Iberian peninsula (Bravo et al., 2008), offshore in New England, Texas and in the Great Lakes region (Bailey and Freedman, 2008).

Many of the topographic features and atmospheric behaviours within complex terrain occur on a smaller spatial scale than those commonly used in synoptic-scale forecasting. This results in limited near-surface model accuracy (Reid and Turner, 2001). However, higher resolution mesoscale models, such as WRF, are better suited for resolving the near-surface atmospheric behaviour in complex terrain, and it has been shown that WRF's cross-mountain flow modeling with respect to blocking, channelling, orography, and thermal forcing all correlate to observations at an acceptable level of accuracy (Rife et al., 2004), (Žagar et al., 2006) and (Jiménez et al., 2010).

Wind energy assessment using modeling techniques relies on the predictability of atmospheric dynamics. Evaluating model accuracy is accomplished by comparing simulated and observed atmospheric conditions spatially and temporally. However, observations are point recordings, while model simulations represent spatial means determined by a model's horizontal and vertical grid spacing (Hanna and Yang, 2001). Thus, differences are expected between observed and simulated conditions simply due to the differences of time and volume averages that each represents (Hanna and Yang, 2001).

WRF version 3.6 was used in this study to simulate airflow over Lake Turkana region for 1 year and generate hourly wind data. The model is discussed in detail below:

4.1.1 WRF Model

The WRF model has superseded the previous industry standard, the MM5 model. The material covered in this section is heavily based on the User's Guide (Wei Wang, 2012), the online tutorial (UCAR, 2012) and the technical notes that provided more details about the internal equations of the model (Skamarock et al., 2008).

WRF model was developed jointly by National Center for Atmospheric Research (NCAR), National Centers for Environmental Predictions (NCEP) and several other agencies and laboratories. It is freely available online and is used world-wide. With the merging of MM5 and WRF, there are now 2 versions of WRF: WRF-NMM (Non-hydrostatic Mesoscale Model) which is mainly used for operational weather forecasting and WRF-ARW (Advanced-Research WRF), more complex and

computationally slower and aimed for atmospheric research (Skamarock et al., 2008).

WRF is not one program but a suite of programs: one core program performs the simulation itself and there are numerous other modules that may be used to process the input or output data. For this study WRF was installed with the ARW core, and the essential modules. A description of the program chain and a flowchart is shown in figure 4.1:

4.1.1.1 WRF Pre-processing System (WPS)

WPS is responsible for defining the location and grid spacing of the desired model domain (including nests), interpolating static data (i.e., terrain, landuse, soil types) to the desired grid spacing, and degribbing and horizontally interpolating meteorological data from another model or data set onto the domain. These processes are accomplished through three steps referred to as Geogrid, Ungrib, and Metgrid. Degribbing is a process of reading GRIB-formatted datasets and writing them into an intermediate format using the Ungrib program. Grids with increasing resolutions, referred to as nests, can be placed within the coarse grids, either with or without feedback to the coarse grids.

The static fields typically have a resolution of 10', 2', or 30", though these are interpolated by Geogrid onto the user's selected grid spacing. Therefore, if the model domain has a resolution of 12 km, there is no benefit of selecting 30" over the 2' data since the higher details of the 30" will be smoothed out. On the other hand, if the horizontal resolution of the domain is a fine scale (e.g., 1 km and less), the static high resolution data is beneficial. If a nested high resolution domain exists inside a coarser grid, different static resolution data sets can be used appropriately.

The pre-existing meteorological data used by the Ungrib and Metgrid programs to make the files that are processed further by the Real program can vary in resolution and time availability. The WPS is essentially responsible for preparing the input data for the Real data initialization program. The Real program vertically interpolates the meteorological fields produced by Metgrid to the defined eta levels within WRF. The Real program creates the initial and boundary condition files needed for the WRF model itself.

Once all of the input and static data has been processed by the WPS system and Real program, the ARW solver is implemented. Specific details about input data and the techniques and options within the ARW solver are discussed next sections.

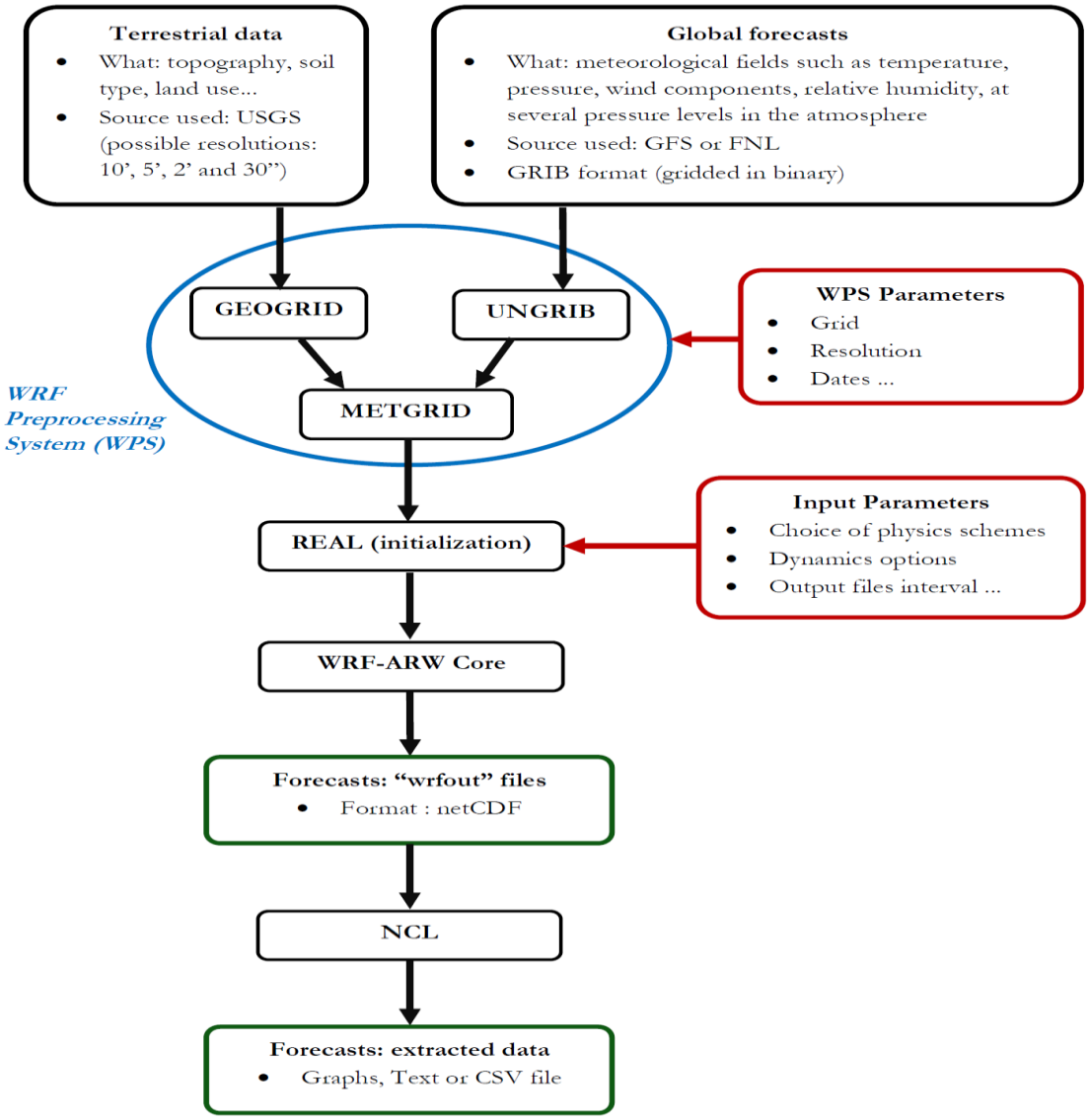

Figure 4.1: WRF model framework flow chart.

4.1.2 WRF Methodology

WRF is a completely compressible Eulerian non-hydrostatic (with a hydrostatic option) model with 3rd order Runge-Kutta time integration and smaller time steps for the acoustic and gravity-wave modes. The spatial discretization horizontally and vertically can be selected anywhere between a 2nd and 6th order advection option (Skamarock et al. 2008).

The WRF model also has turbulent mixing filters that include the subgrid scale turbulence formulation in both coordinate and physical space. Divergence damping, external-mode filtering, vertically implicit acoustic step off-centering, with an explicit filter option are also available. The diffusion options select how the derivatives used in terms of diffusion are calculated. This is accomplished by selecting two parameters within WRF, the "diffusion" and "K" option. If the diffusion option is not turned off, the K option selects how the diffusivity coefficients are calculated. Since a PBL scheme is utilized throughout this study, the K option only evaluates the horizontal diffusion, as the vertical diffusion is performed by the PBL scheme.

The WRF model uses an Arakawa C-grid, which is a staggered grid (Fig. 4.2). The mass variables are defined in the middle of the grid, while the wind components are defined on the edge of the grids. To compute the wind speeds for the center of the grid points (where the 10 m wind and 2 m temperature, etc. variables are defined), the U and V variables are interpolated onto the center of the grid. The vertical grid also uses the staggered grid (Fig. 4.2). The WRF model uses a terrain-following hydrostatic-pressure vertical coordinate denoted by η (Fig. 4.3). The coordinates are defined as:

$$\eta = \frac{(P_h - P_{ht})}{(P_{hs} - P_{ht})}$$

Where P_{hs} is the hydrostatic pressure at the surface and P_{ht} is the hydrostatic pressure at the top of the model domain. The heights selected to be used can either be specified by giving the desired η levels or by selecting how many vertical levels the user wants. If the user does not specify the η levels, then an automated algorithm is used to select the placement of these levels. This algorithm does not place more than 7 levels within the lowest 2 km. Since the model output is reported on the η levels, the ground relative heights are calculated from the geopotential heights. The grid spacing of the vertical levels normally increases with height.

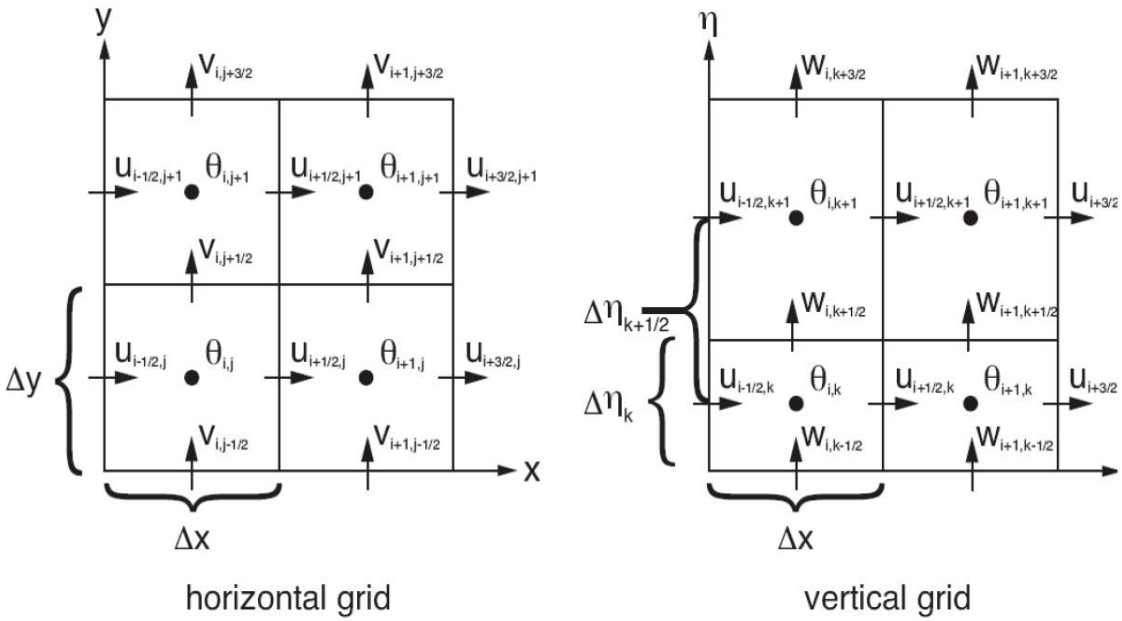

Figure 4.2: Horizontal and vertical grids of the ARW WRF (Skamarock et al. 2008).

The WRF model also has several options for various physics considerations, including microphysics, cumulus, land-surface, PBL physics, and radiation parameterizations. Since the PBL schemes in WRF have the largest impact on the wind speed within the lowest 1km Above Ground Level (A.G.L), a discussion about the purpose of the PBL schemes, as well as details about five main schemes are presented.

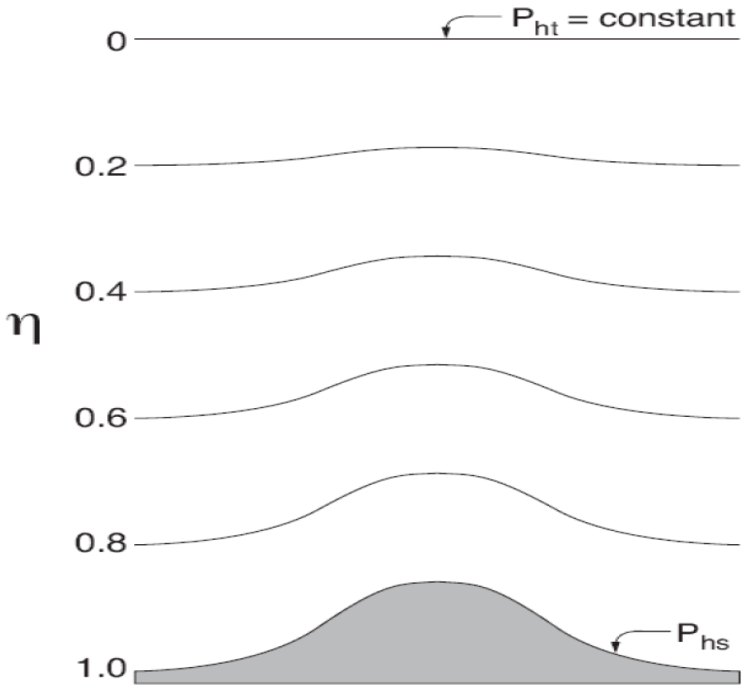

Figure 4.3: WRF η levels (Skamarock et al. 2008).

According to Skamarock et al. (2008), the PBL schemes in WRF represent the vertical subgrid-scale fluxes due to eddy transports in both the boundary layer and the free atmosphere overlying it. How this is represented can vary from scheme to scheme, and is discussed in more detail later in the following subsections. The PBL schemes are responsible for determining the flux profiles within the boundary layer, while the surface fluxes are determined by the surface layer and land-surface schemes (Skamarock et al. 2008). PBL schemes in WRF are one-dimensional and assume a clear scale separation between subgrid eddies and resolved eddies. Once the grid spacing becomes small enough, boundary layer eddies can be resolved (few hundred metres), and the above assumption may not be valid. When using a fine grid, a fully three-dimensional local subgrid turbulence scheme may be more appropriate (Skamarock et al. 2008).

Five main PBL schemes supported in WRF version 3.6 are:

- Yonsei State University (YSU) PBL
- Mellor-Yamada-Janic (MYJ) PBL
- Medium Range Forecast Model (MRF) PBL
- Asymmetrical Convective Model version 2 (ACM2) PBL
- Quasi-Normal Scale Elimination (QNSE) PBL.

These schemes are discussed in detail in the next five subsections.

a. Medium Range Forecast Model (MRF) PBL

The scheme is described by Hong and Pan (1996). This PBL scheme employs a so-called counter-gradient flux for heat and moisture in unstable conditions. It uses enhanced vertical flux coefficients in the PBL, and the PBL height is determined from a critical bulk Richardson number (R_i). It handles vertical diffusion with an implicit local scheme, and it is based on local R_i in the free atmosphere.

b. Yonsei State University (YSU) PBL

The Yonsei State University PBL (Hong et al., 2006) is the next generation of the MRF PBL, also using the counter-gradient terms to represent fluxes due to non-local gradients. This adds to the MRF PBL (Hong and Pan, 1996) an explicit treatment of the entrainment layer at the PBL top. The entrainment is made proportional to the

surface buoyancy flux in line with results from studies with large-eddy models (Noh et al., 2003). The PBL top is defined using a critical bulk Richardson number of zero (compared to 0.5 in the MRF PBL), so is effectively dependent on the buoyancy profile, in which the PBL top is defined at the maximum entrainment layer (compared to the layer at which the diffusivity becomes zero). A smaller magnitude of the counter-gradient mixing in the YSU PBL produces a well-mixed boundary-layer profile, whereas there is a pronounced over-stable structure in the upper part of the mixed layer in the case of the MRF PBL. Details are available in Hong et al. (2006), including the analysis of the interaction between the boundary layer and precipitation physics. In version 3.0, an enhanced stable boundary-layer diffusion algorithm (Hong, 2007) is also devised that allows deeper mixing in windier conditions.

c. Mellor-Yamada-Janjic (MYJ) PBL

This parameterization of turbulence in the PBL and in the free atmosphere (Janjic, 1990, 1996, 2002) represents a non-singular implementation of the Mellor-Yamada Level 2.5 turbulence closure model (Mellor and Yamada, 1982) through the full range of atmospheric turbulent regimes. In this implementation, an upper limit is imposed on the master length scale. This upper limit depends on the TKE as well as the buoyancy and shear of the driving flow. In the unstable range, the functional form of the upper limit is derived from the requirement that the TKE production be non-singular in the case of growing turbulence. In the stable range, the upper limit is derived from the requirement that the ratio of the variance of the vertical velocity deviation and TKE cannot be smaller than that corresponding to the regime of vanishing turbulence. The TKE production/dissipation differential equation is solved iteratively. The empirical constants have been revised as well (Janjic, 1996, 2002).

d. Asymmetrical Convective Model version 2 (ACM2) PBL

The ACM2 (Pleim, 2007) is a combination of the ACM, which is a simple transient model that was originally a modification of the Blackadar convective model, and an eddy diffusion model. Thus, in convective conditions the ACM2 can simulate rapid upward transport in buoyant plumes and local shear induced turbulent diffusion. The partitioning between the local and nonlocal transport components is derived from the fraction of non-local heat flux according to the model of Holtslag and Boville (1993).

The algorithm transitions smoothly from eddy diffusion in stable conditions to the combined local and non-local transport in unstable conditions. The ACM2 is particularly well suited for consistent PBL transport of any atmospheric quantity including both meteorological (u, v, θ, qv) and chemical trace species.

e. Quasi-normal scale elimination (QNSE) PBL

The QNSE PBL scheme employs the diffusivity obtained from the spectral theory to reflect effects of internal wave generation in the presence of turbulence in the stably stratified boundary layer. The vertical scalar mixing is totally suppressed by the stable stratification, whereas vertical momentum mixing continues even at low Froude numbers (*Fr*) (Sukoriansky et al. 2005). The QNSE theory is valid for stable stratification and weakly unstable conditions, while improvement for the unstable case is in progress (Galperin and Sukoriansky 2010).

4.1. 3 Input data

The input data needed for WRF are of two types:

a) Static geographic data from the USGS (United State Geological Survey) stored in a database and downloaded once with WRF: soil altitude, soil type, roughness and other information. There are several possible resolutions, the best is 30" arc.
b) Meteorological data from a global NWP model for the full time period of the WRF simulation (they are used as boundary conditions). The NCEP final analysis data further referred to as NCEP/FNL, is a state-of-the-art data forecasting system which assimilates data from many different sources such as buoys, ships, planes and satellites through the Global Data Assimilation System (GDAS). The data is free for download and covers the world on global grids with a horizontal resolution of 1º, corresponding to ~110km. The actual data is on a 4-times daily (6 hour) basis from the 30th of July, 1999 to the present. The NCEP/FNL has to a great extent been used as the primary input to WRF models in the industry since their release and is currently updated on a daily basis with a lag of 1 hour after the Global Forecast System (GFS) is initialized.

Those global forecasts used as input files are in GRIB format. This is a standard format for meteorological data, in a binary form, defined by the WMO (Dey, 1998).

4.1.4 Model Configuration

The version of WRF used in this study for prediction of winds is version 3.6. WRF model has shown ability to accurately model boundary layer dynamics in complex terrain (Rife et al. 2004, Žagar et al. 2006 and Jimenez et al. 2010). A series of WRF forecasts were conducted during the year 2009 to test WRF wind power modeling accuracy at Lake Turkana wind farm site in Kenya. WRF model was configured with three domains using two-way nesting to attain a horizontal resolution of 2 km over the study area. The three domains were centred over the wind farm site. The horizontal resolution of the outermost domain is 18 km, the intermediate domain is 6 km and the third domain is 2 km (figure 4.4). A WRF configuration of 32 terrain-following hydrostatic pressure levels, with 10 levels in the lowest 200 m, an average spacing of 15 m and with the top most level at 50 hPa was used in the vertical for all three domains.

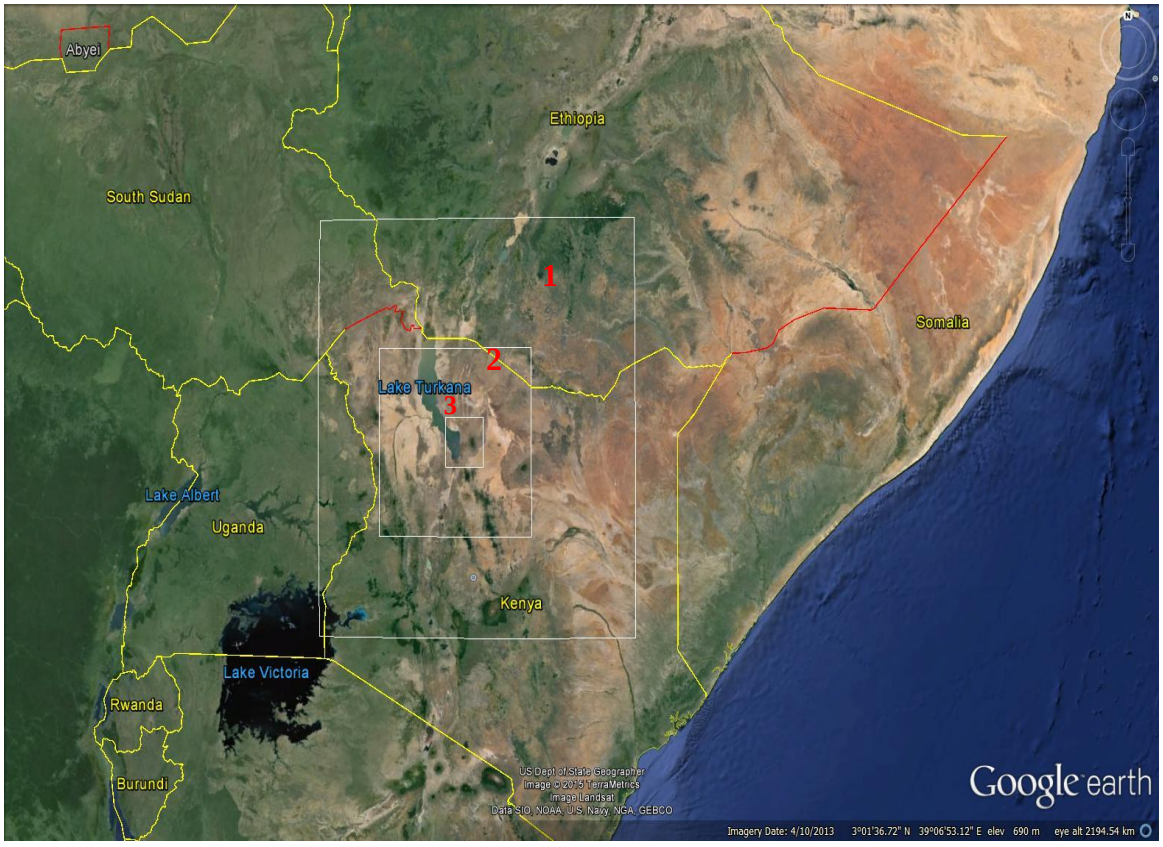

Figure 4.4: WRF simulation domains: three domains two-way nested with 18, 6, and 2 km horizontal resolution.

4.1.5 Validation of WRF simulated winds.

Validation of the WRF model output data was based on 3 sites within the inner grid where actual wind data were available. All three sites: Kalkumpei, Nyiru and Sirima are located in complex terrain. Accurate simulation of wind flow patterns near these sites was expected to be very challenging. Based on the performance of WRF model at these sites, a measure of the confidence of the results and hence of the derived wind maps could be determined. The locations of the validation sites are described in section 3.1.

There are two components to the validation process: the first using wind rose plots to compare the overall wind direction distribution of the modelled and observed data at each site, and the second using a more rigorous statistical analysis of the hourly wind speed data.

4.1.6 Statistical measures

A variety of statistical measures are used for the model evaluation, focusing on wind speed. Six statistical measures listed below were considered to evaluate model performance with respect to wind speed and wind direction. These statistics can be divided into three types: mean statistics, difference statistics, and skill measures.

4.1.6.1 Mean statistics

These statistics provide an overall summary of the model and observed wind data. These statistics are also used in the calculations of other statistical measures:

i. Observed mean
ii. Modelled mean

4.1.6.2 Difference statistics

These statistical measures compare observed hourly data with the corresponding modelled hourly data. The three statistics used in this study are described below.

a) Root Mean Square Error (RMSE)

The RSME can be described as the standard deviation of the difference for hourly prediction and observation pairings at a specific point. Equation below is the formula for computing the RMSE. N is the total number of observed and forecast

values, f represents forecast value while o represents observed value (Reid and Turner 2001, Rife et al. 2004 and Žagar et al. 2006).

$$RMSE = \sqrt{\frac{1}{N}\sum_{i=1}^{N}(f_i - o_i)^2}$$

b) Mean error (ME)

As the name suggests, the mean error is an average of the errors. ME measures the average errors in a set of forecasts, without considering their direction. The formula for calculating ME is given by:

$$ME = \frac{1}{n}\sum F - A$$

Where F represents the forecast value and A represents the observed value

c) Percent Bias (PBIAS)

PBIAS is an average tendency measure of the simulated values to be larger or smaller than their observed ones. The optimal value of PBIAS is 0.0, with low-magnitude values indicating accurate model simulation. Positive values indicate overestimation bias, whereas negative values indicate model underestimation bias. The formula for calculating PBIAS is given by:

PBIAS = 100 * [sum (sim - obs) / sum (obs)]

Where sim represents forecast values and obs represent observed values.

4.1.6.3 Skill measures

Skill measure statistics are given in terms of a score, rather than in absolute terms.

a. Index of Agreement (IOA)

The IOA is calculated using a method described in Willmott (1982). The IOA can take a value between 0 and 1, with 1 indicating perfect agreement. The IOA is the ratio of the total RMSE to the sum of two differences: the difference between each prediction and the observed mean, and the difference between each observation and observed mean.

$$IOA = 1 - \frac{\sum_{i=1}^{N}(P_i - O_i)^2}{\sum_{i=1}^{N}(|P_i - \bar{O}| + |O_i - \bar{O}|)^2}$$

N is the number of observations, P_i are the hourly model predictions, O_i are the hourly observations and $\bar{O}$ is the observation mean.

4.2 Combined mesoscale and microscale modelling

WAsP is the wind energy industry standard model used to assess the mean wind speed and energy output at a specific site or at a high resolution over a wider area. One key requirement for a WAsP analysis is to have a site for which a reliable wind climate is available close to and in a similar environment to the prediction area.

The section below therefore outlines a methodology that was used to evaluate whether prognostic modelling can be used to provide reliable wind climates for sites within an area, which can then be used as input to the diagnostic model WAsP. Limitations of the WAsP model are discussed below, particularly when it is used in complex terrain. The combined mesoscale atmospheric model- WAsP model methodology aims to overcome some of these limitations by providing a source of data over areas of complex terrain that can be used to drive the WAsP model.

4.2.1 WAsP

The WAsP sub-models were first developed by the Risø National Laboratory in 1987, and are commonly used throughout the world in the wind energy industry to get an estimate of available regional wind resources, to site turbines at specific locations, and to estimate wind farm production (Mortensen, 2007). Unlike dynamic models such as WRF, WAsP does not represent the changing state of the atmosphere over time, but is based around the statistical description of the wind field. From this climatological perspective and on small spatial scales, wind variations are affected by surface features such as topographic changes and obstacles. WAsP uses equations to describe these variations of the Earth's surface and their effect on wind speed and direction.

WAsP is based on the physical principles of flows in the boundary layer and attempts to solve the Navier-Stokes momentum equations, estimates the regional wind climate, as well as the wind speed at any specific location and height. This is done by horizontally and vertically extrapolating a record of wind data within the region using steps that take into consideration elevation or topography changes, land use or classification / surface roughness, and local obstacles (Troen and Petersen, 1989).

WAsP has been applied to a wide variety of situations including flat, open terrain (Achberger et al., 2002), offshore locations (Barthelmie et al., 1996), (Lange and Højstrup, 2001), coastal locations (Romeo and Magri, 1994), mountainous terrain (Botta et al., 1992 and Reid, 1997), forested terrain (Suárez et al., 1999), extreme winds (Abild, 1994 and Kristensen et al., 2000) and short-range weather forecasting (Landberg and Mortensen, 1993). Amongst these studies there are huge contrasts in the choice of reference data, both in terms of record length and type e.g. surface observations from anemometers, surface and geostrophic winds from numerical models, upper-level wind data from radiosondes.

Suárez et al., 1999 studied an area of mountainous, forested terrain in western Scotland. Using an anemometer on an exposed ridge as their reference site, they found that WAsP produced an accurate estimate of the mean speed at another nearby hill-top site (7.5 km to the east of southeast). However for two valley locations in the same area the mean speed was underestimated by around 15% and for a site in a saddle and a site on the side of a valley the WAsP overestimates by 15-20%.

Landberg and Mortensen, 1993 compared WAsP and MCP using data from six complex terrain stations in northern Portugal. They demonstrated that WAsP will produce poor results if the reference station and target site are in different climatic zones.

Romeo and Magri, 1994 found that WAsP produced good estimates of the mean speed for a coastal site in southeast Sicily. They used data from a numerical model as the starting point for the analysis.

Barthelmie et al., 1996 found that for offshore locations WAsP tended to over-predict the mean speed. The differences were thought to be due to the incorrect assignment of roughness lengths and stability effects.

Onat and Ersoz, 2011 used five-layer sugeno-type model scripted in MATLAB and WAsP to describe the characteristics of wind climate and energy potential for three regions in Turkey. Their analysis produced detailed wind resource maps and concluded that the regions are well located for the installation of parallel-connected

wind plants to the national network in terms of the reliability of wind and capacity usage rates.

Palaiologou et al., 2011 used GIS and WAsP as basic calculation platforms to test and evaluate measurements from 15 wind turbine sites by creating six alternative scenarios in the island of Lesvos, Greece. They demonstrated that topography plays a critical role in the accuracy of WAsP calculations.

Djamai and Merzouk, 2011 used WAsP to investigate the possibility of setting up a 10 MW wind farm in Adrar, a region located in south Algeria. Lima and Filho, 2012 conducted a wind resource evaluation and wind energy assessment for São João do Cariri in Paraiba state of northeast. They both demonstrated that WAsP program is a robust and reliable tool to make wind characterization and wind energy potential assessment.

4.2.1.1 WAsP Methodology

The method used by WAsP involves the following steps, and is shown in Figure 4.5 below:

1. Analysis of observed wind data into 12 direction sectors, 30° each of which has a Weibull distribution function fitted.
2. Elimination of the effects of terrain, roughness and obstacles on the wind climate data by the application of sub-models (described below).
3. Vertical extrapolation of the 'cleaned' wind data using the logarithmic wind profile model to obtain a regional wind climate (wind atlas) over flat homogeneous terrain for neutral atmospheric conditions. The resulting wind atlas summary is given for a number of roughness criteria and standard levels above the ground.
4. Reverse transformations are then applied to the wind atlas information to account for the terrain, roughness and obstacles surrounding the predicted site. These transformations account for the speed-up (or slow-down) of the airflow when encountering such features. The effects from topographic features are described in Section 2.3, and the effects from surface roughness and obstacles that are more specific to the WAsP model, are given below. The predicted wind climate at each site is given as a Weibull function (to model the wind speed) for each of the twelve wind direction sectors. The

probability of the occurrence of winds falling into each of the direction sectors is also given. For the production of wind maps, the reverse transformations are applied and hence predicted wind climates attained at a specified grid resolution over the map area.

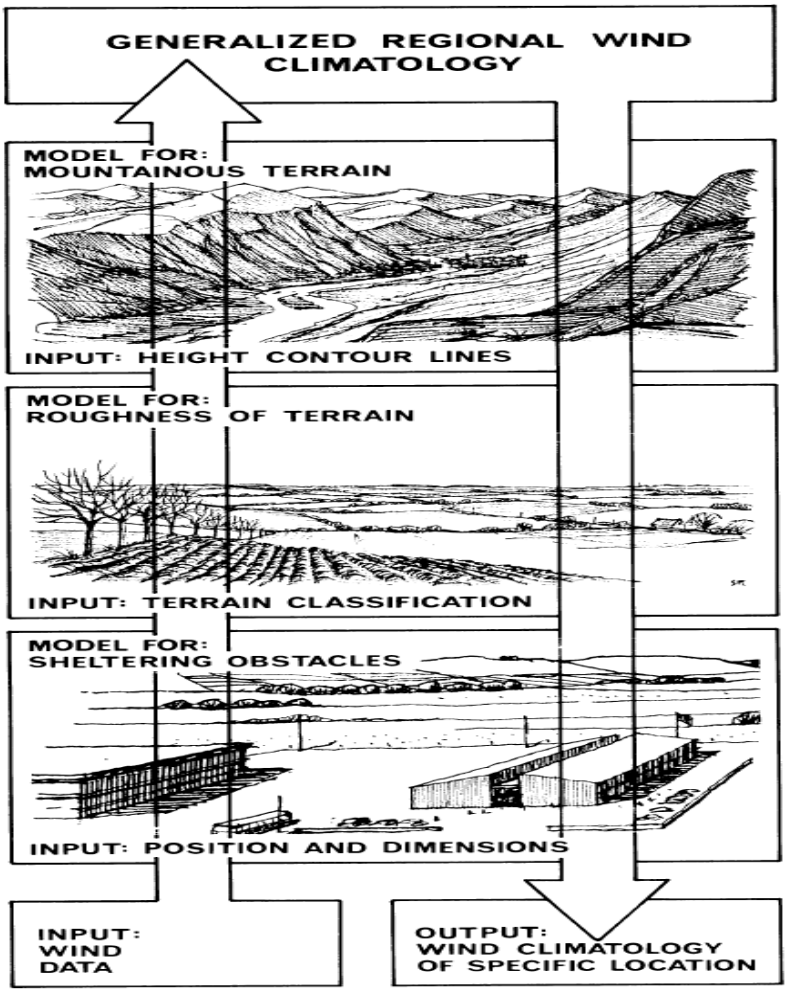

Figure 4.5: The wind atlas method of WAsP. Meteorological models are used to calculate the regional wind climatology from the raw data. In the reverse process – the application of wind atlas data – the wind climate at any specific site may be calculated from the regional climatology (Mortensen, 2007)

4.2.1.2 Description of the sub-models used in WAsP

WAsP is built around three sub-models, incorporating effects of obstacles on airflow in the vicinity of the observation and prediction sites, surface roughness changes within the map area, speed up and turning of the wind due to orographic effects. These sub-models are briefly described below.

4.2.1.2.1 The shelter model

Shelter is defined as the relative decrease in wind caused by an obstacle in the terrain. The shelter model used in WAsP is based on Perera (1981), where shelter by an obstacle at a particular site depends on:

- the distance between the obstacle and site
- the height of the obstacle
- the height of the point of interest at the site
- the length of the obstacle
- The porosity of the obstacle (Landberg, Myllerup et al. 2003)

WAsP considers obstacles as rectangular 'boxes'. Each obstacle is assigned a position relative to the site, its dimensions and porosity. There is a maximum of 50 obstacles that can be specified in one obstacle list.

There is often the problem of whether to classify a feature as an obstacle or roughness element (as described below). The following guidelines are given:

a) If the point of interest (turbine or anemometer) is closer than about 50 obstacle heights to the obstacle and closer than three obstacle heights to the ground, the object should be included as an obstacle.
b) If the point of interest is further away than the above conditions, the object could be included in the roughness description.

There were no obstacles to account for in any of the WAsP analyses completed in this study.

4.2.1.2.2 The roughness change model

The overall effects of the terrain surface and obstacles that lead to resistance to the wind near the ground are referred to as the roughness of the terrain. The roughness change model in WAsP takes into account the influence of changes in roughness near sites of interest. Roughness changes close to sites of interest are generally said to be important for distances up to 10 km (Landberg, Myllerup et al. 2003) However, if there is significant roughness change further away, such as at a coastline, in the direction of a prevailing wind, then the mapped area should be extended to include them, up to 20 km away (Bowen and Mortensen, 1996).

The roughness classifications applied in the WAsP program are made up of 36 azimuth sector divisions from the site (or grid point) of interest, with up to 10 roughness changes permitted in each of these 36 sectors (Landberg, Myllerup et al. 2003) These roughness classifications for each site can be viewed as a roughness rose, but for this study roughness changes are specified in a map file format (see Figure 4.6) that indicate the roughness change boundaries over the area of interest.

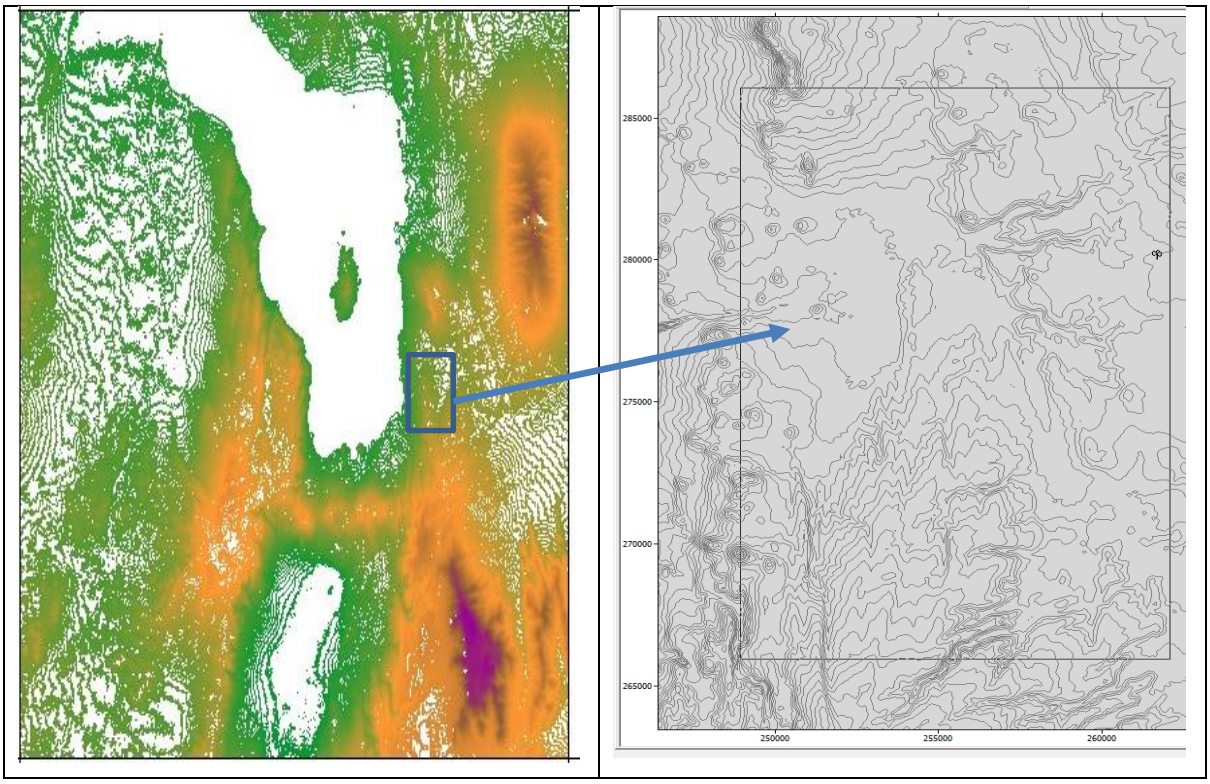

Figure 4.6: Topographical contour map for Lake Turkana region from the SRTM data base, the blue rectangle shows the location of the wind farm (left). The topographical data map for lake Turkana wind farm imported into WAsP, the grey lines represent the elevation contour with 50m intervals (right).

In the wind atlas files generated by WAsP, the roughness criteria are divided into four standard classes. This allows for wind and energy calculations to be done in the same area but for varying land cover characteristics. Roughness class 1 was changed from 0.03 to 0.02 for the file used in this study. The classes and corresponding roughness lengths used in this study are shown in Table 4.1.

Table 4.1: Roughness classes used by WAsP to generate wind atlas files

Roughness class	Roughness length (m)	Terrain description
0	0.0002	Smooth land and water surfaces
1	0.02	Land with shrubs and complex terrain
2	0.1	Less open farmland with trees and buildings
3	0.4	Rough surface with trees and buildings

4.2.1.2.3 The Orographic Model

WAsP utilises the 'BZ-model' to calculate the wind velocity perturbations induced by orographic features such as single hills or more complex terrain. The linear model is limited to neutrally stable airflows over low, smooth hills with attached flows. WAsP simulations in such conditions compare well with measured field data from two benchmark studies at Askervein and Blashval in Scotland (Bowen and Mortensen, 1996). The model was developed specifically for wind energy assessment and has the following features:

- It employs a high resolution, zooming polar grid. This allows for increasing detail in the calculation of flow perturbation profiles close to the sites (or grid points in a wind or energy resource analysis) of interest.
- It incorporates the roughness conditions of the terrain in the vicinity of the sites of interest.
- Its uses a boundary layer thickness of approximately 1000 m to force large-scale airflow around high elevation areas (Landberg, Myllerup et al. 2003)

4.2.1.3 WAsP Inputs

The inputs required to run WAsP are discussed below.

4.2.1.3.1 Wind-climatological inputs

WAsP simulations are based on the observed wind climate (OWC) at the meteorological station site or Meteorological mast location i.e. time-series data of measured wind speeds and directions over one or several years that have been binned into intervals of wind direction (the wind rose) and wind speed (the histograms). Therefore, the quality of the measurement data has direct implications for the

quality of the WAsP simulations of wind climate and annual energy production. Consequently, the wind data must be accurate, representative and reliable.

The wind-climatological input to WAsP is given in the OWC, which contains the wind direction distribution (wind rose) and the sector-wise distributions of mean wind speed (histograms). The observed wind climate file should also contain the wind speed sensor (anemometer) height above ground level in metres and the geographical coordinates of the mast site: latitude and longitude. The latitude is used by WAsP to calculate the Coriolis parameter.

Wind speeds must be given in metres per second [m/s] and wind directions in degrees [˚] clockwise from 0˚ (north) through 360˚. The wind direction indicates the direction from which the wind blows. The observed wind climate is usually given for 12 sectors and the wind speed histograms using 1 m/s wind speed bins.

4.2.1.3.2 Topographical inputs

The topographical inputs to WAsP are given in the vector map, which can contain height contour lines, roughness change lines and lines with no attributes (say the border of the wind farm site). In addition, nearby sheltering obstacles may be specified in a separate obstacle group member and shown on the map.

Map coordinates and elevations must be specified in meters and given in a Cartesian map coordinate system. The map projection and datum should be specified in the Map Editor so that this information is embedded in the map file. All metric coordinates used in the WAsP workspace should of course refer to the same map coordinate system. Obstacle distances and dimensions must likewise be given in metres.

High-resolution gridded (or raster) elevation data exist for many parts of the world, one such data set is the Shuttle Radar Topography Mission (SRTM). The data was collected by a radar system flown on board on the space shuttle Endeavour in February 2000. The objective of this mission was to obtain RADAR data of most of the Earth's land surface to produce high resolution topographic maps. This data is available in TIFF format on USGS website with a resolution of approximately 90 metres by providing the latitude and longitude of the area. The current version of

WAsP cannot employ such data directly, so it is necessary to make a height contour (vector) map from the raster data. One freely available software program that was used to make WAsP vector maps from SRTM data is SAGA GIS.

After importing topographical data map of the region into WAsP, the map on the right of figure 4.6 is produced. It has contour intervals of 50 metres and was used for all different simulations using WAsP. The high density of grey lines indicates a complex terrain with step elevation changes.

4.2.1.3.3 Wind farm inputs

The wind farm inputs to WAsP consist of the layout of the wind farm (turbine site coordinates) and the characteristics of the wind turbine generator(s): hub height, rotor diameter and the site-specific power and thrust curve.

4.2.1.3.4 Wind turbine generator

It is important to use site-specific wind turbine generator data (i.e. power and thrust coefficient curves) when calculating the AEP of the wind farm. These may be chosen by selecting the right performance table in the wind turbine generator window in WAsP, where the tables correspond to specific values of air density and/or noise level. Vestas V52-850kW turbines are equipped with microprocessors which control the pitching of the blades, thus ensuring continuous adjustment to maintain optimal blade angles in relation to the prevailing wind. The power curve used by WAsP for these turbines in its simulations can be seen in Figure 2.4. These numbers are provided by Vestas.

4.2.2 WAsP in complex terrain

The WAsP program generalises a long-term wind data time series at a reference site, which is stored as a wind atlas file and then used to predict the wind climate at other sites. Accurate simulations using WAsP can be obtained if the reference and predicted sites meet the following criteria:

- They are subject to the same weather regime.
- The prevailing weather conditions are close to being neutrally stable.
- The surrounding terrain is sufficiently gentle and smooth to ensure mostly attached flows, and with minimal large-scale terrain effects, such as channelling.

The prediction accuracy also depends on the reliability of the reference site wind data, the methods used to do preliminary data processing and the correct use of the WAsP program (Bowen and Mortensen, 1996). Areas of wind energy potential assessment are not always going to fit the above criteria. Lake Turkana wind farm area lies within a region with complex terrain.

4.2.2.1 Factors affecting the prediction process

The analysis and application procedures in WAsP can be considered as a transfer function model linking the winds from a reference site to a predicted site (Bowen and Mortensen, 2004). WAsP assumes that there are different and unique speed-up ratios between the two sites for each direction sector. These speed-up ratios are dependent on surface roughness and the orography surrounding the sites, and are independent of the wind speed and climatic conditions that are assumed to be neutrally stable. For a well-behaved transfer function model, a high cross-correlation of the wind conditions must exist between the reference site and predicted site (Bowen and Mortensen, 2004).

Bowen and Mortensen (2004) stated that there are a number of factors that can contribute to the overall errors made in a WAsP prediction process. These were separated into the following four categories and are explained in more detail below: Atmospheric conditions, Orography, Weibull fit error and Wind speed records. Only orography was considered to affect WAsP prediction process in this study due to the topography of the study area. Ruggedness index (RIX) was used to determine the turbine locations likely to be affected by topography during the prediction process.

4.2.2.1.1 Atmospheric conditions

The atmospheric conditions that affect WASP prediction occur due to location of predicted and predictor site being at different regional wind climate. The existence of two sites in one climatic condition can be shown using Correlation coefficient. However, prediction errors can still occur even when the sites are found under the same regional wind condition due to non-standard atmospheric conditions such as atmospheric stability and stratification (Niels G. Mortensen et al., 1996).

The individual effect that each of the climate phenomena have on WAsP simulations is complex and requires further investigation (Bowen and Mortensen, 2004). Bowen

and Mortensen (2004) proposed that WAsP errors were likely to be slightly higher if the predicted site was in an unstable and hilly environment and much less if the predicted site was in a stable environment. This is likely to be because the orographic model used in WAsP assumes a neutrally stable atmosphere.

4.2.2.1.2 Weibull fit error and wind direction

Prediction error can occur while forcing the observed data to fit into the Weibull frequency distribution. The directional differences can occur when the incidence flow is changed due to oblique steep ridges.

4.2.2.1.3 Wind speed records

WASP assumes that the two sites (predictor and predicted) are fully correlated. However, if the averaging time is very small this is not always true unless the sites are very close to each other. The measurement time is another factor seen to have effect on the prediction error.

4.2.2.2 WAsP errors

It has been shown that the size of WAsP errors in the analysis and prediction processes are predominately a function of the degree that the operational limits are violated by factors associated with atmospheric conditions and terrain (Bowen and Mortensen, 2004). Overall, the errors can be defined as the analysis error E1, when creating a wind atlas from the reference site, and the application error E2, when creating a wind climate for the predicted site. The overall prediction error of the wind climate is determined by the difference in the two procedure errors (E2–E1).

The orographic component uses a linear model that is limited to neutrally stable airflow over low smooth hills. It is suggested that the critical slope for flow separation to occur is above 0.3 (Wood, 1995). Bowen and Mortensen, 1996 proposed an orographic performance indicator, which attempts to quantify the extent to which the terrain at a particular site exceeds the limits of the orographic model. The resulting ruggedness index (RIX) is a fraction of the surrounding terrain that exceeds a slope of 0.3. The index is calculated for each of the 12 sectors and the overall RIX is the mean RIX for all of the sectors.

4.2.2.3 Using the ruggedness index (RIX) to assess potential WAsP errors

The ruggedness index (RIX) is described in detail in Bowen and Mortensen (1996), Mortensen and Petersen (1997) and Bowen and Mortensen (2004). The following conclusions regarding RIX can be made:

- If the RIX is close to zero, then the terrain is generally less steep than 0.3 and the airflow in the region is likely to be attached.
- If the RIX is greater than zero, then parts of the terrain are steeper than 0.3 and flow separation may occur in some sectors.

Therefore, large RIX values (>5%) can lead to significant errors in the modelling of the airflow.

The sign and magnitude of the prediction error (E2-E1) due to orography was found to be proportional to the difference in the ruggedness of the observed and predicted sites (Bowen and Mortensen, 1996). However, in complex terrain the errors in the analysis and application procedures can effectively cancel each other out, resulting in an accurate prediction. Therefore, if the terrain does differ between sites, an indication of either under-prediction and over-prediction of mean wind speeds can be made based on the difference of the RIX values at each site.

Bowen and Mortensen(1996) therefore proposed that the overall accuracy of WAsP predictions depends on the terrain characteristics near both the reference and predicted sites, and can be summarized as below:

a) If the observed and predicted sites have similar RIX values, then modelling errors are significant but tend to cancel each other out. Both sites should have similar orientation and orography, and also experience similar wind climatic conditions.
b) If the observed site is less rugged than the predicted site, then modelling errors are significant and unequal. The overall prediction will be overestimated.
c) If the observed site is more rugged than the predicted site, then modelling errors are significant and unequal. The overall prediction will be underestimated.

Error indication maps are given using RIX values in the results section. By calculating the difference between the RIX value at reference and predicted site, a

quantitative indication of prediction errors can also be made. In their study, Bowen and Mortensen, 2004 showed that if the difference in RIX values was within about 5%, the wind speed error should be less than 5%. If the absolute difference in RIX values between the sites is 10%, then the wind speed error could potentially be in excess of 30%.

4.2.2.4 WAsP Limitations

Due to some of the simplifications made in the numerical models used within WAsP, the program can produce somewhat inaccurate results when used outside its recommended operational envelope (Bowen and Mortensen, 2004). When a site has complex, rugged terrain or very complex atmospheric conditions, the accuracy of WAsP can be unreliable (Wagner et al., 2009). WAsP analyzes the orography and the site RIX of the entire grid layout. The associated performance indicator (ΔRIX) can identify problematic sites within a project. RIX is defined as the fractional extent of the surrounding terrain which is steeper than a critical slope, which is within the operational envelope of the WAsP flow model (Bowen and Mortensen, 2006). ΔRIX is defined as the difference in the (percentage) fractions between the predicted and reference sites (Bowen and Mortensen, 2004).

This problem can be solved by using several reference sites and cross-referencing sites where wind observations are available. There is also the option for some user corrections at problematic sites which can significantly improve the accuracy of the model in complex terrain (Wagner et al., 2009).

More recently the wind energy industry has been trying to implement the use of Computational Fluid Dynamics (CFD) models. These models develop a steady-state, time-independent solution for the wind and turbulence field (Berge et al., 2006). They solve the mass and momentum conservation of the Navier-Stokes equations (Beaucage et al., 2012). This is a physically more accurate modeling of the flow field when compared to WAsP.

There have been several studies where WAsP has been compared to CFD-models in complex terrains. These studies show that using CFD-models offers an improvement in some cases but not for all (Periera and Guedes, 2010) (VanLuvanee et al., 2009) (Sumner et al., 2010). These CFD-models are very complicated and require

significant computer power, it can take super computers several hours to complete the required calculations (Corbett et al., 2007).

4.2.2.5 Specific aims for combining mesoscale and microscale modelling

It has been highlighted in previous sections that there are many factors that influence WAsP simulations. The effects from topography and atmospheric conditions are considered to be the most significant. Deviations from neutral stability, the forcing of wind speed data to fit the Weibull function, and winds falling in different direction sectors in the analysis and application procedures of WAsP, are all limitations of the mathematical sub-models and were not addressed directly in this study.

Considering the limitations that have been highlighted above, and the overall goals of this research, the methodology described below addressed the following three issues:

i) Using wind data from WRF model to generate a wind climate for WAsP in situations where there is no actual reliable wind data available.

ii) Using WRF model wind data to reduce potential errors that can result when using WAsP if the reference and predicted sites are located in different wind climate areas and/or topography.

iii) Considering the relationship between the 'ruggedness' of sites and the size of the modelling errors, to assess the reliability of WAsP simulations in a complex terrain environment.

4.2.2.6 Combined Mesoscale- Microscale modelling methodology

Wind data from other sources are often used when wind energy assessments are made at sites where there are no actual wind data. The observed and predicted sites shouldn't be in different wind climate and/or topographic environment to avoid significant errors in simulations. The analysis procedure of the WAsP program was used to generate a wind atlas file based on wind observations from 3 meteorological mast locations and their equivalent retrievals from WRF. First, the observed data at the 3 masts were analyzed to generate observed wind climate. Observed wind climate represents as closely as possible the long-term wind climate at anemometer height at the position of the meteorological mast. The observed wind climate was then combined with terrain data described in section 4.2.1.3.2 to generate local wind atlas.

Second, the extracted WRF wind data was analyzed to produce simulated wind climate which was then combined with terrain data described in section 4.2.1.3.2 to generate the local wind atlas.

The resulting wind atlas maps from second procedures above were then compared with the atlas map from the first procedure. This comparison was done to give an idea of how well the combined modelling technique performs relative to techniques currently used within the wind industry.

4.2.2.7 Wind atlas assessment methodology

The 3 wind atlas maps generated from each of the two procedures described in section 4.2.2.6 were compared against each other. Maps for Lake Turkana wind farm were also used to illustrate the spatial differences of mean wind speed and AEP when using the two sources of wind data in the analysis. These maps were generated using wind atlas files based on winds from the 3 mast locations and their equivalent WRF retrievals. The maps are based on 45 m above ground mean wind speed and AEP calculations at 100 m resolution. AEP calculations were based on a Vestas V52 turbine.

These maps were validated using LIDAR data described in section 3.5. Using the LIDAR data, 1139 virtual masts were designed within Lake Turkana wind farm. These virtual masts were then used to validate WAsP modelled data. This was achieved by calculating ME, RMSE and IOA. The formulas for ME, RMSE and IOA are given in section 4.1.5.

4.2.3 Methodology Summary

Methodologies for the mesoscale and microscale modelling were introduced first in this chapter. The validation for the Weather Research and Forecast model was more comprehensive, using hourly wind data from 3 sites over Lake Turkana region. The combined mesoscale and microscale modelling methodology involved using both WRF and WAsP models to predict wind and energy in areas where there are no reliable wind data. Limitations of the WAsP model were discussed in detail in this chapter. Recognising and understanding the model limitations is important to help overcome and be aware of when errors are likely to occur. The next chapter presents and discusses the results obtained from the methodologies presented in this chapter.

5. CHAPTER 5

This chapter presents and discusses the results obtained using the methods described in Chapter four to achieve the objectives outlined in Section 1.2.

5.1 WRF model

Hindcast model simulations using the Advanced Research WRF Version 3.6 were generated for 2009 calendar year with the following specifications: The setup consists of a main grid (with horizontal resolution of 18 km) and 2 nested domains (with 6 km and 2 km grids respectively). The wind farm is located within the innermost domain (Fig. 4.4).

The model was run with five different PBL schemes, as indicated in Table 5.1: Asymmetric Convective Model version 2 (Pleim, 2007), Medium Range Forecast Model (Troen and Mahrt, 1986), Mellor-Yamada-Janjic (Mellor and Yamada, 1982), Yonsei State University Scheme (Hong et al., 2006) and the Quasi-Normal Scale Elimination (Sukoriansky et al., 2006). Land surface model and the surface layer physics presented in table 5.1 and recommended by (Wang et al., 2012) were used. Simulation 1 used WRF Single-Moment microphysics. All other parameterizations remain the same for the 6 simulations.

The model was initialized and forced at the boundaries by 1° NCEP/FNL data using 2-way nesting and 32 vertical levels, with 8 levels within the lowest 500 m. The model physics options include: Thompson graupel scheme except for simulation 1, Kain-Fritsch cumulus parameterization, 6th order numerical diffusion, and positive definite advection of moisture and scalars. No data assimilation or grid nudging was used in the simulations.

Table 5.1: Description of the six simulations: PBL parameterizations, associated land surface models and surface layer physics schemes, as recommended in Wang et al. (2012)

Simulation	**PBL Physics**	**Surface Layer Physics**	**Land Surface Physics**
1	Yonsei State University scheme	MM5 similarity (with WRF Single-Moment microphysics)	Noah Land Surface Model
2	ACM2 PBL scheme	Pleim-Xiu surface layer	Pleim-Xiu Land Surface Model
3	MRF PBL scheme	MM5 similarity	Noah Land Surface Model
4	Mellor-Yamada-Janjic scheme	Eta similarity	Noah Land Surface Model
5	Quasi-Normal Scale Elimination PBL	QNSE (Quasi-Normal Scale Elimination)	Noah Land Surface Model
6	Yonsei State University scheme	MM5 similarity – (with New Thompson microphysics)	Noah Land Surface Model

5.1.1 Post-processing the WRF output files

NCAR Command Language (NCL) and Integrated Data Viewer (IDV) were used to extract the desired data from the netCDF WRF output files. NCL is an interpreted language with built-in functions that enables the user to write scripts which execute a series of actions while IDV has a graphical user interface that allows the user to key in latitude, longitude and altitude and extract time series wind speed data. Scripts written in R (appendix 1) were used to compute the various statistical results presented in this study.

5.1.2 Observations

The WRF model simulations were validated against measurements from three meteorological masts described in section 3.3 and situated within the inner most domain (Figure 5.1).

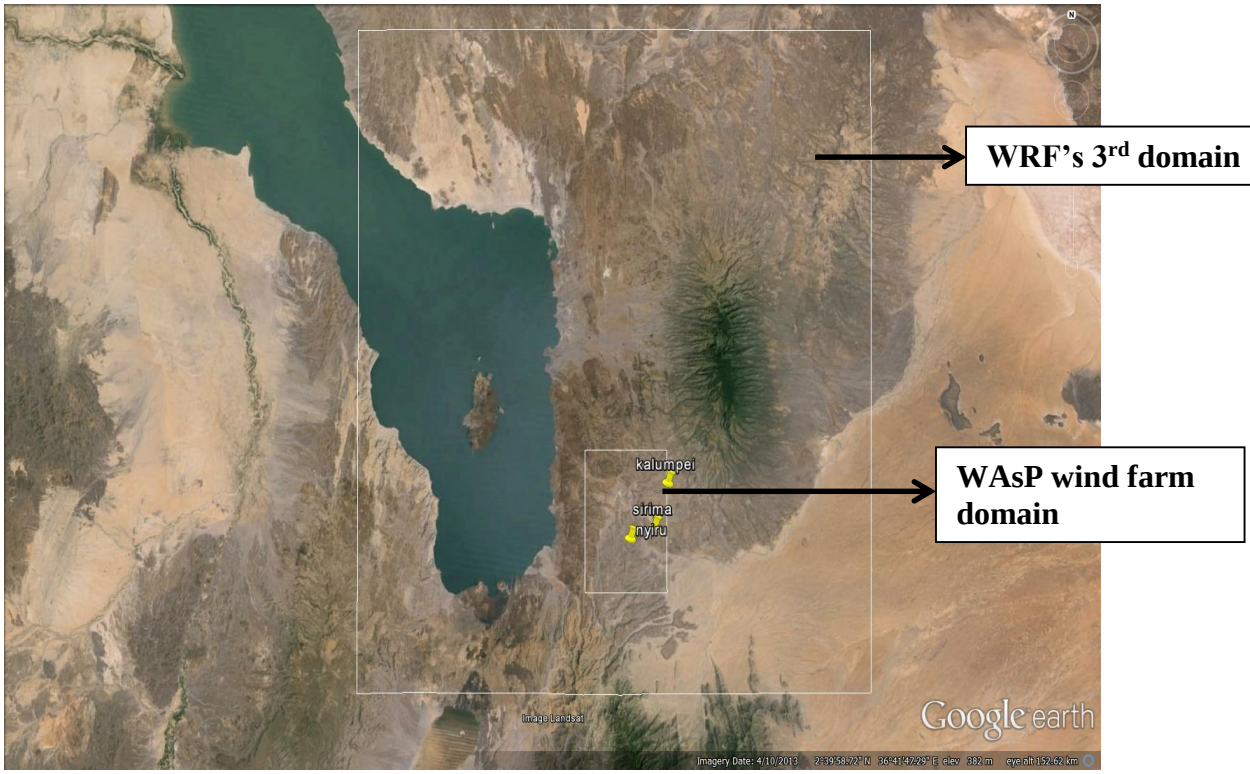

Figure 5.1: Location of WAsP wind farm domain and the 3 masts within WRF's 3rd domain.

5.1.3 Validation of WRF Modelled data

Wind rose plots and a comparative statistics are used to evaluate the performance of WRF model. WRF hindcast wind speed was validated against observations at Kalkumpei (38.5 m), Nyiru (46 m) and Sirima (38 m). This section is divided into 2 sections: Annual and monthly statistics. The validation analysis is the process through which the modeled datasets are compared against actual recorded datasets. The similarity between modeled and observed datasets was determined through statistical validation. Statistics such as mean, mean error, percent bias, root mean square error and index of agreement helped us to determine that similarity. Annual wind rose plots are given for the three validation sites for the 6 WRF simulations in Figures 5.2, 5.3 and 5.4.

5.1.4 Annual statistics

Presented in table 5.2 are error statistics between WRF forecast sets and the observations at Kalkumpei, Nyiru and Sirima for 2009. The smallest Mean Error (ME), Root Mean Square Error (RMSE), percent bias error (Pbias) per station and the largest Index of Agreement (IOA) are highlighted in bold.

Table 5.2: Error statistics between WRF forecast sets and the observations at Kalkumpei, Nyiru and Sirima for 2009.

Mean wind speed

	Observed (m/s)	Sim1 (m/s)	Sim2 (m/s)	Sim3 (m/s)	Sim4 (m/s)	Sim5 (m/s)	Sim6 (m/s)
Kalkumpei	10.44	10.48	8.38	10.33	11.56	11.36	10.45
Nyiru	10.75	10.59	8.58	10.59	11.57	11.34	10.58
Sirima	11.10	9.61	7.69	9.61	10.54	10.30	9.56

Kalkumpei

Simulation	MAST/WRF			
	ME (m/s)	RMSE	Pbias	IOA
1	-0.03	**2.30**	-0.3	0.65
2	2.06	3.13	24.6	0.52
3	0.11	2.49	1.1	0.61
4	-1.11	2.56	-9.7	0.65
5	-0.92	2.68	-8.1	0.59
6	**-0.01**	2.31	**-0.1**	**0.66**

Nyiru

Simulation	MAST/WRF			
	ME (m/s)	RMSE	Pbias	IOA
1	**0.15**	2.47	**1.5**	0.60
2	2.16	3.26	25.2	0.49
3	0.15	2.57	1.5	0.58
4	-0.82	2.65	-7.1	0.60
5	-0.59	2.82	-5.2	0.55
6	0.16	**2.46**	1.6	**0.61**

Sirima

Simulation	MAST/WRF			
	ME (m/s)	RMSE	Pbias	IOA
1	1.48	2.82	15.5	0.56
2	3.40	4.21	44.3	0.43
3	1.49	3.00	15.5	0.54
4	**0.56**	**2.52**	**5.3**	**0.61**
5	0.80	2.90	-7.8	0.55
6	1.54	2.85	16.1	0.56

5.1.4.1 Kalkumpei

The observed wind rose shows a dominant wind direction from the southeast and a secondary peak from the east (figure 5.2). The modelled wind roses show a similar distribution, with the dominant wind direction from the southeast, however they fail to capture the secondary peak from the east. Simulation 6 data predicted the closest mean with a difference of 0.01 m/s and percent bias of -0.1 followed by simulation 1 with a difference of 0.03 m/s and percent bias of -0.3. Both simulation 1 and 6 used Yonsei State University PBL scheme.

5.1.4.2 Nyiru

The observed wind rose shows a dominant wind direction from the southeast and secondary peak from the east and south-southeast (figure 5.3). The modelled wind roses show a similar distribution, with the dominant wind direction from the southeast, simulation 3 almost correctly captures the secondary peak from the south-southeast. Simulation 1 data predicted the closest mean with a difference of 0.15 m/s followed by simulation 6 with a difference of 0.16 m/s. both simulation 1 and 6 used Yonsei State University PBL scheme.

5.1.4.3 Sirima

The observed wind rose shows two dominant wind direction from the east and southeast (figure 5.4). On the contrary, the modelled wind roses show a distinct dominant wind direction from the southeast only. This could be partly be attributed the erroneous wind direction at this site discussed in section 3.2. Simulation 4 data predicted the closest mean with a difference of 0.56 m/s followed by simulation 5 with a difference of 0.80 m/s. Simulation 4 used Mellor-Yamada-Janjic PBL scheme

while simulation 5 used Quasi-Normal Scale Elimination PBL scheme. 0.56 m/s was a relatively large difference compared to 0.01 m/s and 0.16 m/s at Kalkumpei and Nyiru respectively. Possible explanations for the poor model performance at Sirima can be linked to the mast location. At the Sirima meteorological mast was atop a very exposed ridgeline that can be subject to sporadic wind gusts and rapidly changing wind directions are difficult to model.

5.1.4.4 Discussion

Boundary layer winds simulated by the WRF model using six different PBL schemes have been evaluated against observations at three locations in Lake Turkana with a focus on the representation of the wind characteristics under different atmospheric conditions. Table 5.2 shows that the modelled mean wind speeds are lower than the actual mean wind speeds at Sirima. On the other hand the modelled wind speeds are higher than the actual mean wind speeds at Kalkumpei for simulations that use Yonsei State University PBL scheme (with WRF Single-Moment microphysics), Mellor-Yamada-Janjic PBL scheme, Quasi-Normal Scale Elimination PBL scheme and Yonsei State University PBL scheme (with New Thompson microphysics). However, simulations that use Asymmetric Convective Model PBL scheme and MRF PBL scheme under-predicts wind speeds.

For Nyiru, the modelled wind speeds are higher than the actual mean wind speeds for simulations that use Mellor-Yamada-Janjic PBL scheme and Quasi-Normal Scale Elimination PBL scheme while simulations that use Yonsei State University PBL scheme (with WRF Single-Moment microphysics), Asymmetric Convective Model PBL scheme, MRF PBL scheme and Yonsei State University PBL scheme (with New Thompson microphysics) under-predicts wind speeds. All modeled data under - predicted the annual average wind speed at Sirima.

The overall lowest bias (0.01 m/s) was that which used Yonsei State University PBL scheme at Kalkumpei while the highest bias is that which uses the Asymmetric Convective Model PBL scheme (3.40 m/s) at Sirima. The wind speeds simulated by the various PBL simulations except Asymmetric Convective Model PBL scheme are within 1 m/s of the observations at Kalkumpei and Nyiru stations. The Asymmetric Convective Model PBL scheme has the biggest mean errors and underestimates wind speeds at all three locations. Yonsei State University PBL scheme has small mean

errors at both Kalkumpei and Nyiru mast locations. It underestimates wind speeds at Nyiru while overestimating at Kalkumpei. Mellor-Yamada-Janjic PBL scheme performs well at Sirima mast compared to the other four options.

The best RMSE values for Kalkumpei, Nyiru and Sirima are 2.30 m/s, 2.46 m/s and 2.52 m/s respectively. Based on these RMSE values, it can be deduced that WRF model performed well in predicting winds at Lake Turkana wind farm site. Similar results have been reported by Emery et al., 2001 who suggested that a benchmark for RMSE was less than or equal to 2 m/s. However, in complex terrain, like the current site, this value could easily be contaminated by a relatively small number of larger errors. In a validation study of TAPM (Hurley et al., 2002) in complex terrain at Cape Grim on the southwest corner of Tasmania, RMSE values of wind speed and the wind components were averaged to be 3.1 m/s. It was concluded that the model had performed well in predicting the observed meteorology at this site.

Overall, the IOA scores in table 5.2 are good with 0.66, 0.61 and 0.61 for Kalkumpei, Nyiru and Sirima respectively. These simulations used Yonsei State University PBL scheme (with New Thompson microphysics) at Kalkumpei and Nyiru and Mellor-Yamada-Janjic PBL scheme at Sirima. (Emery et al., 2001) suggests that IOA scores above 0.6 indicate good model performance.

WRF-modelled wind speeds were similar to those observed, with accurate wind direction simulation. Taking into account all the metrics in Table 5.2 and the discussion on Sirima presented in section 5.1.4.3, the best performing PBL scheme for Lake Turkana wind farm region was the Yonsei State University scheme. In summation, WRF performance using this PBL scheme was good for the near-surface wind field simulation at Lake Turkana wind farm domain.

Kalkumpei

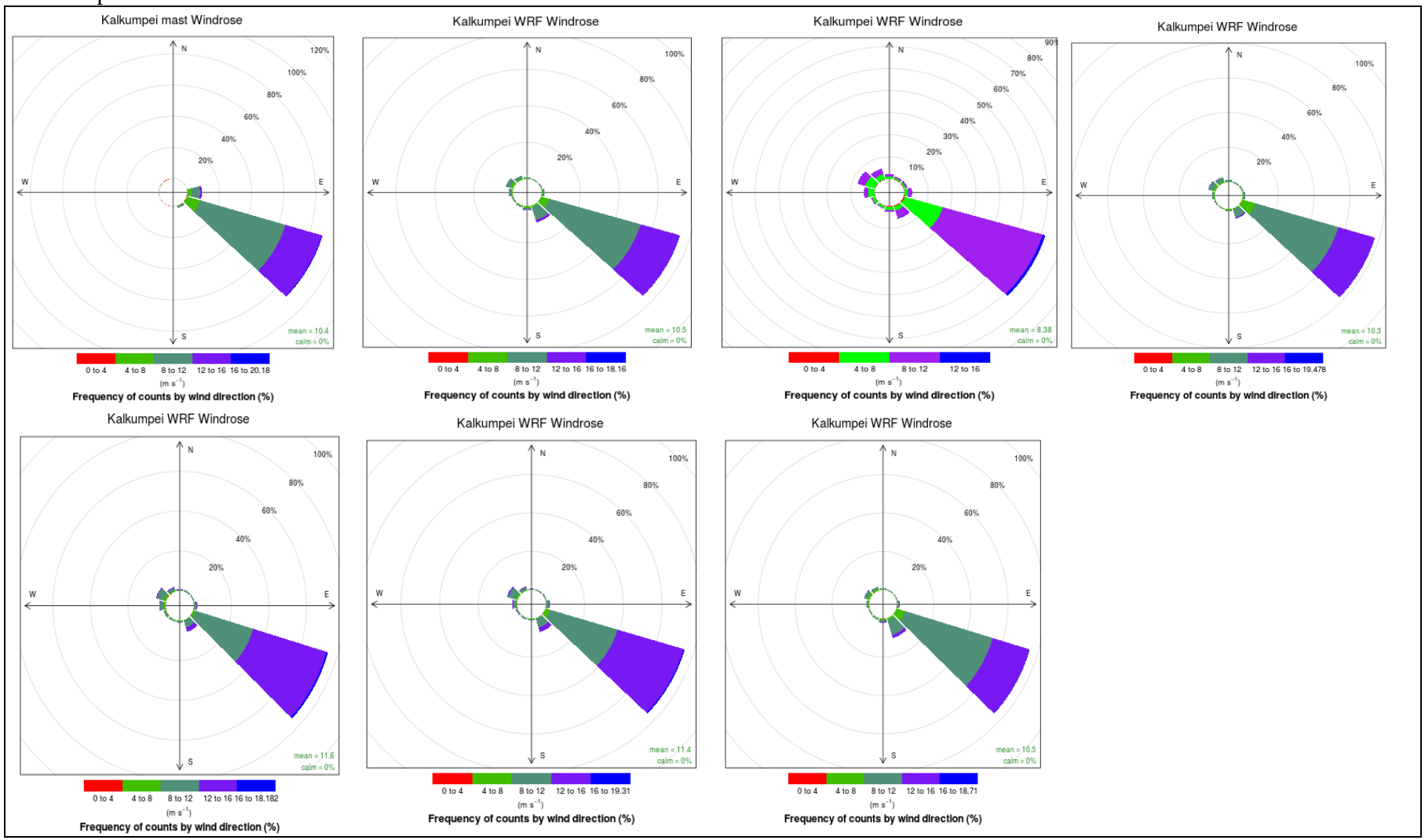

Figure 5.2: Annual Windroses for observed and modelled data (from left to right: observed then simulation 1 to 6) at Kalkumpei for 2009.

Nyiru

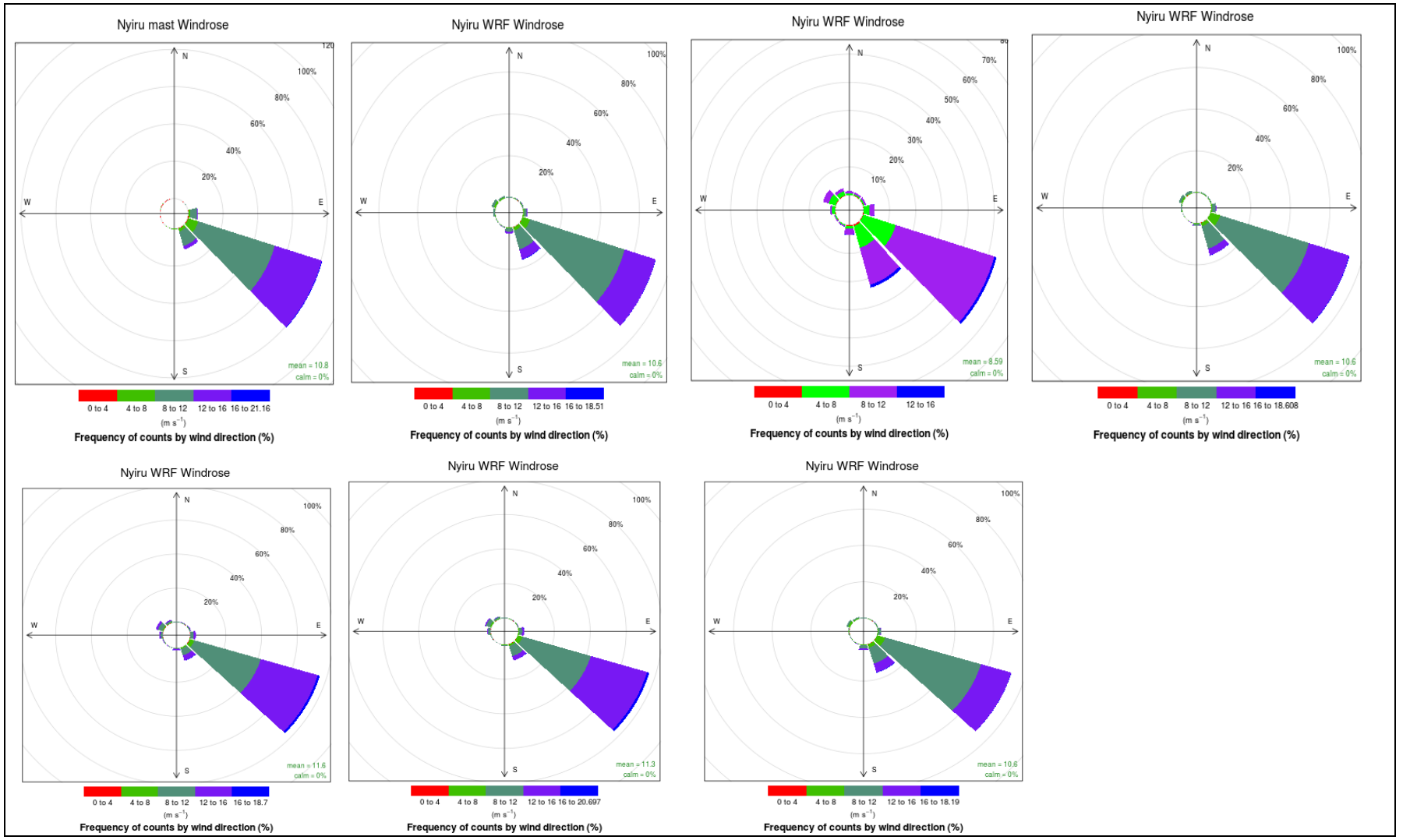

Figure 5.3: Annual Windroses for observed and modelled data (from left to right: observed then simulation 1 to 6) at Nyiru for 2009.

Sirima

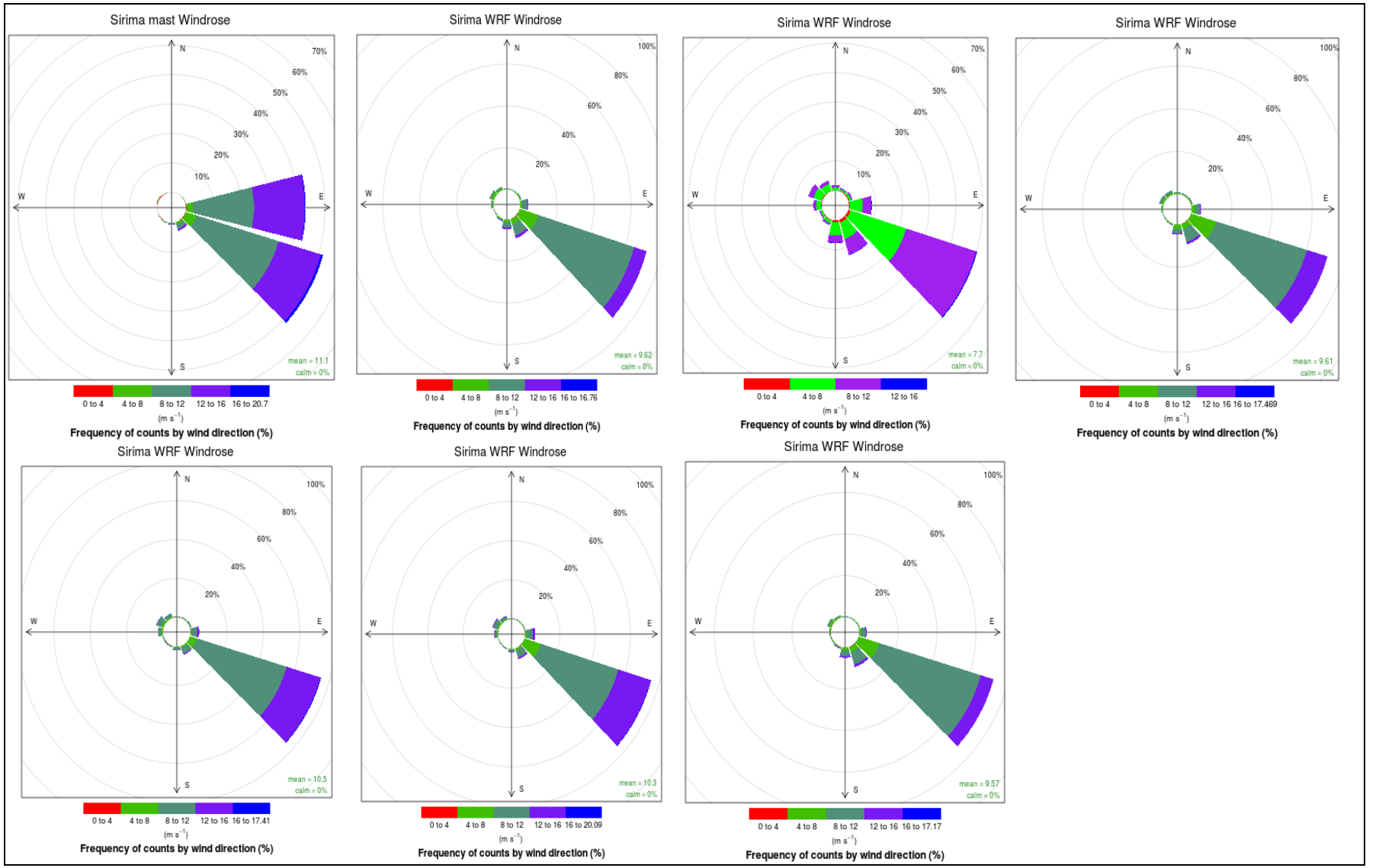

Figure 5.4: Annual Windroses for observed and modelled data (from left to right: observed then simulation 1 to 6) at Sirima for 2009.

5.1.5 Seasonal and Monthly statistics

The seasonal variation of mean wind speeds over the three mast locations is discussed in this section, focusing particularly on the temporal variation both monthly and seasonally for the four northern hemisphere seasons of 2009.

The statistics provide some interesting features in the mean wind speed pattern for different times of the year. It is clear from figures 5.5, 5.10 and 5.15 that the start of winter has the lowest mean wind speeds for all three locations. The wind speeds then increase gradually till the end of winter. Wind speeds then decline gradually throughout spring and start to increase again at the start of summer season. The summer season has the strongest winds in this region.

The final month for spring and autumn records the lowest wind speeds for the respective seasons. August has the strongest winds at the three locations. The winds decline gradually during autumn. The wind speeds increase gradually during winter and summer months and decrease gradually during spring and autumn months. All simulations capture the winter peak, spring minimum and summer peak but the summer peak extends into October. All the six simulations predict that October has the strongest winds at the three locations. Simulations 1 to 5 predict May has the lowest wind speeds. Simulation 6 predicts lowest wind speeds for Nyiru only. Figure 1.3 illustrates a simplified model showing cross-equatorial monsoon flow diverting into the Turkana channel. This flow is responsible for higher wind speed during both summer and winter seasons.

5.1.5.1 Kalkumpei

Simulations that best simulate the observed wind speed are considered in this section and reference will be made on figures 5.5, 5.6, 5.7, 5.8 and 5.9. Simulation 6 has the lowest or second lowest mean error for 10 of 12 months. Simulation 5 performs well in predicting wind speeds for July and August with a mean error of 0.43 m/s with a percent bias of -3.6 and -3.5 respectively. This indicates that Yonsei State University PBL scheme does a good job in predicting wind speed for this station for all months except July and August during which Quasi-Normal Scale Elimination PBL scheme does a better job. November has the least mean error of 0.01 m/s. October has the highest mean error of 0.82 m/s with a percent bias of 8.7 as the model erroneously predicts this to be the windiest months of the year.

Summer months have the lowest root mean square errors of 1.9, 1.48 and 1.58 for June, July and August respectively. October has the highest root mean square error of 2.79 m/s. Mellor-Yamada-Janjic and Yonsei State University are the best PBL schemes for predicting wind speed at Kalkumpei during the summer months. Based on RMSE, Yonsei State University PBL scheme does a good job in predicting wind speed for this station for all months except July and August during which Mellor-Yamada-Janjic PBL scheme does a better job.

Summer months have the highest index of agreement of 0.74, 0.8 and 0.74 for June, July and August respectively. October has the lowest index of agreement of 0.37 and it's the only instance below 0.5. Mellor-Yamada-Janjic and Yonsei State University are the best PBL schemes for predicting wind speed at Kalkumpei during the summer months. Based on the four statistical measures, Yonsei State University PBL scheme does a good job in predicting wind speed for this station for all months except July and August during which Mellor-Yamada-Janjic PBL scheme does a better job.

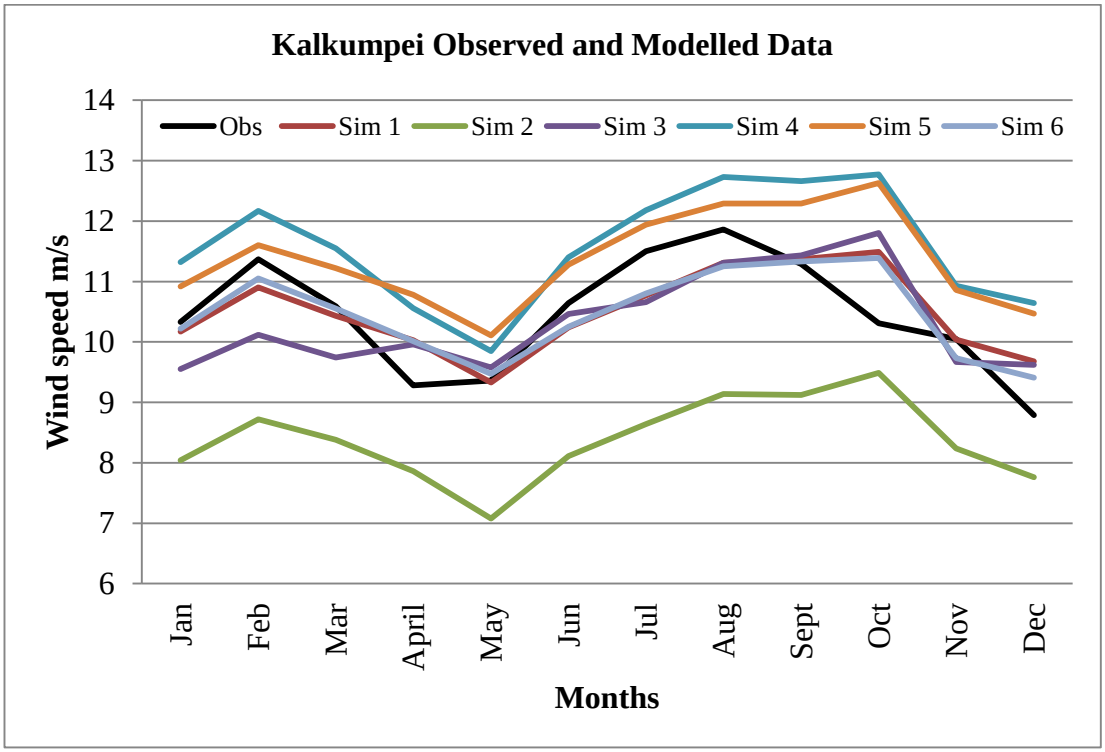

Figure 5.5: Mean measured and modeled data at Kalkumpei for 2009.

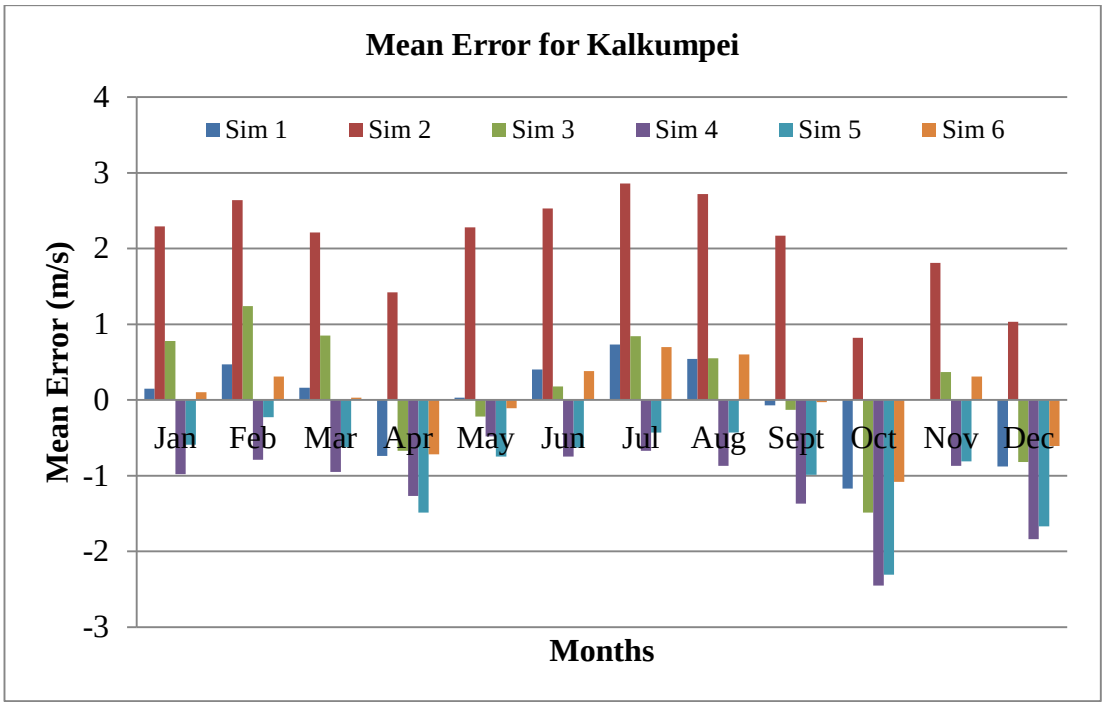

Figure 5.6: Monthly mean error at Kalkumpei for 2009.

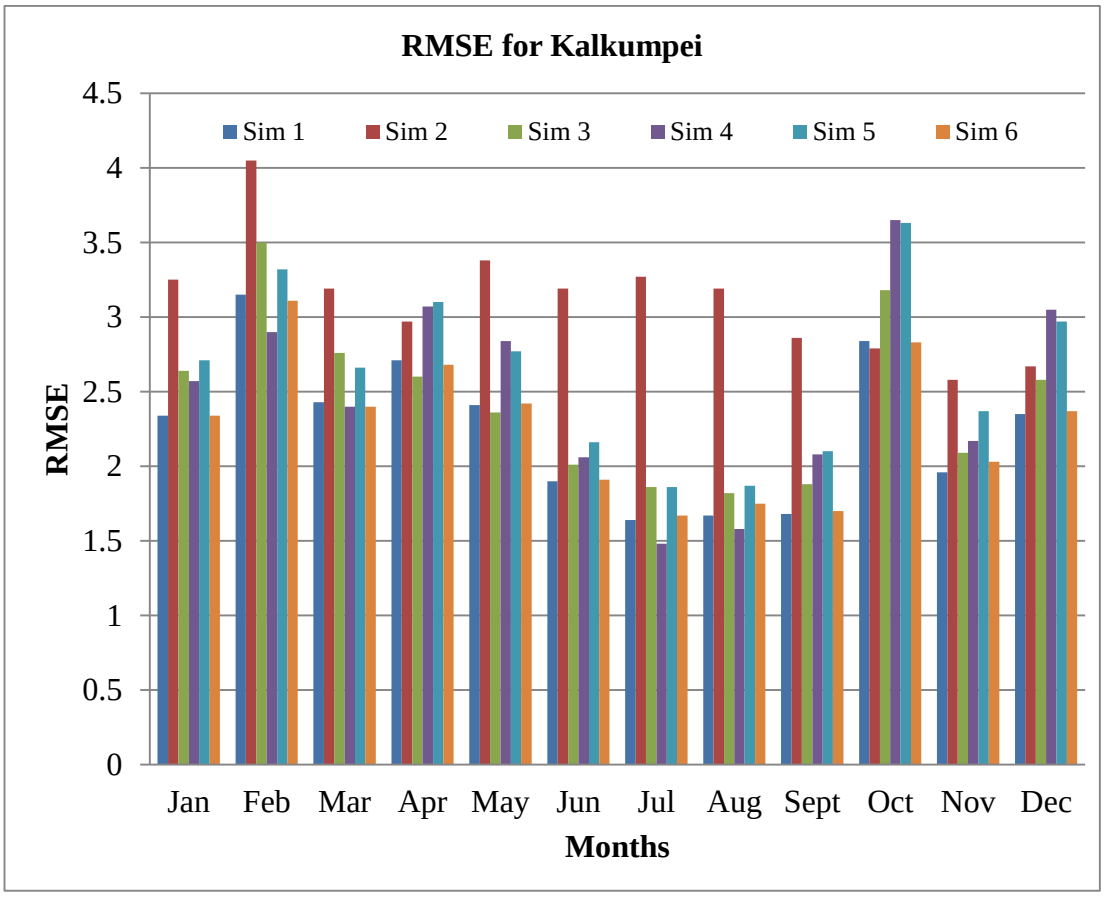

Figure 5.7: Monthly root mean square error at Kalkumpei for 2009.

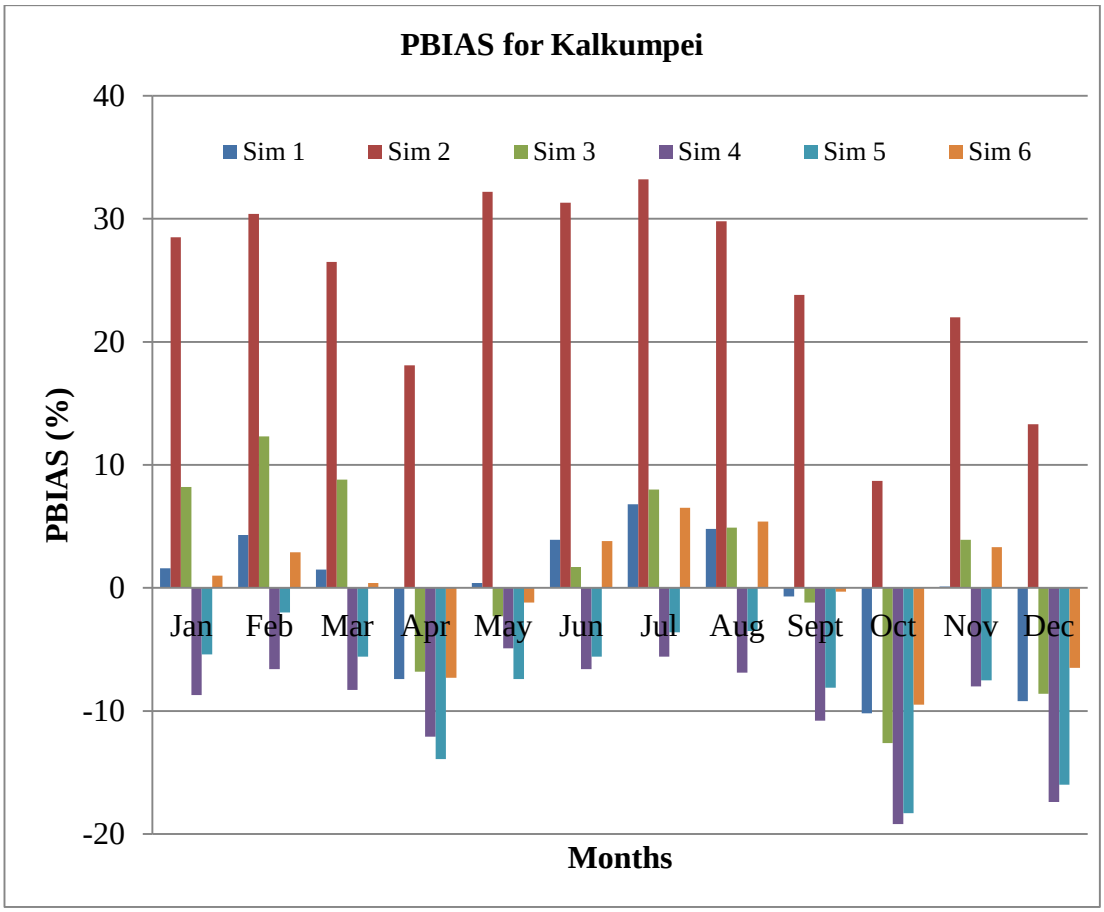

Figure 5.8: Monthly percentage bias at Kalkumpei for 2009.

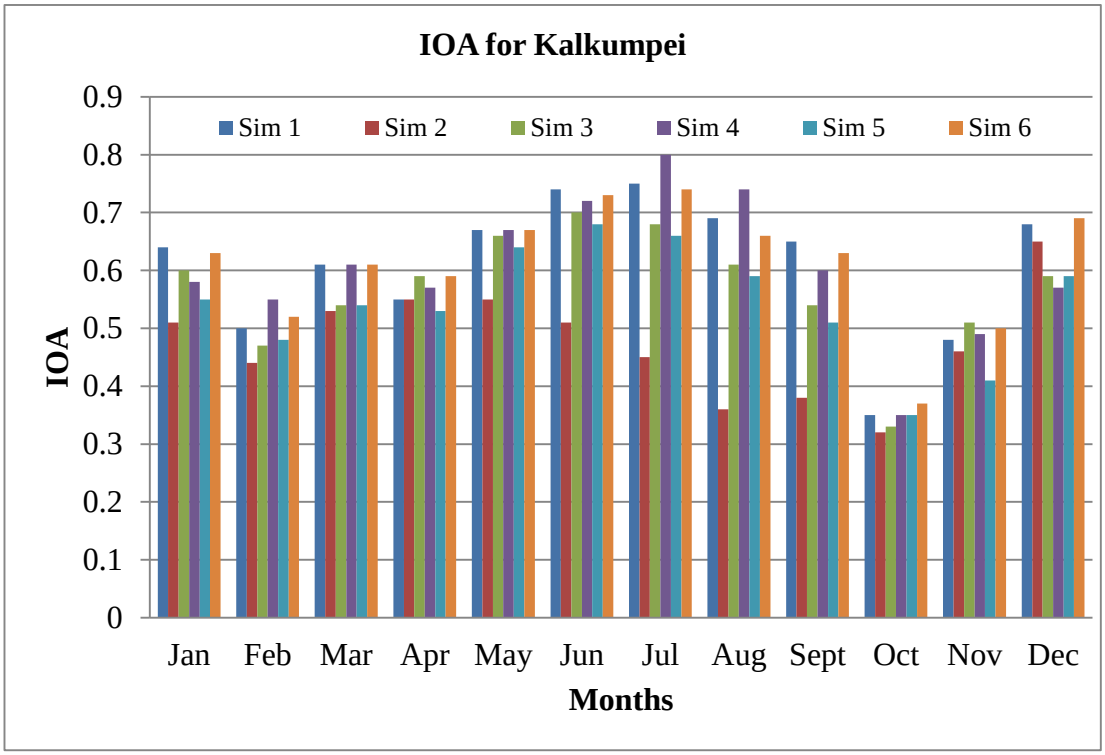

Figure 5.9: Monthly index of agreement at Kalkumpei for 2009.

5.1.5.2 Nyiru

Simulations that best simulate the observed wind speed are considered in this section and reference will be made on figures 5.10, 5.11, 5.12, 5.13 and 5.14. Simulations 4 and 5 perform well in predicting summer wind speeds with mean error of 0.2 m/s, 0.22 m/s and -0.01 m/s for June, July and August respectively and with a percent bias of 1.9, 1.9 and -0.1 respectively. October has the highest mean error of 0.86 m/s with a percent bias of 8.8 because the model erroneously predicts this to be the windiest months of the year. August has the least mean error of 0.01 m/s with a percent bias of -0.1. This implies that Quasi-Normal Scale Elimination PBL scheme does a better job for predicting June wind speeds while Mellor-Yamada-Janjic PBL scheme does a better job for both July and August. Yonsei State University PBL scheme does a good job in predicting wind speed at this station for January, February, March, April and November. The mean error for these months are: -0.28 m/s, -0.2 m/s, -0.03 m/s, -0.44 m/s and 0.26 m/s respectively, with percent biases of -2.7, -1.8, -0.3, -4.4 and 2.7 respectively.

July, August and September have the lowest root mean square errors of 1.57, 1.68 and 1.83 respectively. October has the highest root mean square error of 2.91 m/s. Mellor-Yamada-Janjic was the best PBL schemes for predicting wind speed at Nyiru during the summer months. Based on RMSE, Yonsei State University PBL scheme does a good job in predicting wind speed for this station for all months except between June and September during which Mellor-Yamada-Janjic PBL scheme does a better job.

June, July and December have the highest index of agreement of 0.72, 0.7 and 0.73 respectively. The index of agreement reduces progressively with the season for both summer and winter. Mellor-Yamada-Janjic PBL scheme was the best for predicting wind speed at Nyiru during the summer while Yonsei State University PBL scheme was the best during winter. Based on the four statistical measures, Yonsei State University PBL scheme does a good job in predicting wind speed for this station for all months except between May and September when Mellor-Yamada-Janjic PBL scheme does a better job.

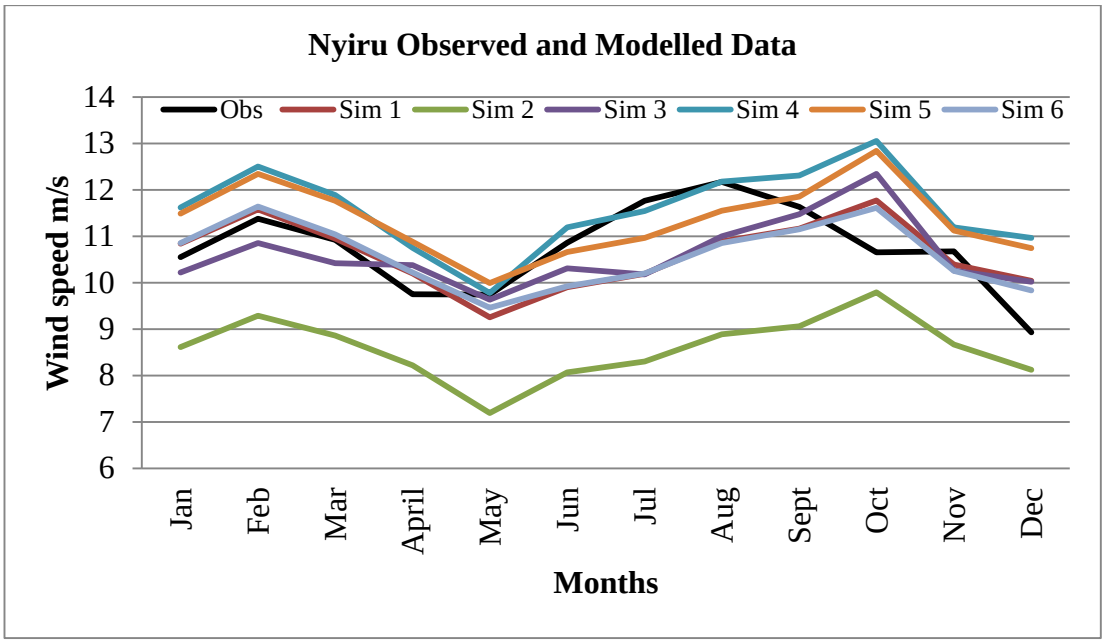

Figure 5.10: Mean measured and modeled data at Nyiru for 2009.

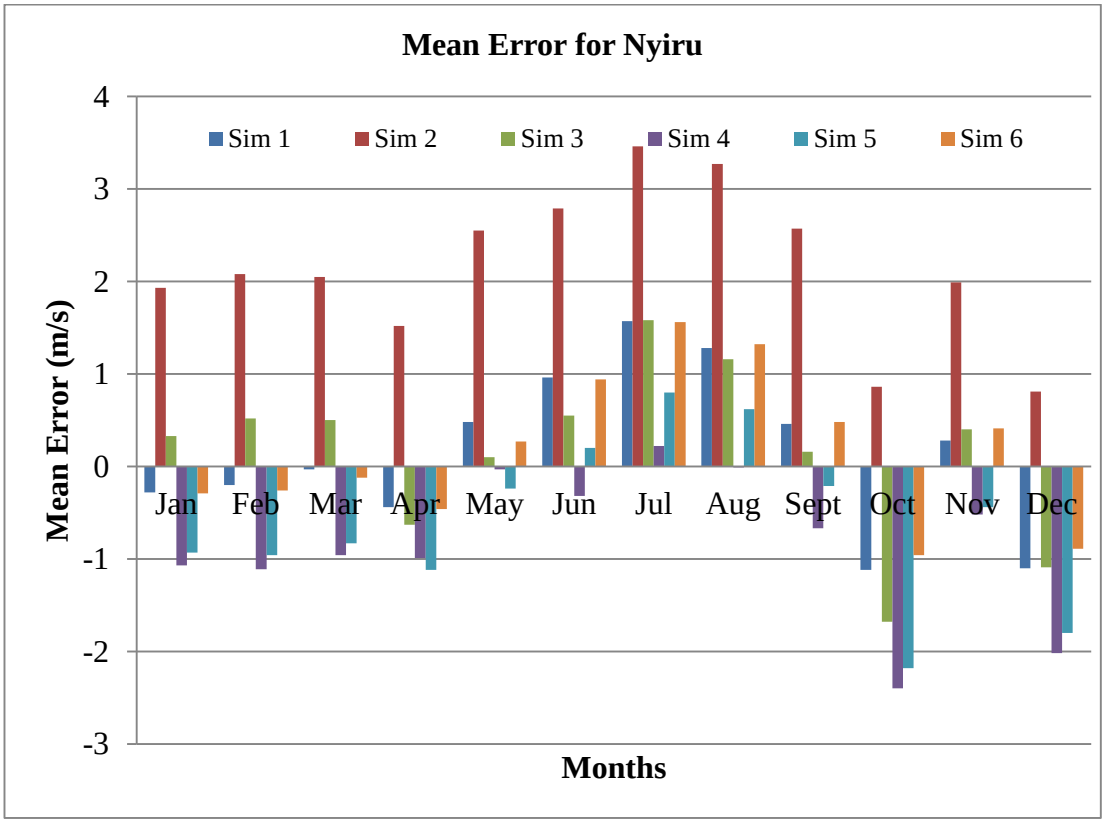

Figure 5.11: Monthly mean error at Nyiru for 2009.

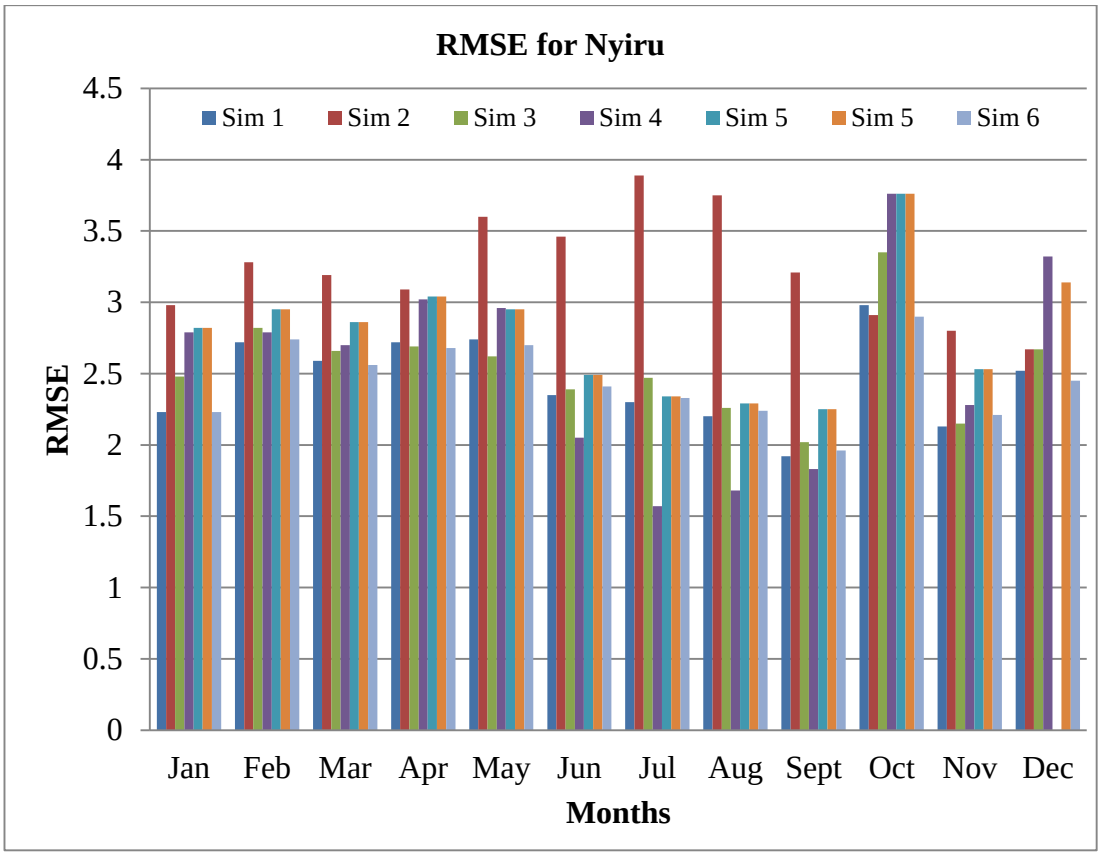

Figure 5.12: Monthly root mean square error at Nyiru for 2009.

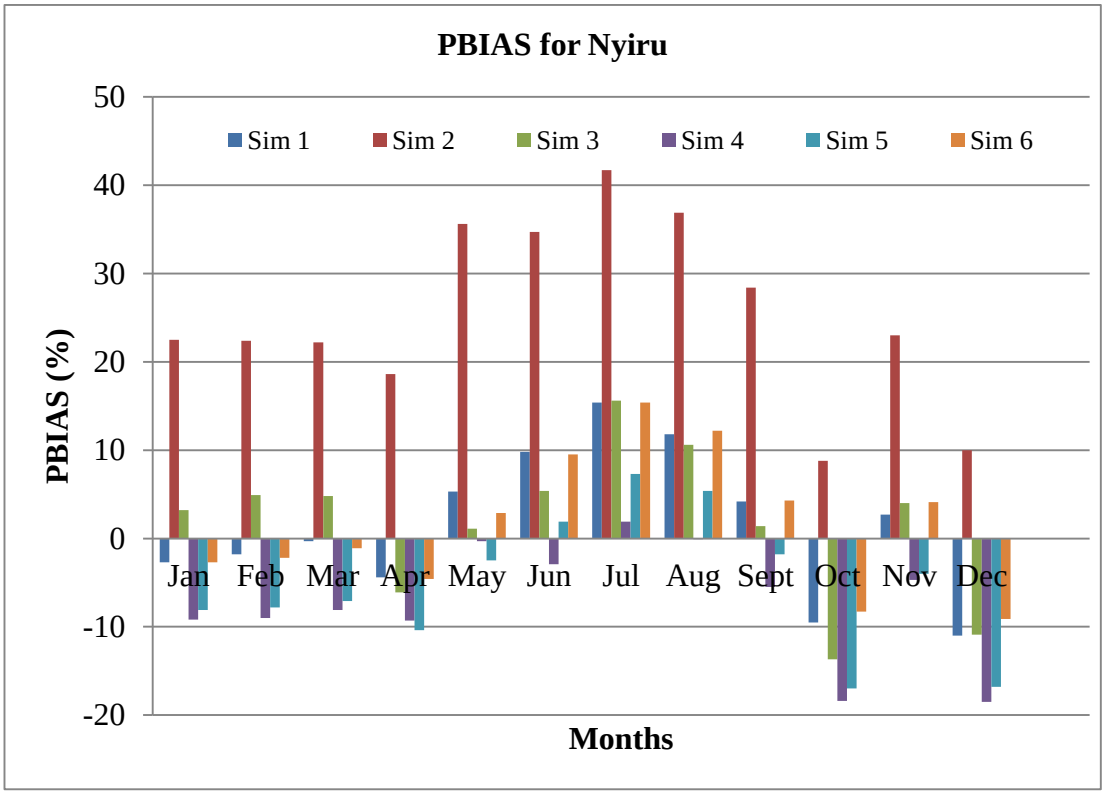

Figure 5.13: Monthly percentage bias at Nyiru for 2009.

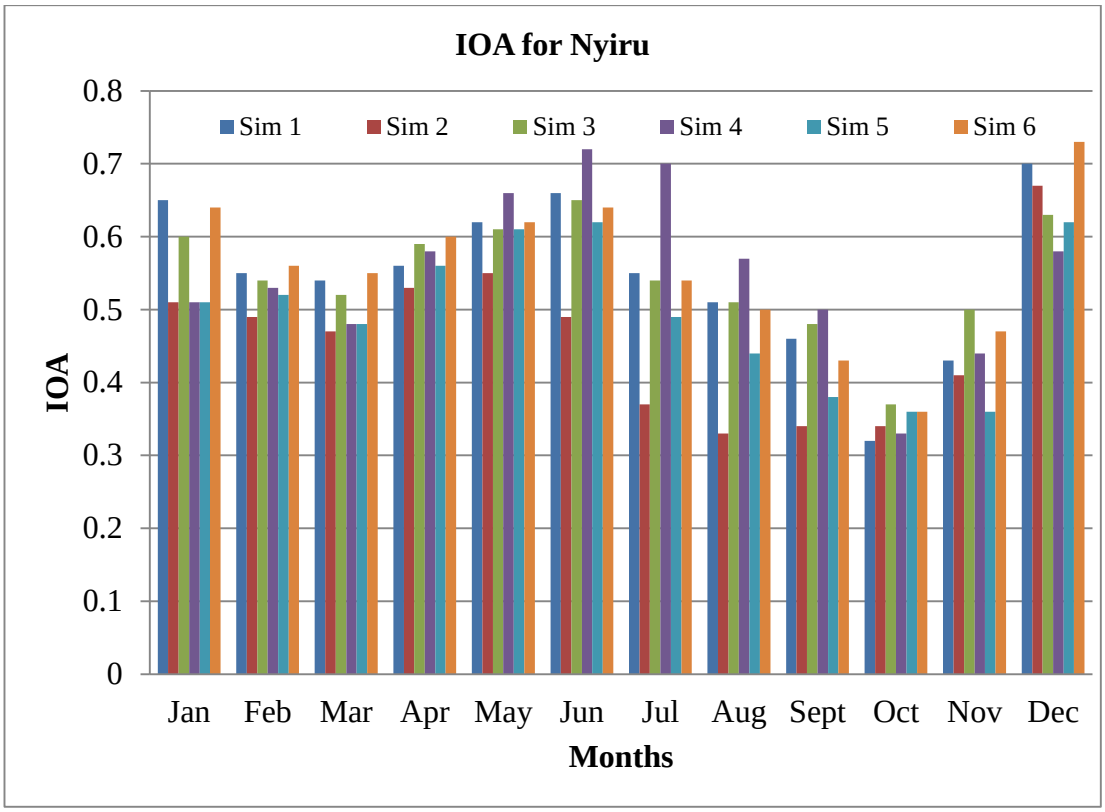

Figure 5.14: Monthly index of agreement at Nyiru for 2009.

5.1.5.3 Sirima

Simulations that best simulate the observed wind speed are considered in this section and reference will be made on figures 5.15, 5.16, 5.17, 5.18 and 5.19. All the simulations under predict wind speed at Sirima with the only exception being simulation 3, 4 and 5 for the month of October. Simulations 5 and 3 perform well in predicting wind speeds for April, May and December with mean error of 0.17 m/s, -0.2 m/s and -0.32 m/s respectively and with a percent bias of 1.8, -1.8 and -3.4 respectively. July has the highest mean error of 1.28 m/s with a percent bias of 12. April has the least mean error of 0.17 m/s with a percent bias of 1.8. July, August and September have the lowest root mean square errors of 1.95, 1.85 and 1.74 respectively. February has the highest root mean square error of 3.08 m/s.

The months of May, June and December have the highest IOA of 0.66, 0.67 and 0.72 respectively. October has the lowest index of agreement of 0.38. Based on the four statistical measures, Mellor-Yamada-Janjic was the best PBL schemes for predicting wind speed at Sirima for all months except between October and January when Yonsei State University PBL scheme does a better job.

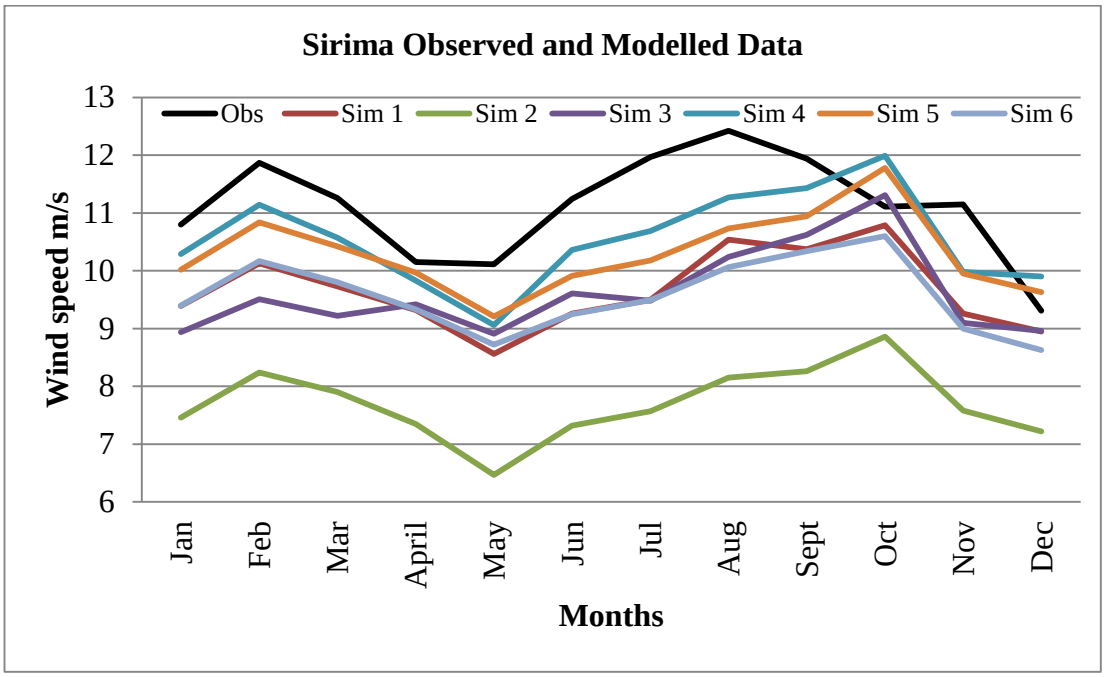

Figure 5.15: Mean measured and modeled data at Sirima for 2009.

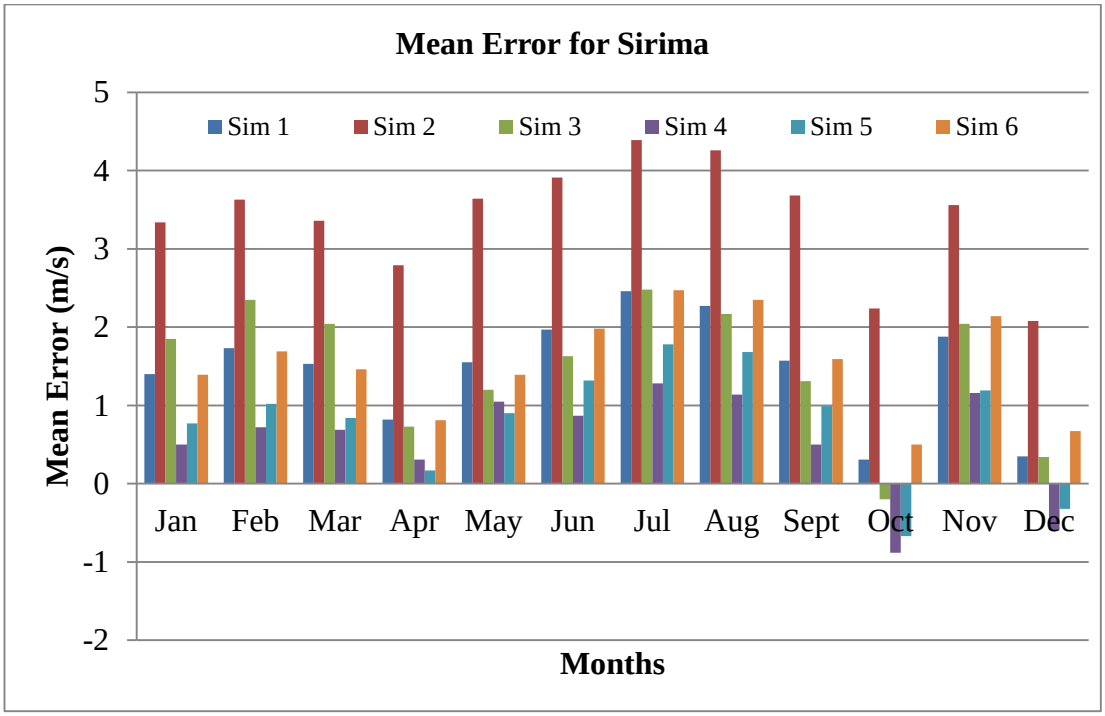

Figure 5.16: Monthly mean error at Sirima for 2009.

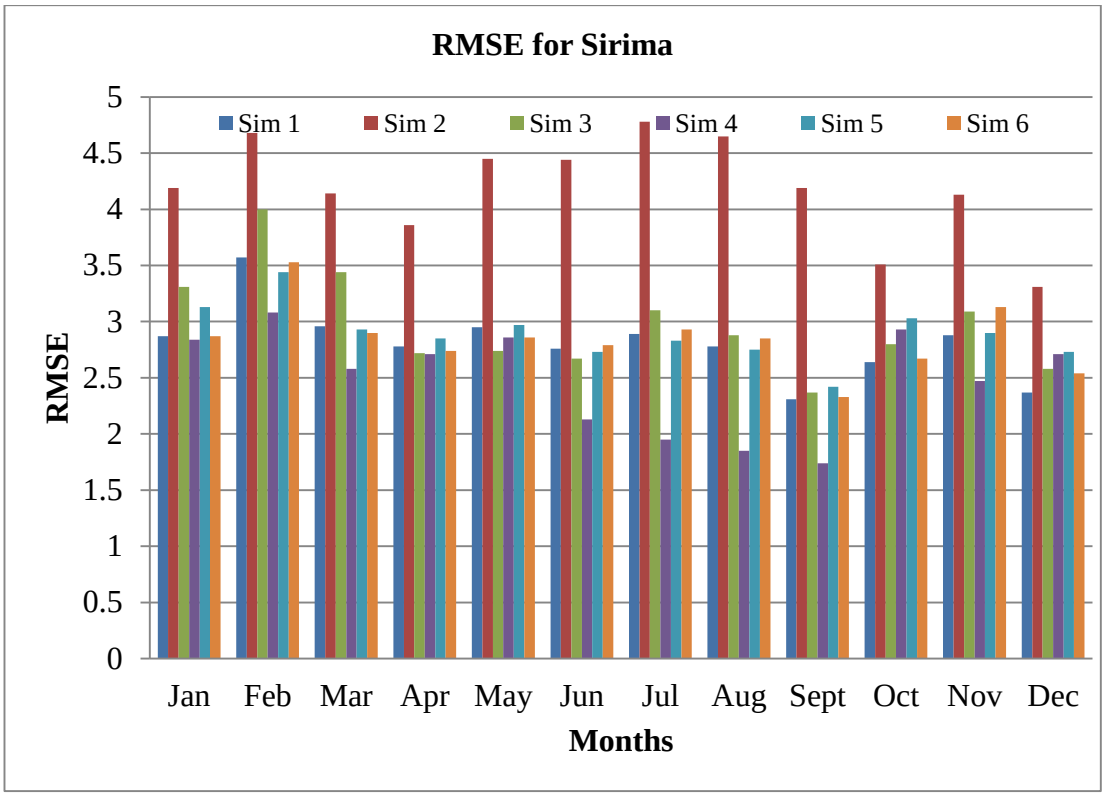

Figure 5.17: Monthly root mean square error at Sirima for 2009.

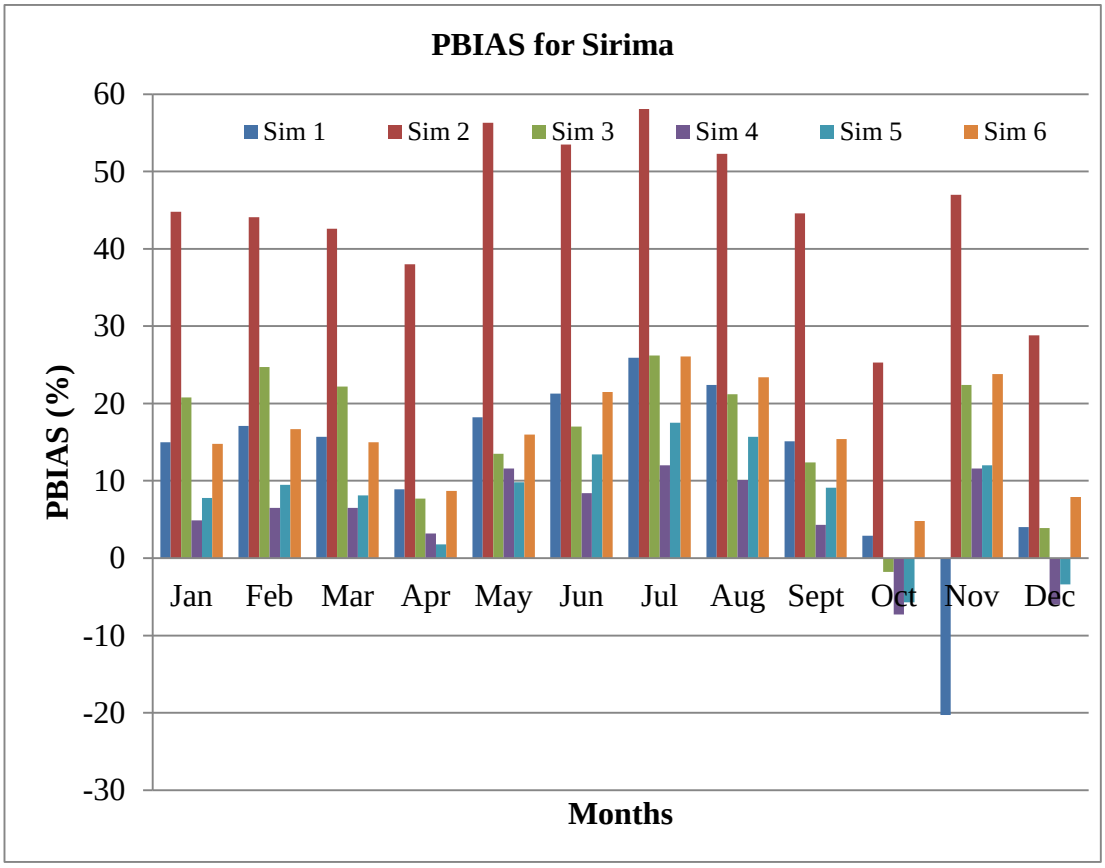

Figure 5.18: Monthly percentage bias at Sirima for 2009.

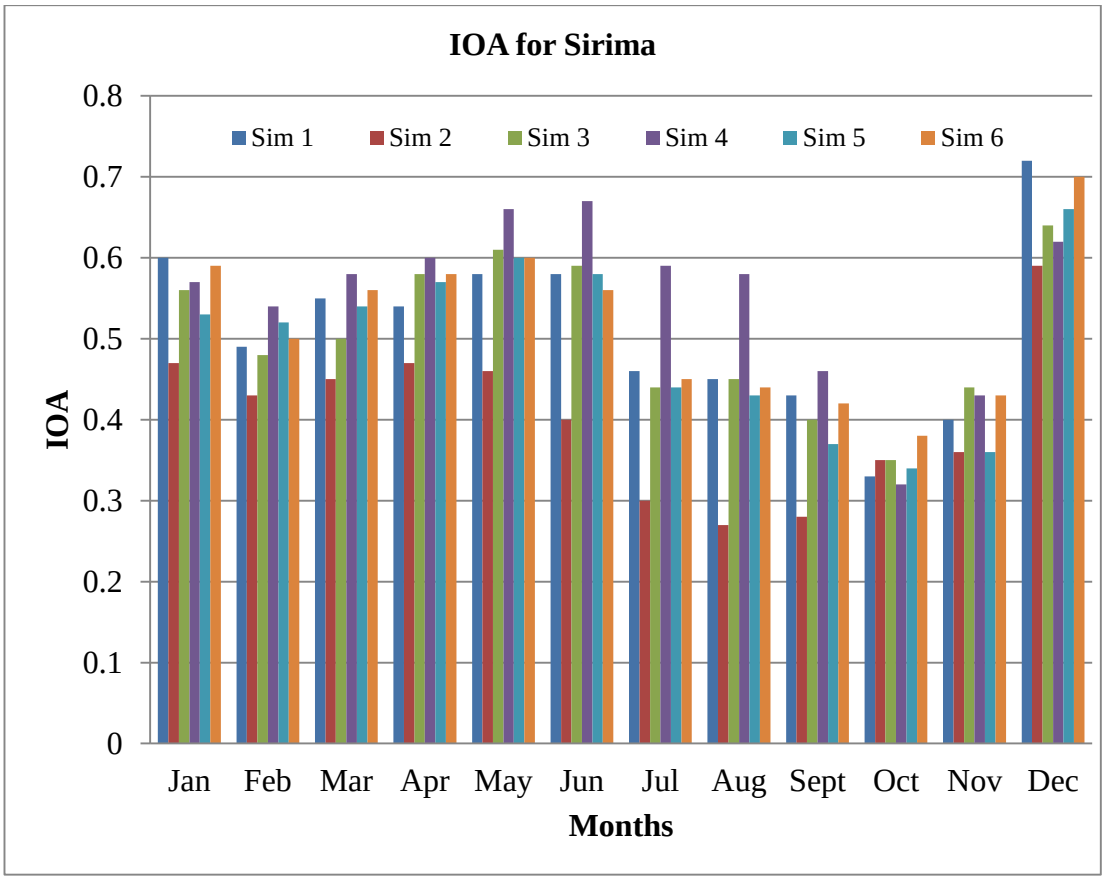

Figure 5.19: Monthly index of agreement at Sirima for 2009.

5.1.5.4 Discussion

The results and discussion presented in this section are based on the wind rose plot comparisons and summary statistics for the three validation sites. Table 5.2 shows that WRF simulations using Yonsei State University PBL scheme produced the best annual results at Kalkumpei with a mean difference of -0.01 m/s, percent bias of -0.1, RMSE of 2.30 m/s and Index of Agreement (IOA) of 0.66 and the predominant south east wind direction was correctly captured by the model at this location. Summer months have the highest IOA and lowest RMSE.

WRF simulations using Yonsei State University PBL scheme produced the best annual results at Nyiru with a mean difference of 0.15 m/s, percent bias of 1.5, RMSE of 2.46 m/s and IOA of 0.61. The predominant south east wind direction was correctly captured by the model at this location. WRF simulation using Yonsei State University PBL scheme generated good results at both Kalkumpei and Nyiru because a topographic correction (topo_wind=1) was incorporated during WRF simulation. This correction improves surface wind biases using sub-grid variance and resolved

topography to modify surface friction effect and enhanced flow at hill tops (Jiménez and Dudhia, 2012).

WRF run using Mellor-Yamada-Janjic scheme produced the best annual results at Sirima with a mean difference of 0.56 m/s, percent bias of 5.3, RMSE of 2.52 m/s and IOA of 0.61. July, August and September have the lowest root mean square errors of 1.95 m/s, 1.85 m/s and 1.74 m/s respectively while May, June and December have the highest IOA of 0.66, 0.67 and 0.72 respectively. The Mellor-Yamada-Janjic was the best PBL schemes for predicting wind speed at Sirima for all months except between October and January when Yonsei State University PBL scheme does a better job. The location of Sirima mast atop a very exposed ridgeline favors WRF simulation using TKE closure PBLs. It therefore doesn't occur as a surprise that MYJ PBL scheme performs better at this location. Based on the analysis and results presented in this work, it can be concluded that WRF model can be used to generate wind data that can be used directly in wind resource assessment.

5.2. WAsP Modelling

Conventionally, wind resource assessment and wind farm calculations are based on wind data measured at or near the wind farm site. The WAsP software used in this research is an implementation of wind atlas methodology (Troen et al., 1986). The results presented consists of three regional wind atlases that were derived from wind data at three mast locations and used to make wind and annual energy simulations at the wind farm site. The wind data used is described in section 3.3.

5.2.1 Wind resource mapping for 45 m turbine hub height

This section deals with the determination of reference conditions and it's analysis to produce wind climate summary for Lake Turkana wind farm site. Wind resource map is the map showing average wind speed, power density and annual energy production of a wind farm site at 45 m hub height using Vestas V52-850kW turbine.

The analysis and prediction of the regional wind climate was calculated by considering 5 reference roughness lengths (0.00 m, 0.02 m, 0.10 m, 0.40 m, 1.50 m) and 5 reference heights (20 m, 40 m, 45 m, 70 m, 90 m) above ground level. Roughness length of 0.0002 m is recommended by WAsP for water bodies like Lake

Turkana which is to the west of the wind farm (figure 1.1). The roses of Weibull parameters have 12 sectors each. The grid set used is given below.

A useful feature in WAsP is the wind resource grid displayed as a map over a selected area. This can be used to locate potentially high AEP sites. The maps for the wind farm mean wind speed, power density, AEP and RIX using data from 3 mast locations are shown and discussed in the sections that follow.

Structure:	131 columns and 201 rows at 100 resolution gives 26331 calculation sites
Boundary:	(248950, 265950) to (262050, 286050)
Nodes:	(249000, 266000) to (262000, 286000)
Height a.g.l.:	45 m
Wind turbine generator:	Vestas V52-850 kW

5.2.1.1 Kalkumpei Regional wind climate summary

Table 5.3 presents WAsP mean and emergent wind speed using wind data collected at Kalkumpei mast before factoring in topography.

Table 5.3: Results from the observed wind climate in WAsP. The emergent wind speeds are the weighted sums of the Weibull distributions in all directions.

Parameter	Measured	Emergent	Discrepancy
Mean wind speed [m/s]	10.25	10.35	1.0%
Mean power density [W/m²]	792	792	0.0%

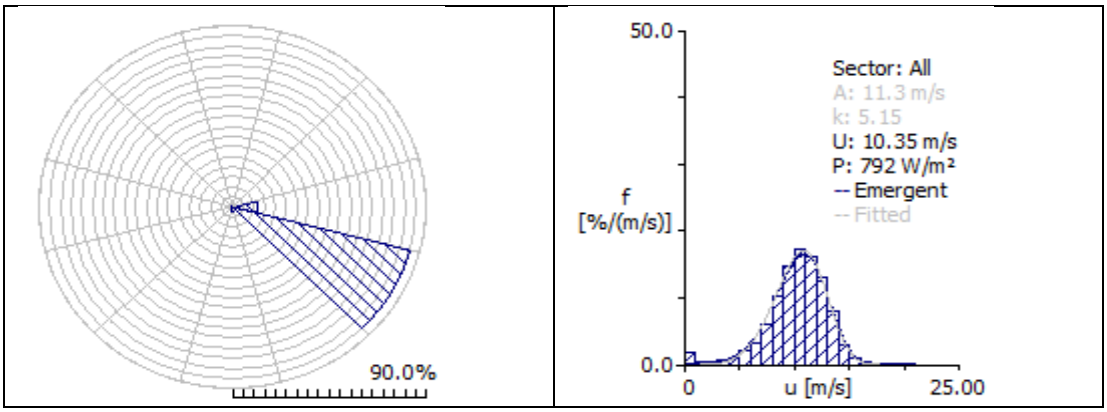

Figure 5.20: Wind Rose for the annual data collected at Kalkumpei meteorological mast and wind speed distribution (Weibull) for all sectors (wind directions) from WAsP.

Table 5.4: Lake Turkana regional wind climate using Kalkumpei data.

Height	Parameter	0.00 m	0.02 m	0.10 m	0.40 m	1.50 m
20.0 m	Weibull A [m/s]	13.10	10.21	8.75	7.16	5.92
	Weibull k	4.97	4.53	4.61	4.46	4.53
	Mean speed U [m/s]	12.02	9.32	8.00	6.53	5.40
	Power density E [W/m²]	1231	589	370	204	115
40.0 m	Weibull A [m/s]	13.96	11.48	10.08	8.57	7.39
	Weibull k	5.07	4.79	4.84	4.65	4.71
	Mean speed U [m/s]	12.83	10.51	9.24	7.83	6.77
	Power density E [W/m²]	1488	830	562	346	222
45.0 m	Weibull A [m/s]	14.11	11.71	10.32	8.82	7.66
	Weibull k	5.10	4.86	4.90	4.70	4.75
	Mean speed U [m/s]	12.97	10.74	9.47	8.07	7.01
	Power density E [W/m²]	1536	881	603	377	247
70.0 m	Weibull A [m/s]	14.73	12.67	11.29	9.81	8.67
	Weibull k	5.09	5.18	5.18	4.93	4.96
	Mean speed U [m/s]	13.54	11.66	10.39	9.00	7.96
	Power density E [W/m²]	1747	1111	786	517	357
90.0 m	Weibull A [m/s]	15.11	13.31	11.89	10.41	9.29
	Weibull k	5.05	5.27	5.40	5.12	5.13
	Mean speed U [m/s]	13.89	12.26	10.97	9.57	8.54
	Power density E [W/m²]	1888	1287	917	616	437

Results for mean wind speed, power density, annual energy production and RIX using Kalkumpei data are presented in the following sections.

Mean Speed

Figure 5.21 show the wind speed resource map at 45 m hub height with contour lines and proposed turbine locations. The wind speed ranges from a minimum of 5.36 m/s, represented by the blue colour on the map, to a maximum value of 16.55 m/s

represented by the red colour. The mean wind speed was 10.72 m/s, according to the WASP 11 Wind Atlas Calculations.

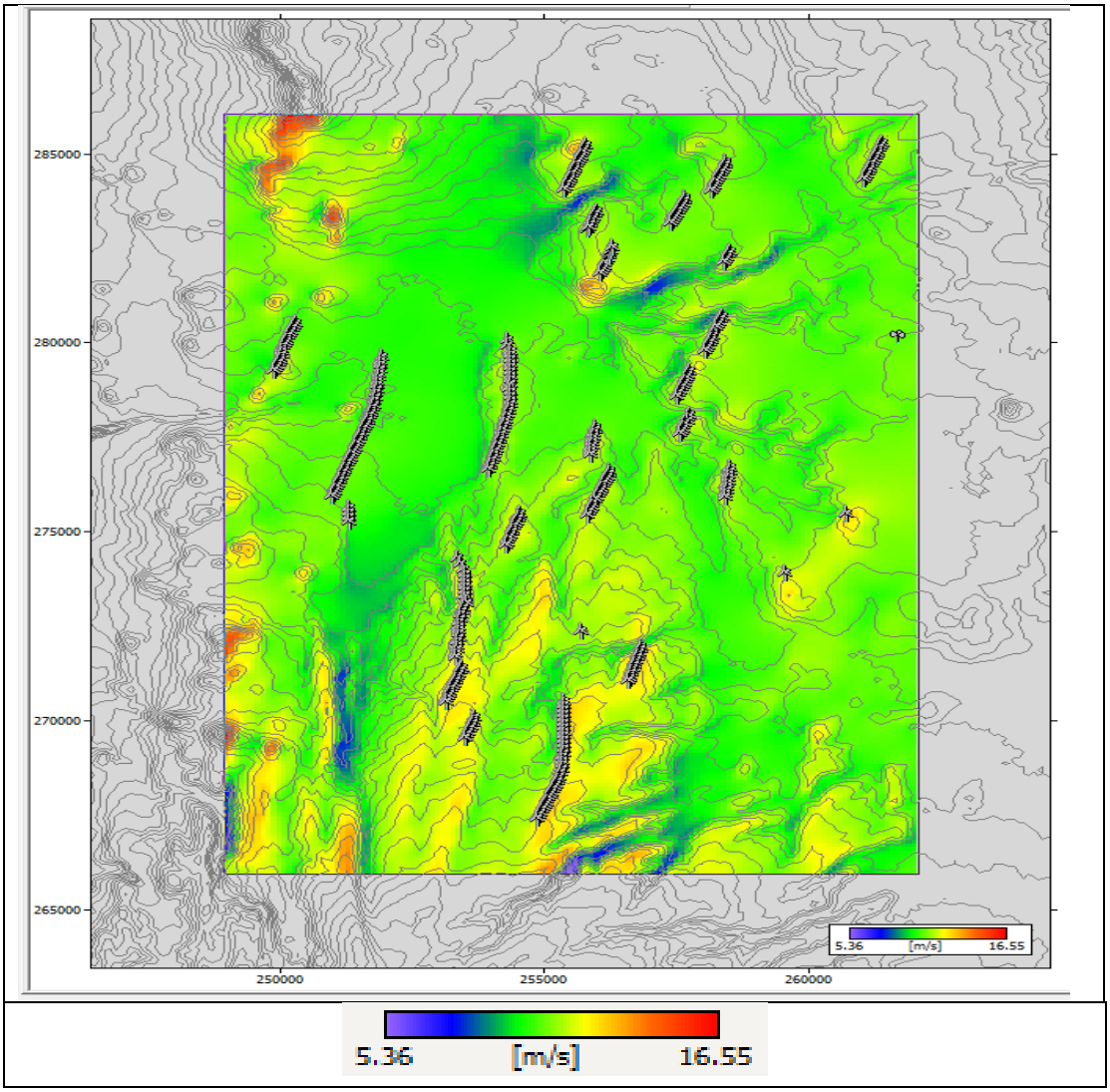

Figure 5.21: Wind speed Resource Map at 45 m wind turbine height using Kalkumpei mast data.

Maximum Value:	16.55 m/s at (250200, 286000)
Minimum Value:	5.36 m/s at (255500, 266000)
Mean Value:	10.72 m/s

Power Density

Similar to the wind speed resource map, figure 5.22 show the analysis result for the site power density at 45 m hub height with contour lines and proposed turbine locations. According to the WAsP 11 Wind Atlas calculations, the mean value for the power density production was 893 W/m².

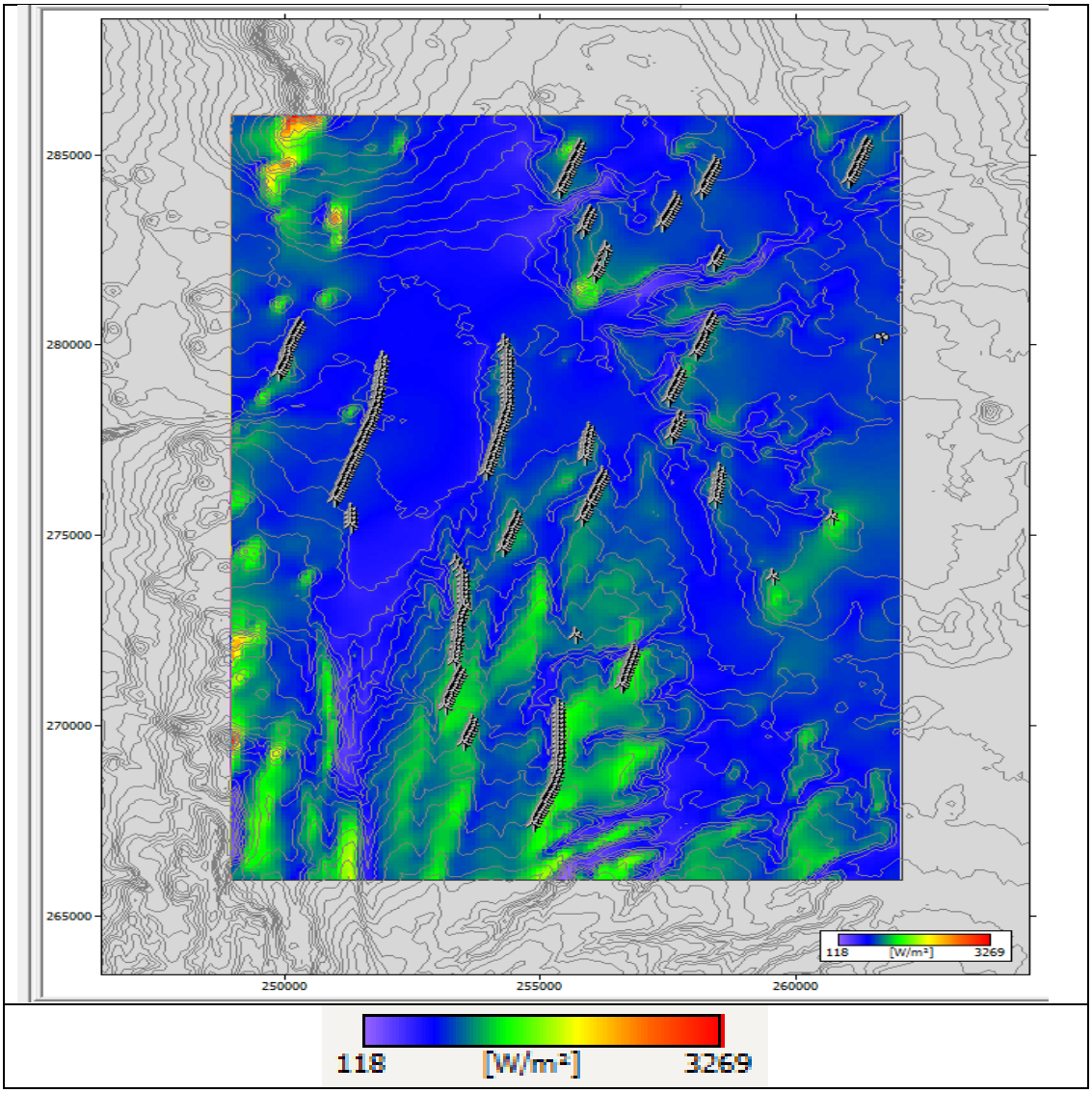

Figure 5.22: Power density Map at 45 m wind turbine hub heights using Kalkumpei mast data.

Maximum Value:	3269 W/m² at (250200, 286000)
Minimum Value:	118 W/m² at (255500, 266000)
Mean Value:	893 W/m²

Annual Energy Production (AEP)

Similar to the wind speed and power density resource maps, the figure 5.23 shows the analysis result for the site Annual energy production at 45 m hub height.

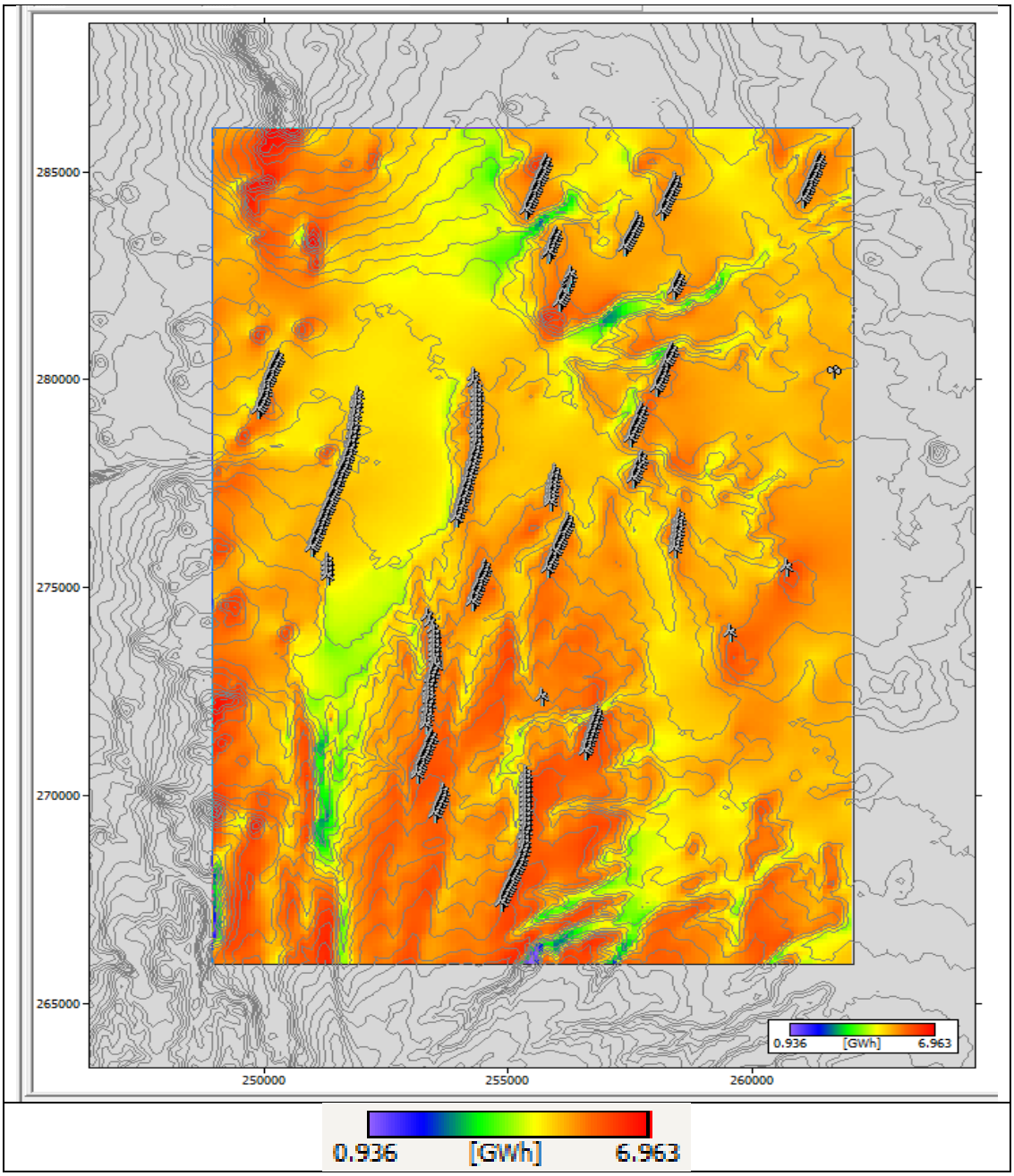

Figure 5.23: Annual Energy Production Map at 45 m wind turbine hub heights using Kalkumpei mast data.

Maximum Value:	6.963 GWh at (250500, 286000)
Minimum Value:	0.936 GWh at (255500, 266000)
Mean Value:	5.146 GWh

RIX [%]

Similar to the wind speed and power density resource maps, the figure 5.24 shows the analysis result for the ruggedness index at 45 m hub height. RIX was not used as a measure of WAsP accuracy because: Lake Turkana region is close to the equator

thus the Coriolis force is very minimal and the wind direction is predominantly south-east. However, figure 5.24 shows that the proposed turbine locations are in regions where RIX values are close to 0. This map applies to both Nyiru and Sirima locations.

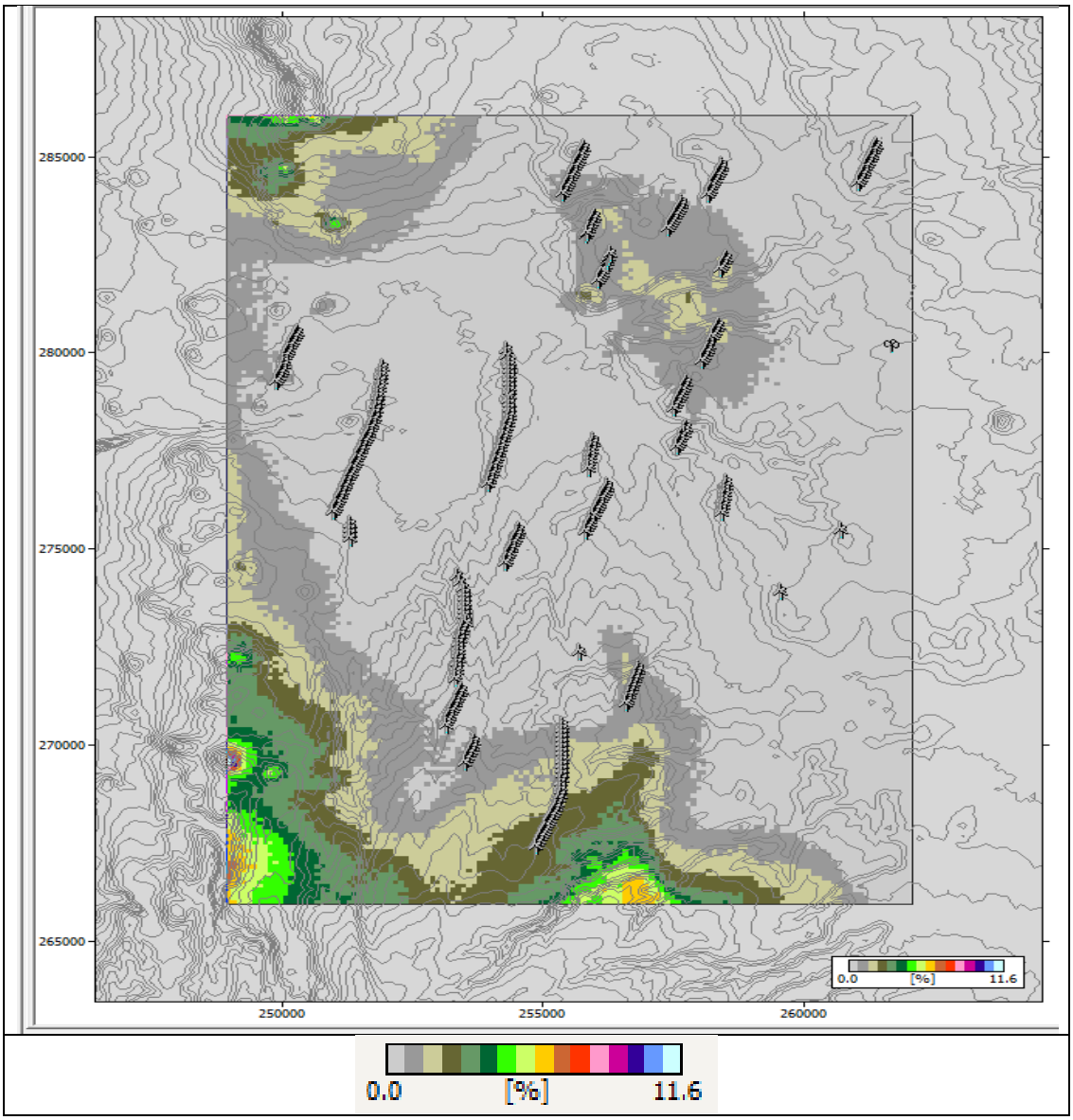

Figure 5.24: Ruggedness index Map at 45 m wind turbine hub heights using Kalkumpei mast data.

Maximum Value:	11.6% at (249000, 269600)
Minimum Value:	0.0% at (262000, 274900)
Mean Value:	0.8%

5.2.1.2 Nyiru Regional wind climate summary

Table 5.5 presents WAsP mean and emergent wind speed using wind data collected at Nyiru mast before factoring in topography.

Table 5.5: Results from the observed wind climate in WAsP. The emergent wind speeds are the weighted sums of the Weibull distributions in all directions.

Parameter	Measured	Emergent	Discrepancy
Mean wind speed [m/s]	10.75	10.75	0.0%
Mean power density [W/m²]	871	873	0.2%

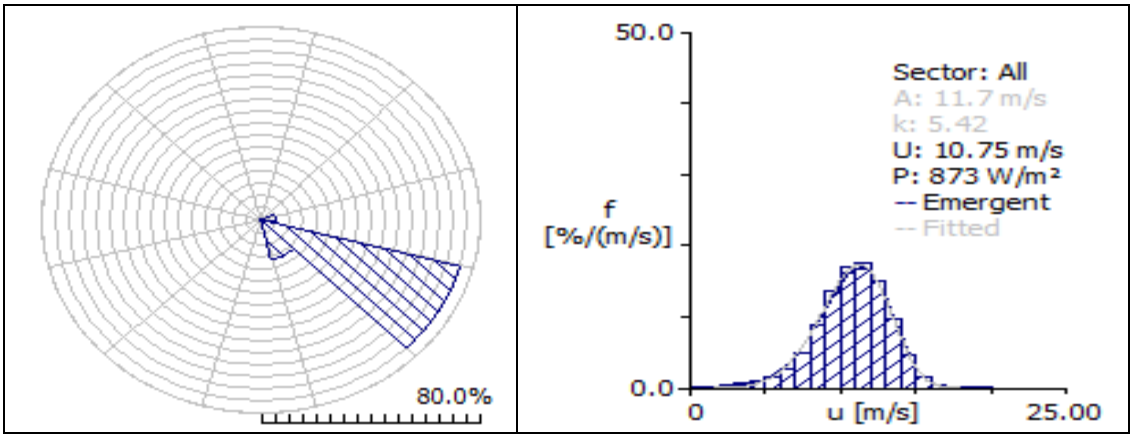

Figure 5.25: Wind Rose for the annual data collected at Nyiru meteorological mast and wind speed distribution (Weibull) for all sectors (wind directions) from WAsP.

Table 5.6: Lake Turkana regional wind climate using Nyiru data.

Height	Parameter	0.00 m	0.02 m	0.10 m	0.40 m	1.50 m
20.0 m	Weibull A [m/s]	12.32	9.60	8.22	6.73	5.55
	Weibull k	5.42	4.89	4.91	4.74	4.76
	Mean speed U [m/s]	11.37	8.81	7.54	6.16	5.08
	Power density E [W/m²]	1019	486	304	168	94
40.0 m	Weibull A [m/s]	13.15	10.85	9.50	8.08	6.95
	Weibull k	5.56	5.24	5.21	4.99	4.99
	Mean speed U [m/s]	12.15	9.99	8.75	7.42	6.38
	Power density E [W/m²]	1237	696	468	289	184
45.0 m	Weibull A [m/s]	13.30	11.08	9.74	8.32	7.20
	Weibull k	5.59	5.32	5.28	5.05	5.05
	Mean speed U [m/s]	12.29	10.21	8.97	7.65	6.62
	Power density E [W/m²]	1279	742	504	316	205
70.0 m	Weibull A [m/s]	13.91	12.05	10.70	9.29	8.19
	Weibull k	5.56	5.74	5.63	5.34	5.31
	Mean speed U [m/s]	12.85	11.16	9.89	8.56	7.55
	Power density E [W/m²]	1464	952	666	437	299
90.0 m	Weibull A [m/s]	14.29	12.72	11.32	9.89	8.79
	Weibull k	5.52	5.77	5.85	5.57	5.52

	Mean speed U [m/s] Power density E [W/m²]	13.20 1588	11.78 1119	10.48 787	9.14 526	8.12 370

Results for mean wind speed, power density, annual energy production and RIX using Nyiru data are presented in the following sections.

Mean Speed

Figure 5.26 show the wind speed resource map at 45 m hub height with contour lines and proposed turbine locations. The wind speed ranges from a minimum of 5.10 m/s, represented by the blue colour on the map, to a maximum value of 15.75 m/s represents by the red colour. The mean wind speed was 10.16 m/s, according to the WASP 11 Wind Atlas Calculations.

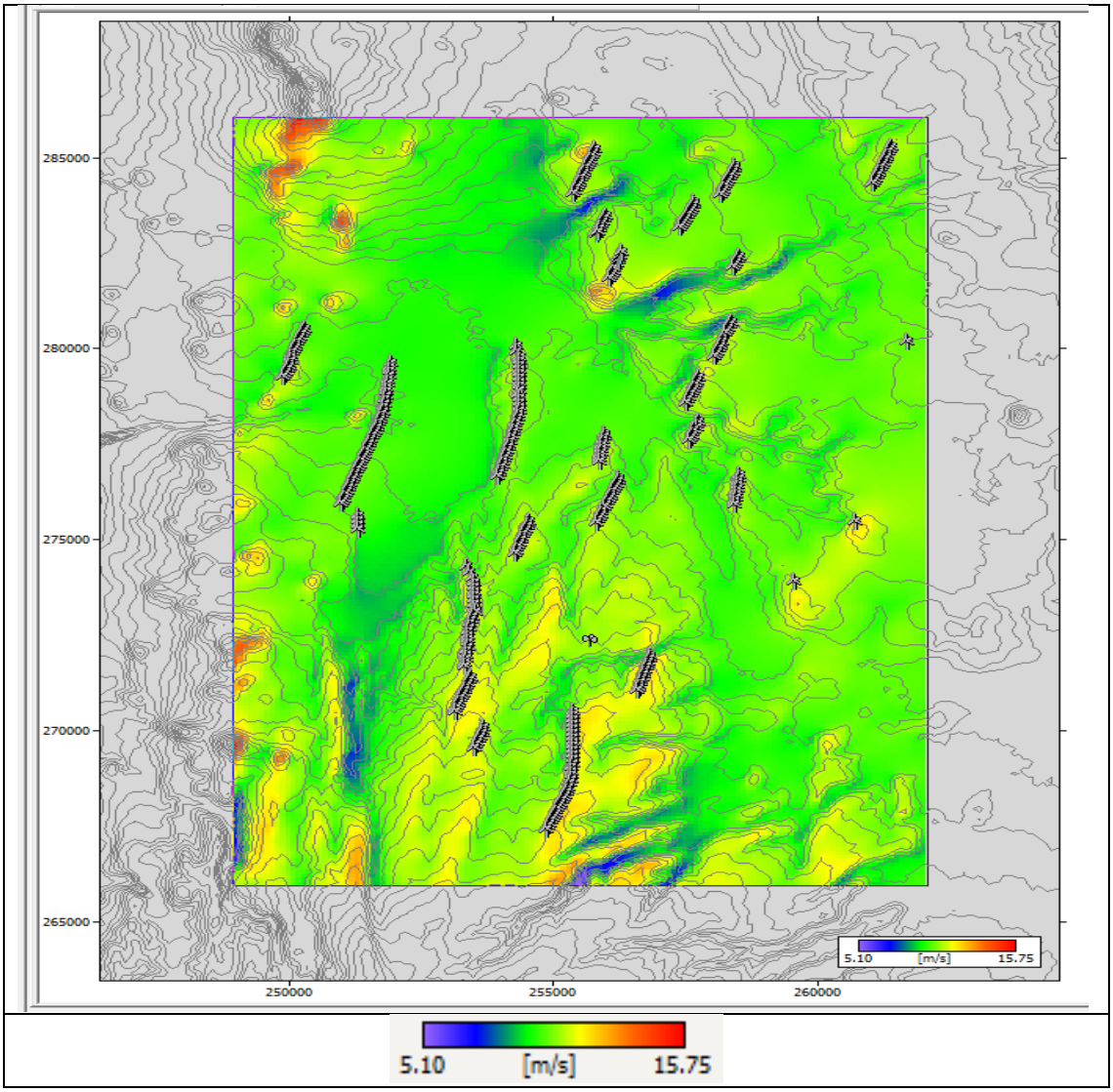

Figure 5.26: Wind speed Resource Map at 45 m wind turbine height using Nyiru mast data.

Maximum Value:	15.75 m/s at (250200, 286000)
Minimum Value:	5.10 m/s at (255500, 266000)
Mean Value:	10.16 m/s

Power Density

Similar to the wind speed resource map, figure 5.27 show the analysis result for the site power density at 45 m hub height with contour lines and proposed turbine locations. According to the WAsP 11 Wind Atlas calculations, the mean value for the power density production was 744 W/m².

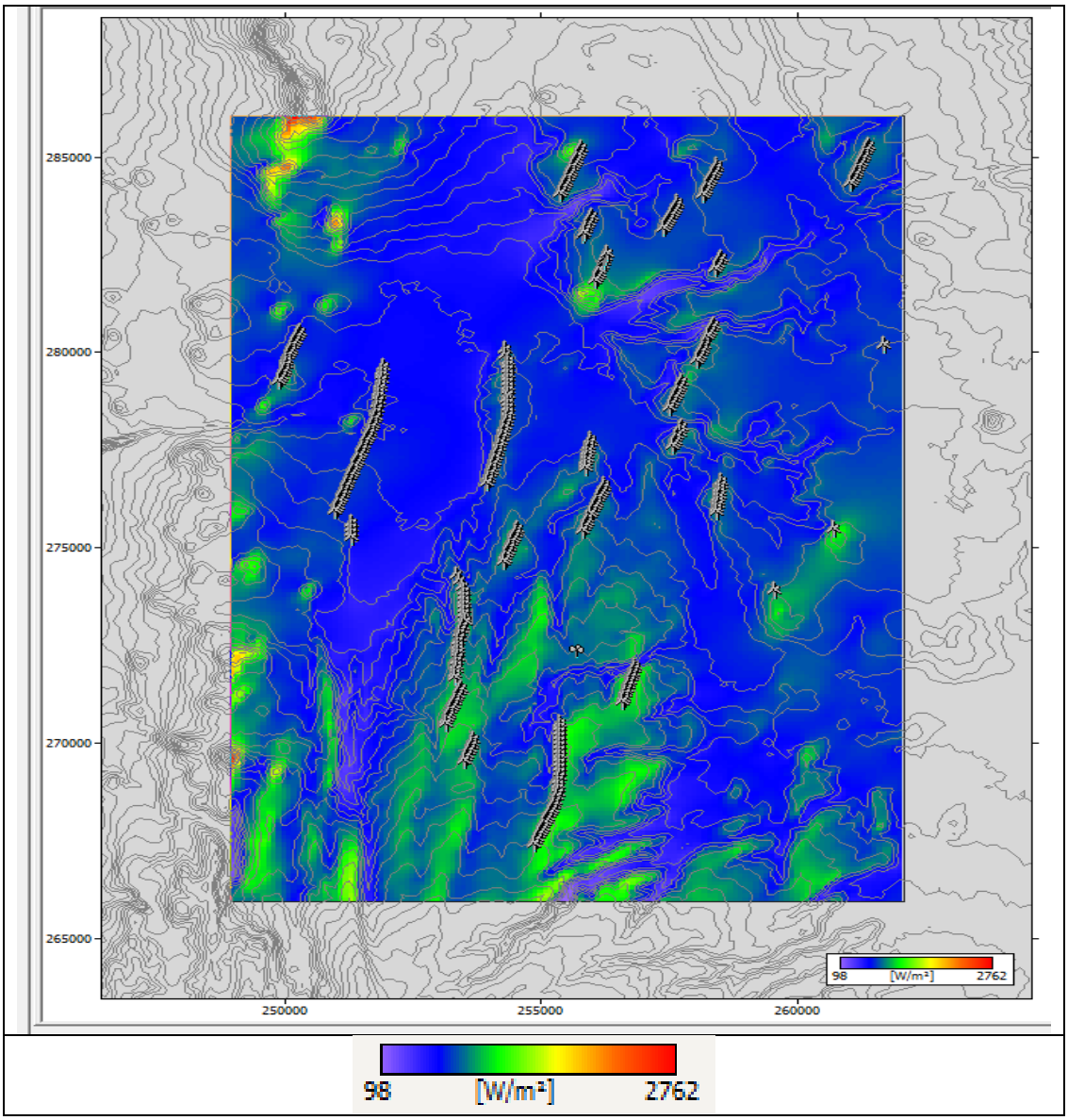

Figure 5.27: Power density Map at 45 m wind turbine hub heights using Nyiru mast data.

Maximum Value:	2762 W/m² at (250200, 286000)
Minimum Value:	98 W/m² at (255500, 266000)
Mean Value:	744 W/m²

Annual Energy Production (AEP)

Similar to the wind speed and power density resource maps, the figure 5.28 shows the analysis result for the site Annual energy production at 45 m hub height.

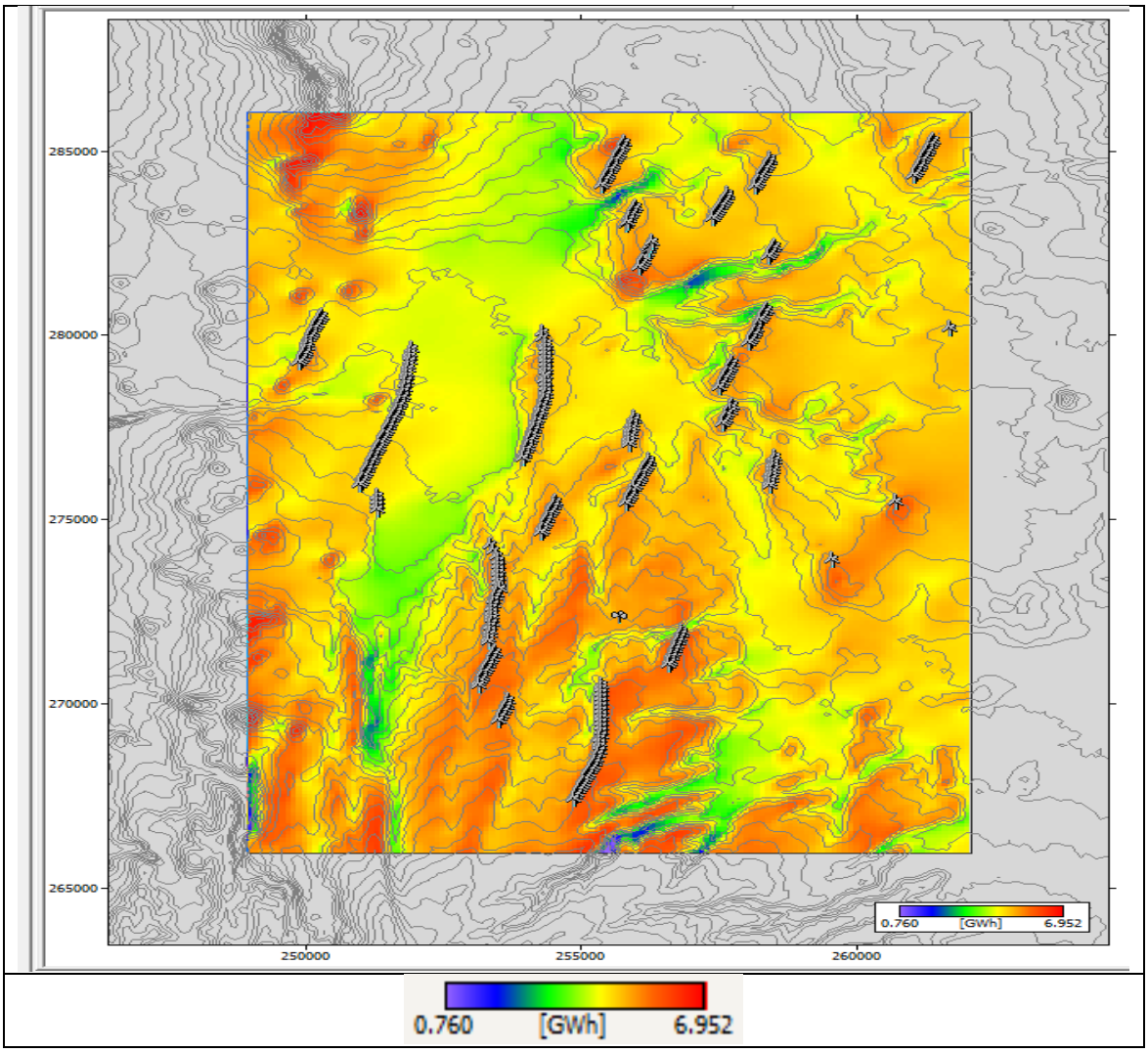

Figure 5.28: Annual Energy Production Map at 45 m wind turbine hub heights using Nyiru mast data.

Maximum Value:	6.952 GWh at (250200, 286000)
Minimum Value:	0.760 GWh at (255500, 266000)
Mean Value:	4.791 GWh

5.2.1.3 Sirima Regional wind climate summary

Table 5.7 presents WAsP mean and emergent wind speed using wind data collected at Sirima mast before factoring in topography.

Table 5.7: Results from the observed wind climate in WAsP. The emergent wind speeds are the weighted sums of the Weibull distributions in all directions.

Parameter	Measured	Emergent	Discrepancy
Mean wind speed [m/s]	11.10	11.06	-0.4%
Mean power density [W/m²]	952	953	0.2%

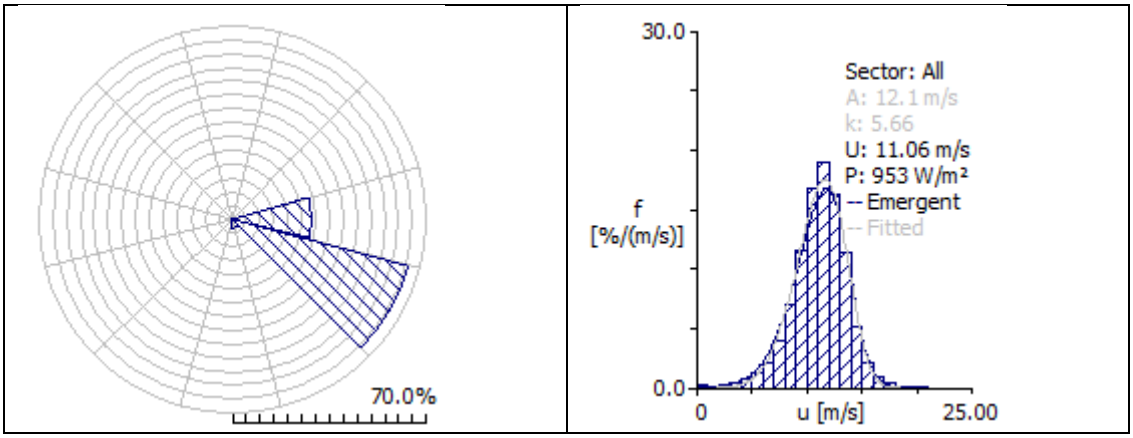

Figure 5.29: Wind Rose for the annual data collected at Sirima meteorological mast and wind speed distribution (Weibull) for all sectors (wind directions) from WAsP.

Table 5.8: Lake Turkana regional wind climate using Sirima data.

Height	Parameter	0.00 m	0.02 m	0.10 m	0.40 m	1.50 m
20.0 m	Weibull A [m/s]	12.37	9.64	8.25	6.76	5.58
	Weibull k	5.39	4.96	4.90	4.91	4.87
	Mean speed U [m/s]	11.40	8.85	7.56	6.20	5.12
	Power density E [W/m²]	1030	490	308	169	95
40.0 m	Weibull A [m/s]	13.20	10.89	9.54	8.11	6.99
	Weibull k	5.53	5.31	5.20	5.18	5.11
	Mean speed U [m/s]	12.19	10.03	8.78	7.46	6.43
	Power density E [W/m²]	1252	704	474	291	187
45.0 m	Weibull A [m/s]	13.35	11.13	9.78	8.36	7.25
	Weibull k	5.56	5.40	5.27	5.24	5.16
	Mean speed U [m/s]	12.33	10.26	9.01	7.69	6.67
	Power density E [W/m²]	1294	750	510	318	208
70.0 m	Weibull A [m/s]	13.97	12.11	10.75	9.33	8.24
	Weibull k	5.52	5.83	5.63	5.55	5.44
	Mean speed U [m/s]	12.90	11.21	9.93	8.62	7.60
	Power density E [W/m²]	1482	964	675	442	304

90.0 m	Weibull A [m/s]	14.35	12.78	11.37	9.93	8.84
	Weibull k	5.48	5.85	5.85	5.80	5.65
	Mean speed U [m/s]	13.24	11.84	10.53	9.20	8.18
	Power density E [W/m²]	1608	1135	798	532	376

Results for mean wind speed, power density, annual energy production and RIX using Sirima data are presented in the following sections.

Mean Speed

Figure 5.30 show the wind speed resource map at 45 m hub height with contour lines and proposed turbine locations. The wind speed ranges from a minimum of 5.93 m/s, represented by the blue colour on the map, to a maximum value of 16.20 m/s represents by the red colour. The mean wind speed was 10.19 m/s, according to the WASP 11 Wind Atlas Calculations.

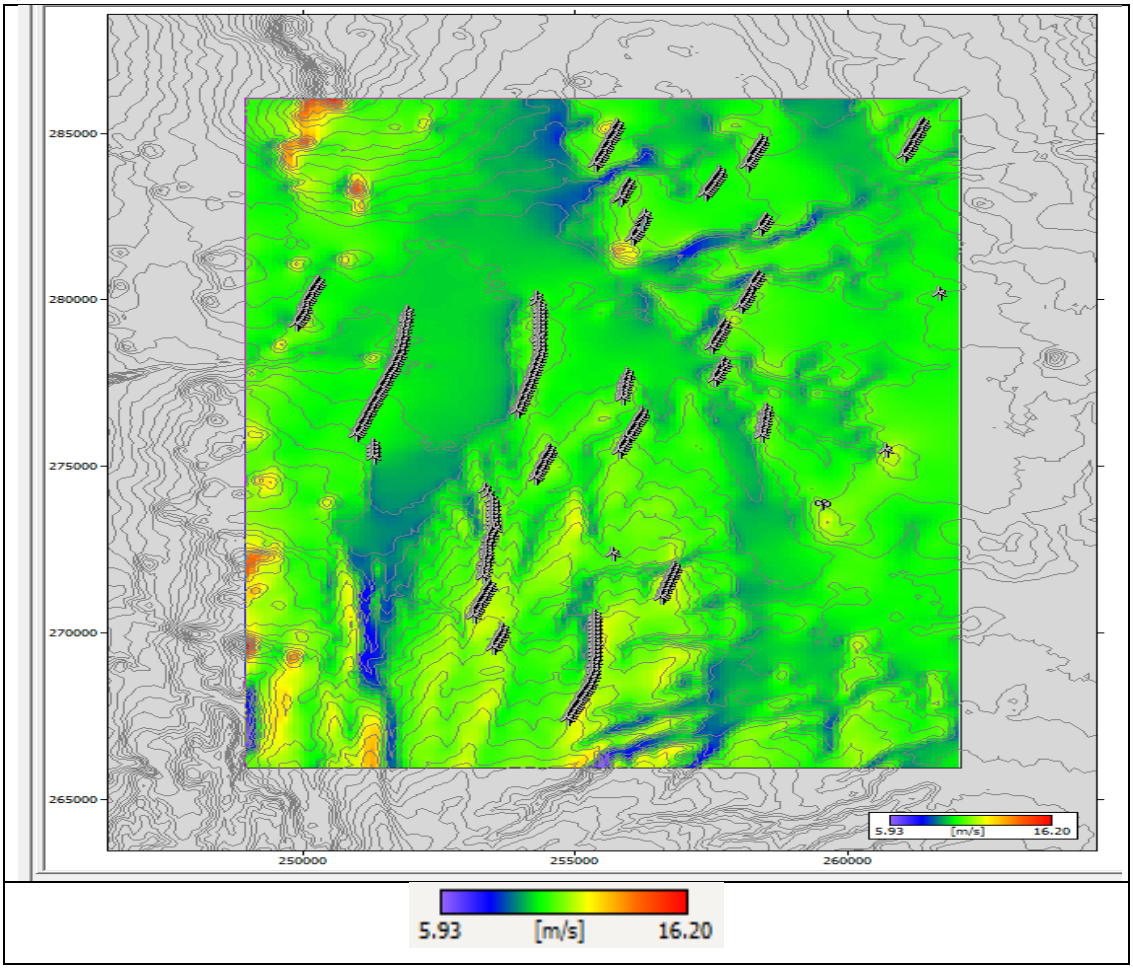

Figure 5.30: Wind speed Resource Map at 45 m wind turbine height using Sirima mast data.

Maximum Value:	16.20 m/s at (249000, 269600)
Minimum Value:	5.93 m/s at (249000, 266800)
Mean Value:	10.19 m/s

Power Density

Similar to the wind speed resource map, figure 5.31 show the analysis result for the site power density at 45 m hub height with contour lines and proposed turbine locations. According to the WAsP 11 Wind Atlas calculations, the mean value for the power density production was 751 W/m².

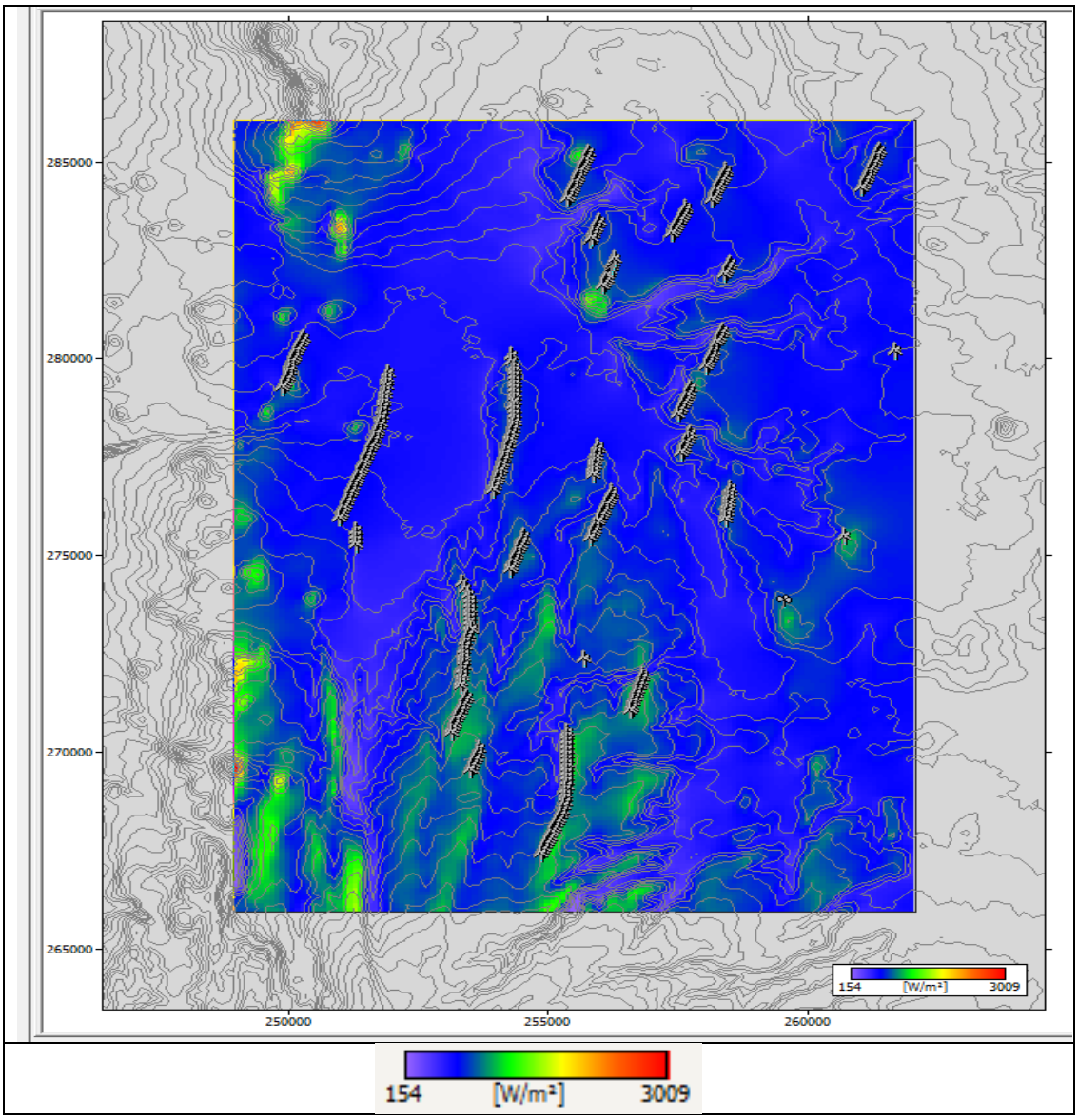

Figure 5.31: Power density Map at 45 m wind turbine hub heights using Sirima mast data.

Maximum Value:	3009 W/m² at (249000, 269600)
Minimum Value:	154 W/m² at (249000, 266800)
Mean Value:	751 W/m²

Annual Energy Production (AEP)

Similar to the wind speed and power density resource maps, the figure 5.32 shows the analysis result for the site Annual energy production at 45 m hub height.

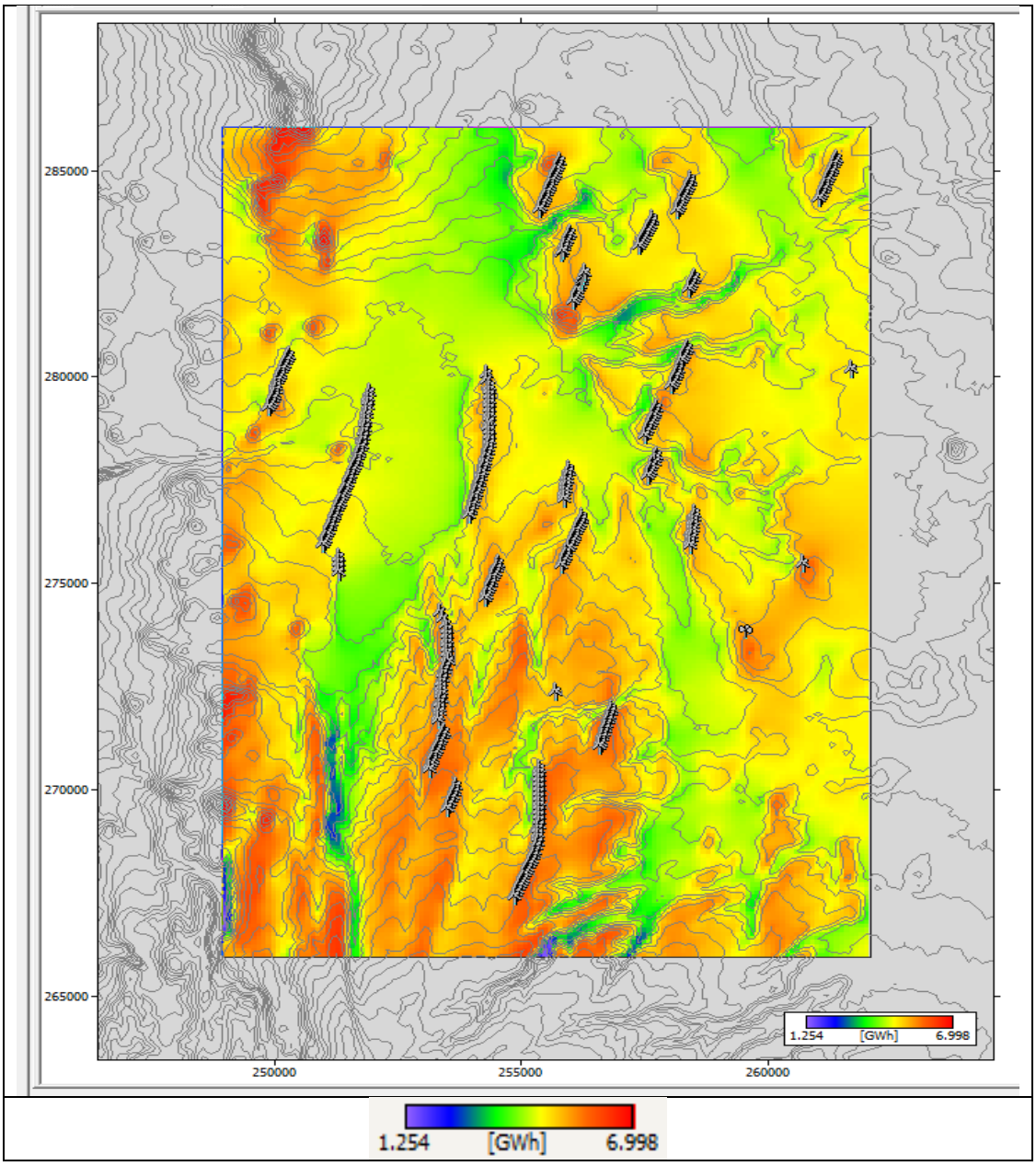

Figure 5.32: Annual Energy Production Map at 45 m wind turbine hub heights using Sirima mast data.

Maximum Value:	6.998 GWh at (249000, 269600)
Minimum Value:	1.254 GWh at (249000, 266800)
Mean Value:	4.825 GWh

5.2.2 Accuracy of WAsP simulations

Simulations of the mean wind speeds and wind power densities using data measured at the three sites (Kalkumpei, Nyiru and Sirima) by WAsP 11 are presented in Table 5.9. Note that the values presented in table 5.9 are WAsP simulations after factoring in topography while values in tables 5.3, 5.5 and 5.7 are observed mean wind speeds.

Table 5.9: Score tables for simulations at Lake Turkana using 3 masts. Top row contains the reference sites, left-hand column the predicted sites. Upper table: mean wind speeds and mean wind power densities. Lower table: percentage differences between predicted and measured wind speeds and power densities.

Site		Kalkumpei	Nyiru	Sirima	Measured
Kalkumpei	m/s	10.65	9.82	9.73	10.25
	W/m^2	862	665	644	792
Nyiru	m/s	11.29	10.69	10.65	10.75
	W/m^2	1026	853	840	871
Sirima	m/s	11.64	11.00	11.24	11.10
	W/m^2	1131	936	988	952
Site		Kalkumpei	Nyiru	Sirima	Measured
Kalkumpei	m/s	-3.90	4.19	5.07	0
	W/m^2	-8.83	16.03	18.68	0
Nyiru	m/s	-5.02	0.55	0.93	0
	W/m^2	-17.79	2.06	3.55	0
Sirima	m/s	-4.86	0.90	-1.26	0
	W/m^2	-18.80	1.68	-3.78	0

Similar simulations were reported by (Bowen and Mortensen, 2004) using WAsP 11. The errors vary in sign and are sometimes large. However, good simulations are obtained for site pair combinations involving Nyiru and Sirima mast locations, including all the self-prediction cases.

5.3 Combined mesoscale and microscale modelling results

The combined mesoscale and microscale modelling results are presented in this section. WRF data from simulation 6 described in section 5.1.3 was used as an input into WAsP model. A script was used to extract wind speed and direction at a specific latitude and longitude corresponding to the 3 mast locations from the nearest WRF

output grid cell. The roughness lengths described in section 5.2.1 are also used in this section together with the topography map described in section 4.2.1.3.2. The results of this analysis are described in the sections below.

5.3.1 Kalkumpei Regional wind climate summary using WRF simulated data

Table 5.10 presents WAsP mean and emergent wind speed using WRF simulated wind data at Kalkumpei mast before factoring in topography.

Table 5.10: Results from WRF simulated data at Kalkumpei in WAsP. The emergent wind speeds are the weighted sums of the Weibull distributions in all directions.

Parameter	Measured	Emergent	Discrepancy
Mean wind speed [m/s]	10.46	10.36	-0.9%
Mean power density [W/m²]	777	779	0.2%

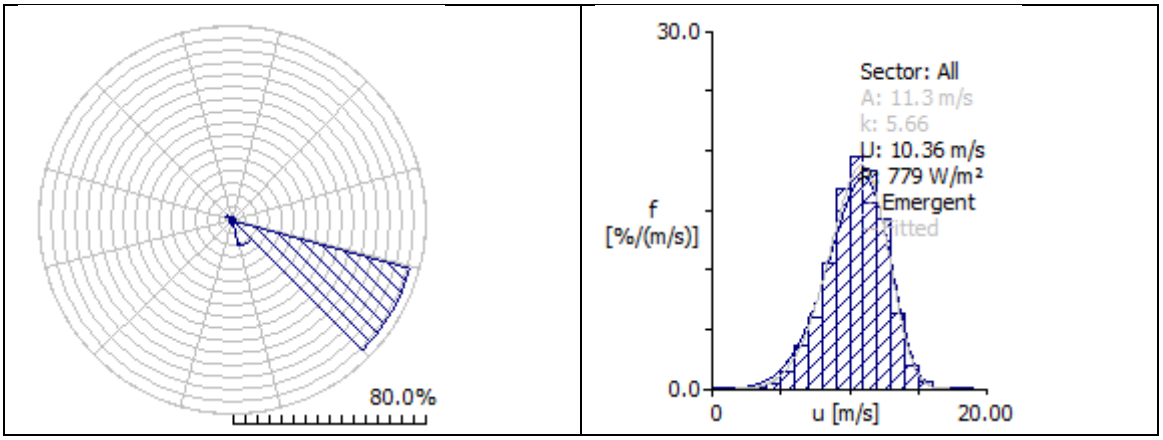

Figure 5.33: Wind Rose for the annual WRF simulated data at Kalkumpei and wind speed distribution (Weibull) for all sectors (wind directions) from WAsP.

Table 5.11: Lake Turkana regional wind climate using WRF simulated data at Kalkumpei.

Height	Parameter	0.00 m	0.02 m	0.10 m	0.40 m	1.50 m
20.0 m	Weibull A [m/s]	13.00	10.14	8.68	7.11	5.88
	Weibull k	5.35	4.90	4.90	4.76	4.72
	Mean speed U [m/s]	11.98	9.30	7.96	6.51	5.38
	Power density E [W/m²]	1197	572	359	197	112
40.0 m	Weibull A [m/s]	13.86	11.41	10.01	8.51	7.34
	Weibull k	5.47	5.22	5.18	4.99	4.93
	Mean speed U [m/s]	12.79	10.50	9.21	7.81	6.74
	Power density E [W/m²]	1450	811	547	337	217
45.0 m	Weibull A [m/s]	14.02	11.65	10.25	8.76	7.60
	Weibull k	5.50	5.30	5.24	5.05	4.98

	Mean speed U [m/s]	12.94	10.73	9.44	8.05	6.98
	Power density E [W/m²]	1498	862	588	367	241
70.0 m	Weibull A [m/s]	14.64	12.63	11.23	9.75	8.62
	Weibull k	5.49	5.69	5.57	5.32	5.22
	Mean speed U [m/s]	13.51	11.68	10.37	8.98	7.93
	Power density E [W/m²]	1707	1094	770	505	349
90.0 m	Weibull A [m/s]	15.02	13.28	11.84	10.36	9.23
	Weibull k	5.46	5.77	5.80	5.53	5.40
	Mean speed U [m/s]	13.86	12.29	10.96	9.57	8.52
	Power density E [W/m²]	1846	1273	902	605	429

Results for mean wind speed, power density and annual energy production using WRF simulated data at Kalkumpei are presented in the following sections.

Mean Speed

Figure 5.34 shows the wind speed resource map at 45 m hub height with contour lines and proposed turbine locations. The wind speed ranges from a minimum of 5.49 m/s, represented by the blue colour on the map, to a maximum value of 16.39 m/s represents by the red colour. The mean wind speed was 10.66 m/s, according to the WASP 11 Wind Atlas Calculations.

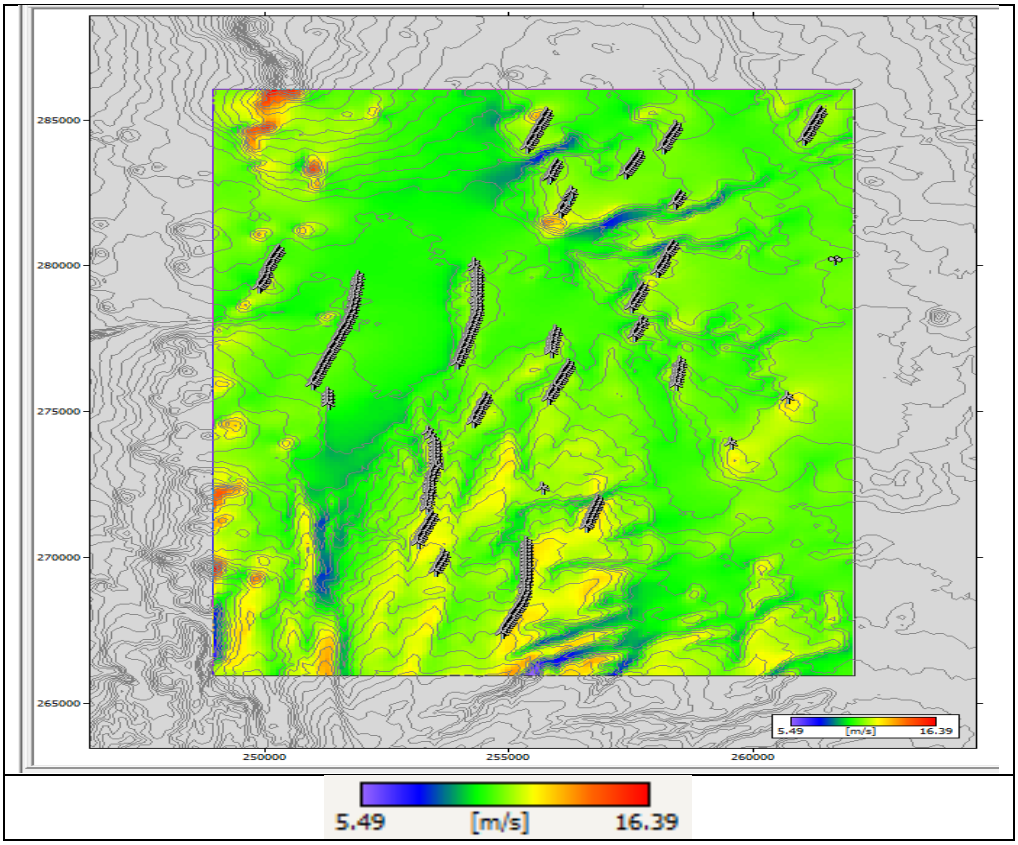

Figure 5.34: Wind speed Resource Map at 45 m wind turbine height using WRF simulated data at Kalkumpei.

Maximum Value:	16.39 m/s at (250200, 286000)
Minimum Value:	5.49 m/s at (255500, 266000)
Mean Value:	10.66 m/s

Power Density

Similar to the wind speed resource map, figure 5.35 show the analysis result for the site power density at 45 m hub height with contour lines and proposed turbine locations. According to the WAsP 11 Wind Atlas calculations, the mean value for the power density production was 862 W/m².

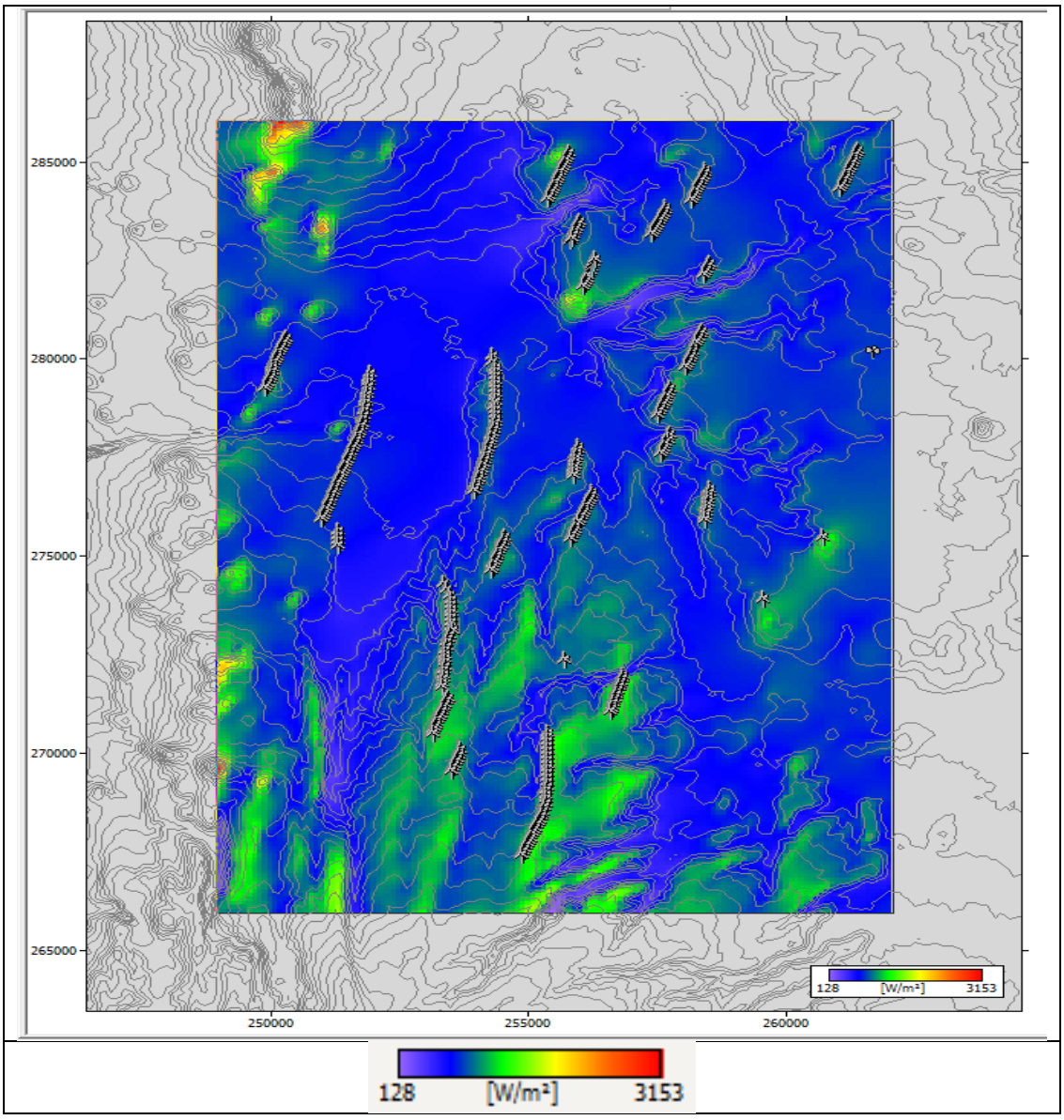

Figure 5.35: Power density Map at 45 m wind turbine hub heights using WRF simulated data at Kalkumpei.

Maximum Value:	3153 W/m² at (250200, 286000)
Minimum Value:	128 W/m² at (255500, 266000)
Mean Value:	862 W/m²

Annual Energy Production (AEP)

Similar to the wind speed and power density resource maps, the figure 5.36 shows the analysis result for the site Annual energy production at 45 m hub height.

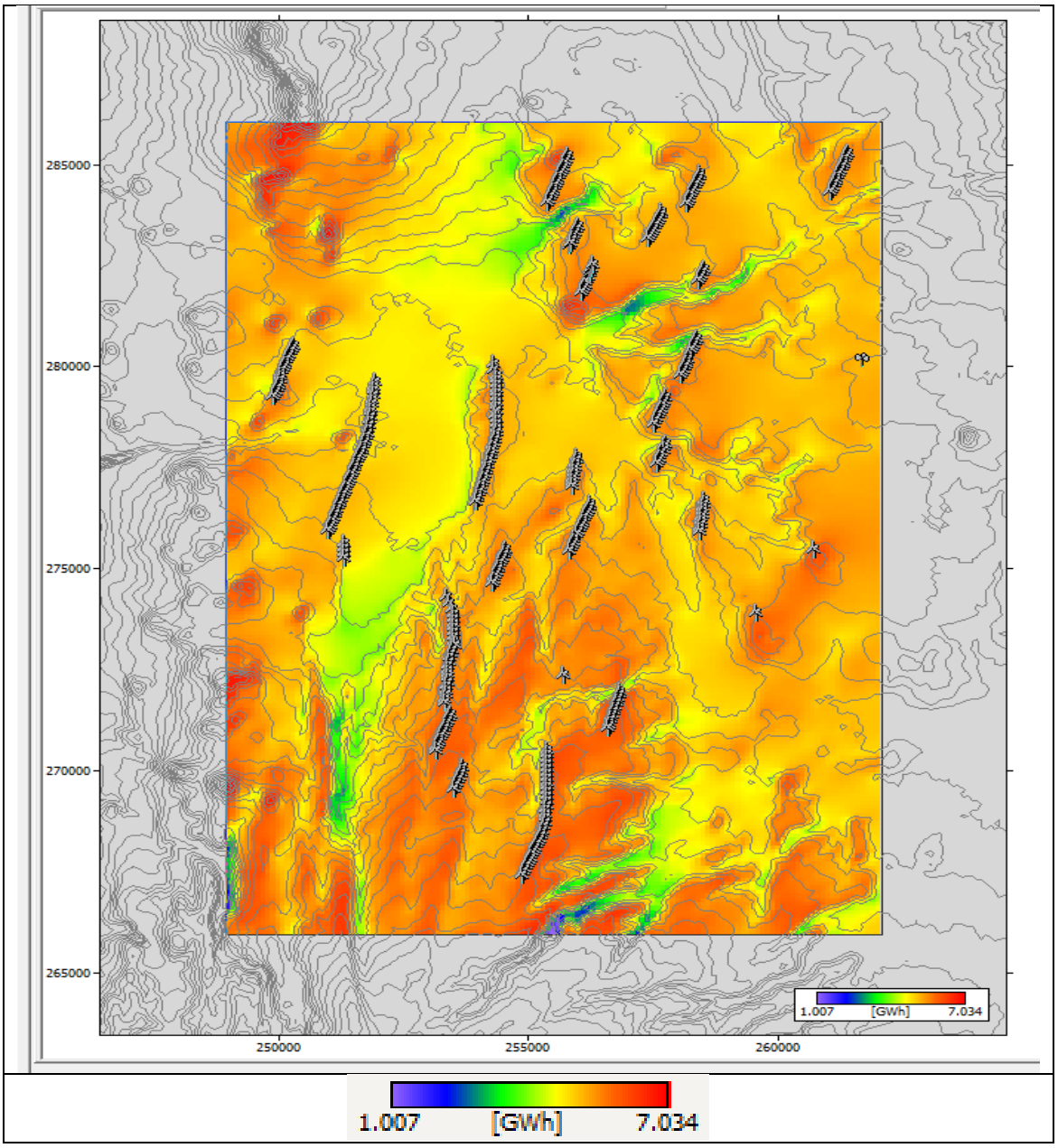

Figure 5.36: Annual Energy Production Map at 45 m wind turbine hub heights using WRF simulated data at Kalkumpei.

Maximum Value:	7.034 GWh at (249000, 269600)
Minimum Value:	1.007 GWh at (255500, 266000)
Mean Value:	5.141 GWh

5.3.2 Nyiru Regional wind climate summary using WRF simulated data

Table 5.12 presents WAsP mean and emergent wind speed using WRF simulated wind data at Nyiru mast before factoring in topography.

Table 5.12: Results from WRF simulated data at Nyiru in WAsP. The emergent wind speeds are the weighted sums of the Weibull distributions in all directions.

Parameter	Measured	Emergent	Discrepancy
Mean wind speed [m/s]	10.58	10.43	-1.4%
Mean power density [W/m²]	805	807	0.2%

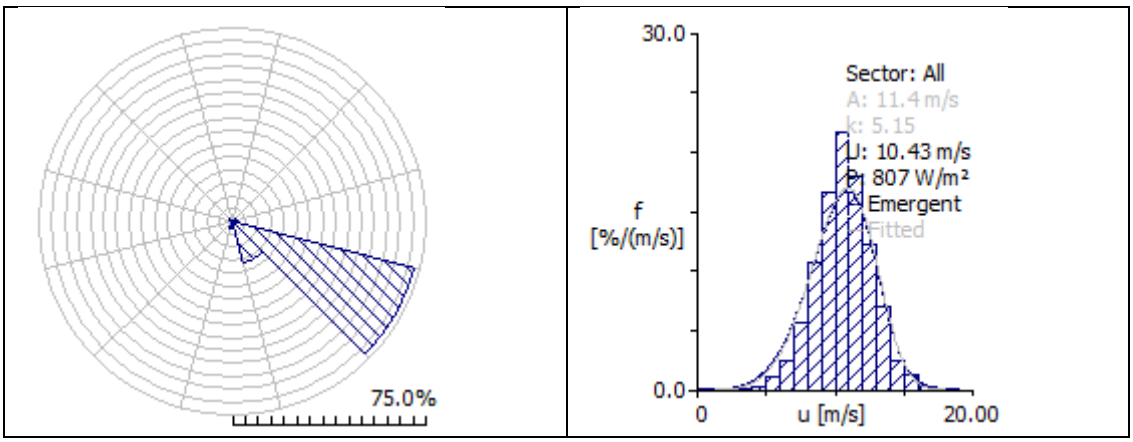

Figure 5.37: Wind Rose for the annual WRF simulated data at Nyiru and wind speed distribution (Weibull) for all sectors (wind directions) from WAsP.

Table 5.13: Lake Turkana regional wind climate using WRF simulated data at Nyiru.

Height	Parameter	0.00 m	0.02 m	0.10 m	0.40 m	1.50 m
20.0 m	Weibull A [m/s]	12.03	9.39	8.03	6.59	5.44
	Weibull k	4.84	4.54	4.28	4.62	4.44
	Mean speed U [m/s]	11.03	8.58	7.31	6.02	4.96
	Power density E [W/m²]	956	458	288	158	89
40.0 m	Weibull A [m/s]	12.85	10.62	9.29	7.92	6.82
	Weibull k	4.97	4.89	4.56	4.89	4.67
	Mean speed U [m/s]	11.79	9.74	8.48	7.26	6.23
	Power density E [W/m²]	1161	656	442	272	175
45.0 m	Weibull A [m/s]	12.99	10.85	9.52	8.16	7.06
	Weibull k	5.01	4.97	4.63	4.96	4.72
	Mean speed U [m/s]	11.93	9.96	8.70	7.49	6.46
	Power density E [W/m²]	1200	699	475	297	194

70.0 m	Weibull A [m/s]	13.59	11.81	10.46	9.11	8.03
	Weibull k	4.97	5.40	4.97	5.27	4.99
	Mean speed U [m/s]	12.48	10.89	9.60	8.39	7.37
	Power density E [W/m²]	1375	897	627	413	284
90.0 m	Weibull A [m/s]	13.97	12.48	11.06	9.71	8.62
	Weibull k	4.94	5.43	5.18	5.52	5.20
	Mean speed U [m/s]	12.82	11.51	10.18	8.96	7.94
	Power density E [W/m²]	1493	1058	739	498	350

Results for mean wind speed, power density and annual energy production using WRF simulated data at Nyiru are presented in the following sections.

Mean Speed

Figure 5.38 show the wind speed resource map at 45 m hub height with contour lines and proposed turbine locations. The wind speed ranges from a minimum of 5.49 m/s, represented by the blue colour on the map, to a maximum value of 16.39 m/s represents by the red colour. The mean wind speed was 10.66 m/s, according to the WASP 11 Wind Atlas Calculations.

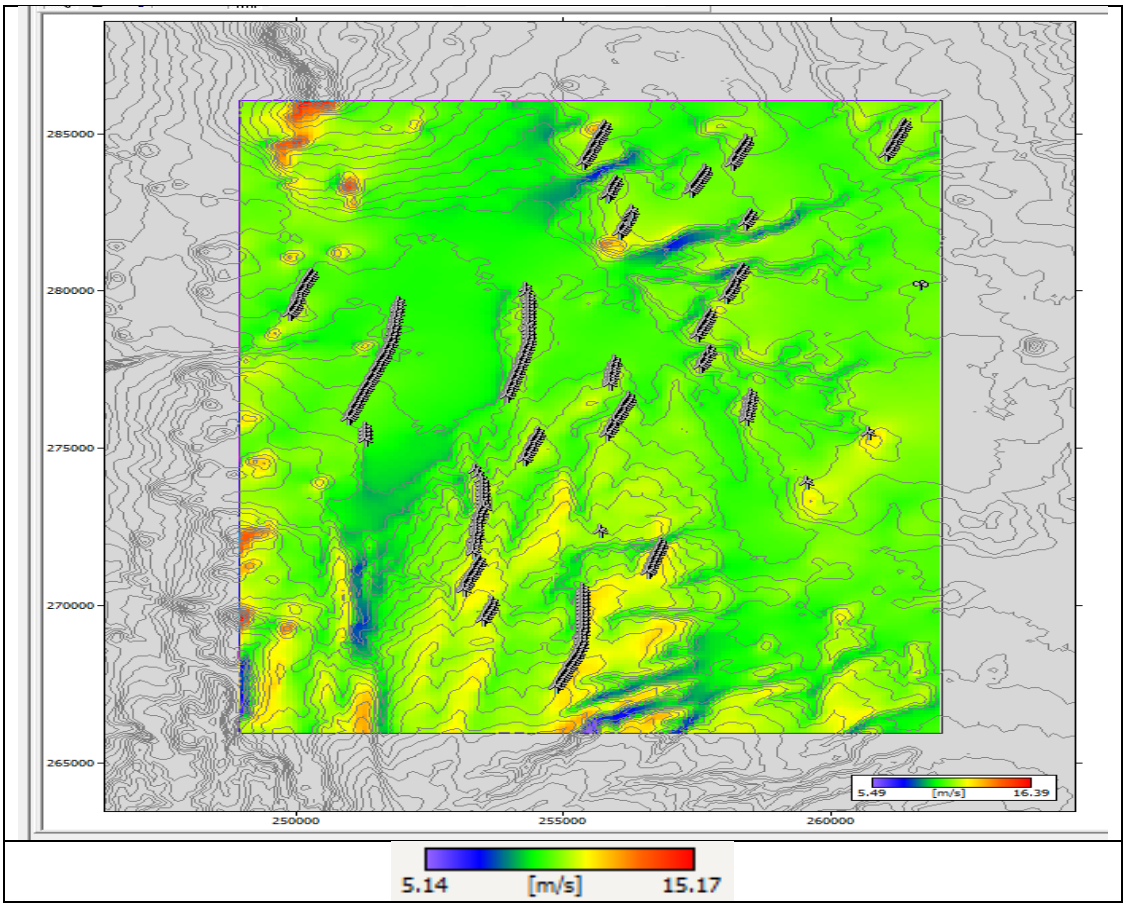

Figure 5.38: Wind speed Resource Map at 45 m wind turbine height using WRF simulated data at Nyiru.

Maximum Value:	15.17 m/s at (250200, 286000)
Minimum Value:	5.14 m/s at (255500, 266000)
Mean Value:	9.86 m/s

Power Density

Similar to the wind speed resource map, figure 5.39 show the analysis result for the site power density at 45 m hub height with contour lines and proposed turbine locations. According to the WAsP 11 Wind Atlas calculations, the mean value for the power density production was 691 W/m².

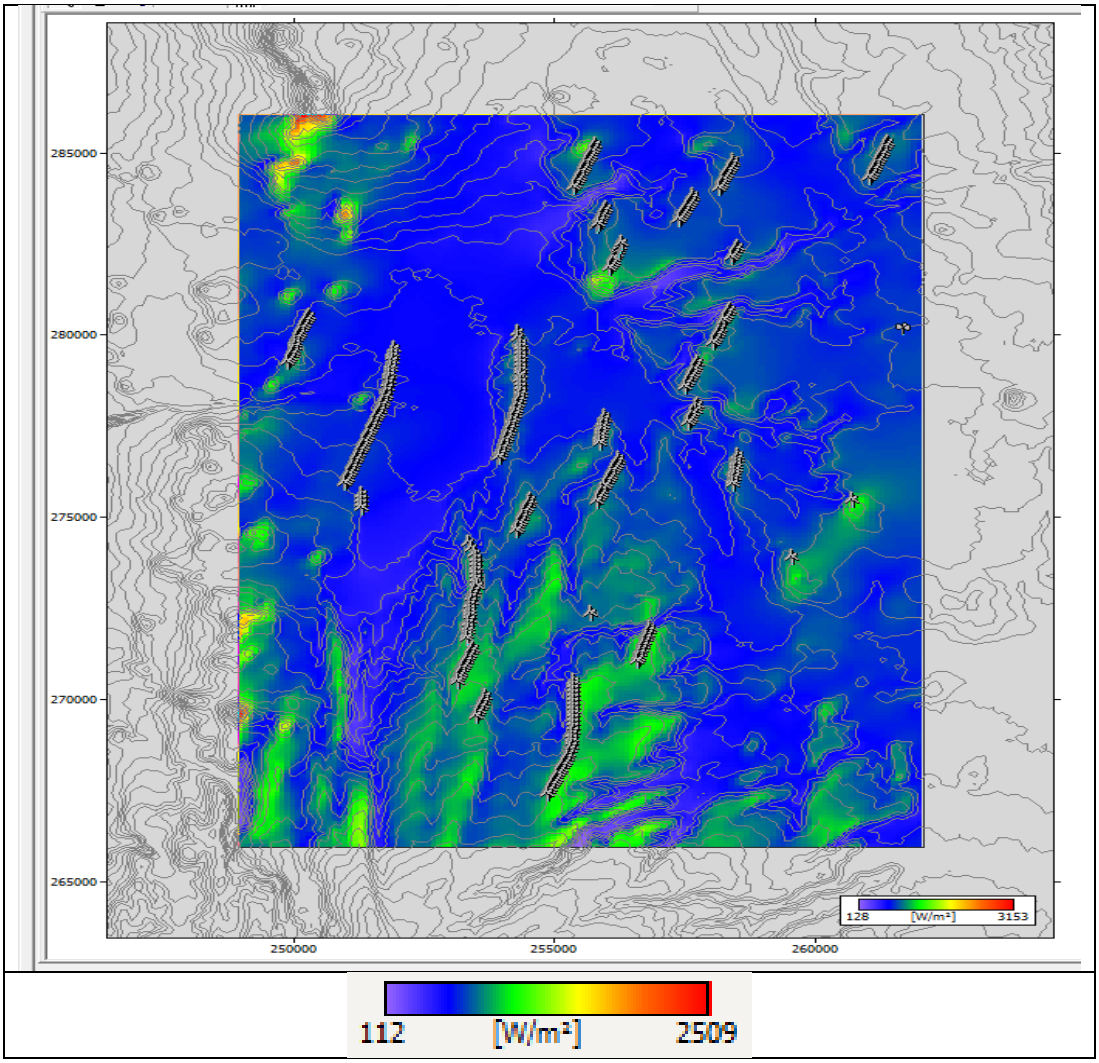

Figure 5.39: Power density Map at 45 m wind turbine hub heights using WRF simulated data at Nyiru.

Maximum Value:	2509 W/m² at (250200, 286000)
Minimum Value:	112 W/m² at (255500, 266000)
Mean Value:	691 W/m²

Annual Energy Production (AEP)

Similar to the wind speed and power density resource maps, the figure 5.40 shows the analysis result for the site Annual energy production at 45 m hub height.

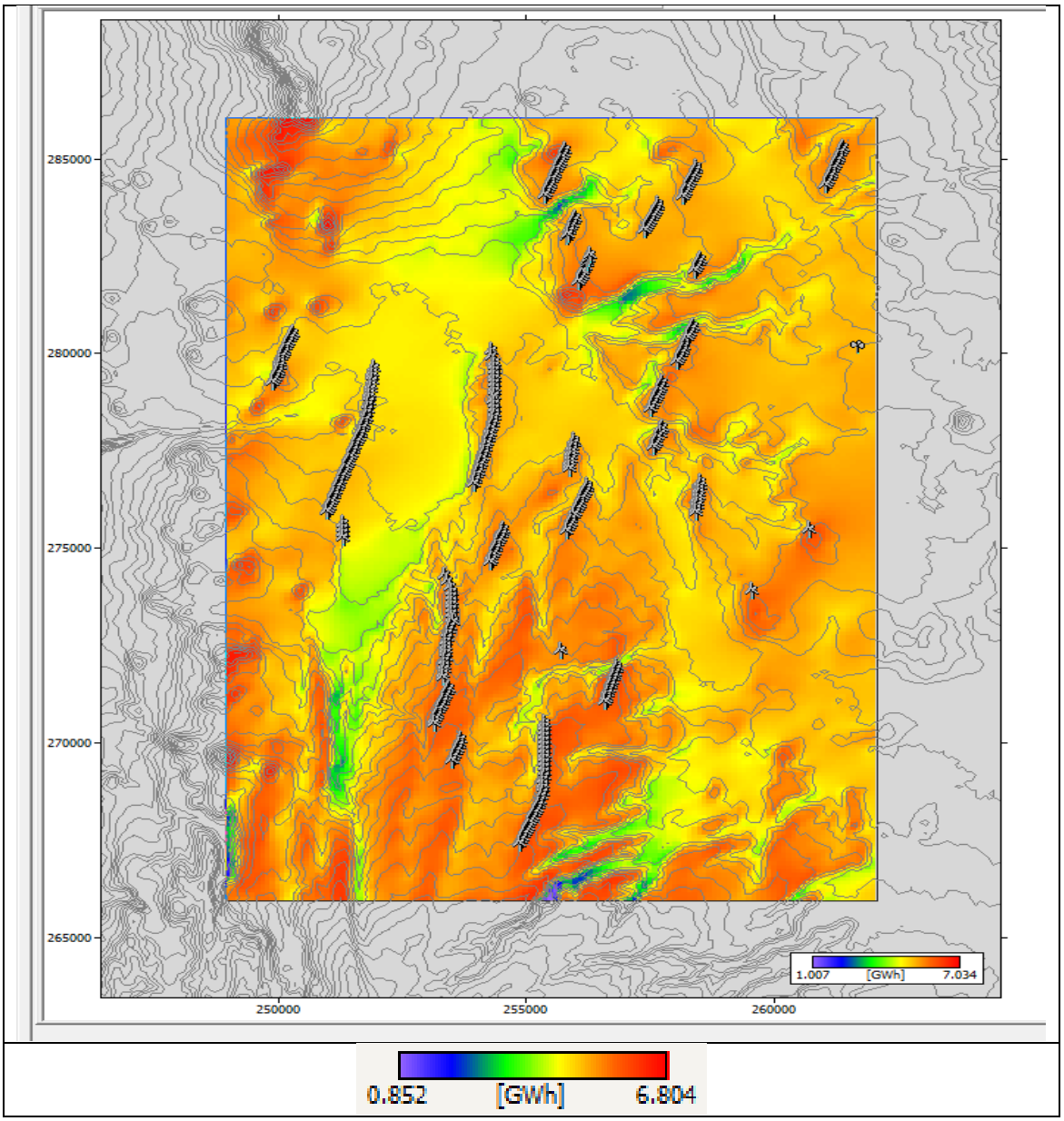

Figure 5.40: Annual Energy Production Map at 45 m wind turbine hub heights using WRF simulated data at Nyiru.

Maximum Value:	6.804 GWh at (249000, 269600)
Minimum Value:	0.852 GWh at (255500, 266000)
Mean Value:	4.520 GWh

5.3.3 Sirima Regional wind climate summary using WRF simulated data

Table 5.14 presents WAsP mean and emergent wind speed using WRF simulated wind data at Sirima mast before factoring in topography.

Table 5.14: Results from WRF simulated data at Sirima in WAsP. The emergent wind speeds are the weighted sums of the Weibull distributions in all directions.

Parameter	Measured	Emergent	Discrepancy
Mean wind speed [m/s]	9.57 m/s	9.49	-0.8%
Mean power density [W/m²]	602 W/m²	603 W/m²	0.2%

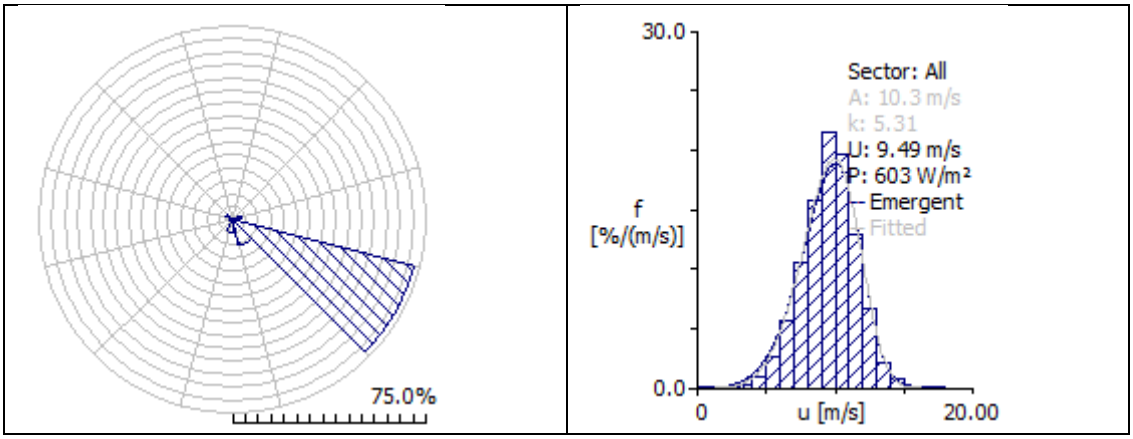

Figure 5.41: Wind Rose for the annual WRF simulated data at Sirima and wind speed distribution (Weibull) for all sectors (wind directions) from WAsP.

Table 5.15: Lake Turkana regional wind climate using WRF simulated data at Sirima.

Height	Parameter	0.00 m	0.02 m	0.10 m	0.40 m	1.50 m
20.0 m	Weibull A [m/s]	10.60	8.29	7.10	5.81	4.78
	Weibull k	5.00	4.57	4.45	4.19	4.05
	Mean speed U [m/s]	9.73	7.57	6.47	5.28	4.34
	Power density E [W/m²]	652	314	198	109	61
40.0 m	Weibull A [m/s]	11.35	9.45	8.26	7.01	6.02
	Weibull k	5.19	5.01	4.81	4.48	4.31
	Mean speed U [m/s]	10.44	8.67	7.57	6.39	5.48
	Power density E [W/m²]	798	461	310	191	121
45.0 m	Weibull A [m/s]	11.49	9.67	8.48	7.23	6.25

	Weibull k	5.20	5.13	4.90	4.55	4.37
	Mean speed U [m/s]	10.57	8.89	7.78	6.60	5.69
	Power density E [W/m²]	828	494	335	209	135
70.0 m	Weibull A [m/s]	12.07	10.62	9.38	8.11	7.13
	Weibull k	5.14	5.62	5.35	4.90	4.67
	Mean speed U [m/s]	11.10	9.82	8.65	7.44	6.52
	Power density E [W/m²]	961	651	450	293	200
90.0 m	Weibull A [m/s]	12.44	11.30	9.99	8.67	7.68
	Weibull k	5.09	5.57	5.50	5.17	4.90
	Mean speed U [m/s]	11.44	10.44	9.22	7.98	7.04
	Power density E [W/m²]	1053	785	542	356	248

Results for mean wind speed, power density and annual energy production using WRF simulated data at Sirima are presented in the following sections.

Mean Speed

Figure 5.42 show the wind speed resource map at 45 m hub height with contour lines and proposed turbine locations. The wind speed ranges from a minimum of 4.68 m/s, represented by the blue colour on the map, to a maximum value of 13.42 m/s represents by the red colour. The mean wind speed was 8.79 m/s, according to the WASP 11 Wind Atlas Calculations.

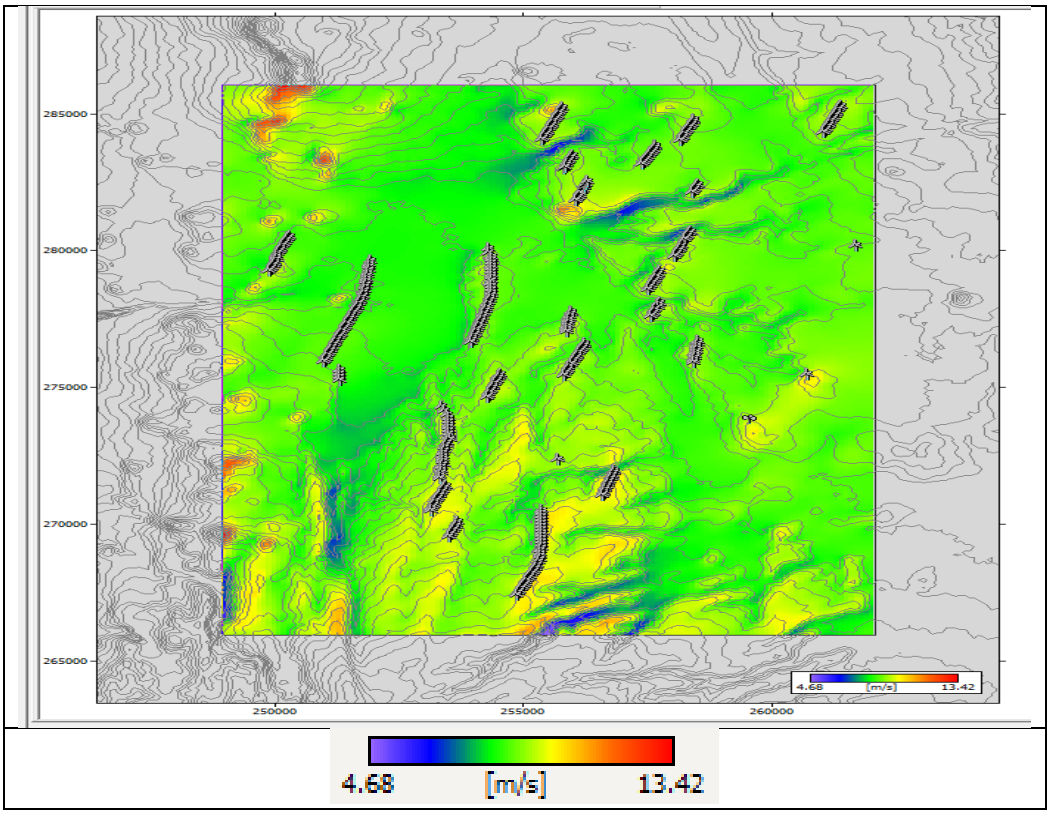

Figure 5.42: Wind speed Resource Map at 45 m wind turbine height using WRF simulated data at Sirima.

Maximum Value:	13.42 m/s at (250200, 286000)
Minimum Value:	4.68 m/s at (255500, 266000)
Mean Value:	8.79 m/s

Power Density

Similar to the wind speed resource map, figure 5.43 shows the analysis result for the site power density at 45 m hub height, the first figure with contour lines together with proposed turbine locations and the second is without contour lines. According to the WAsP 11 Wind Atlas calculations, the mean value for the power density production was 485 W/m².

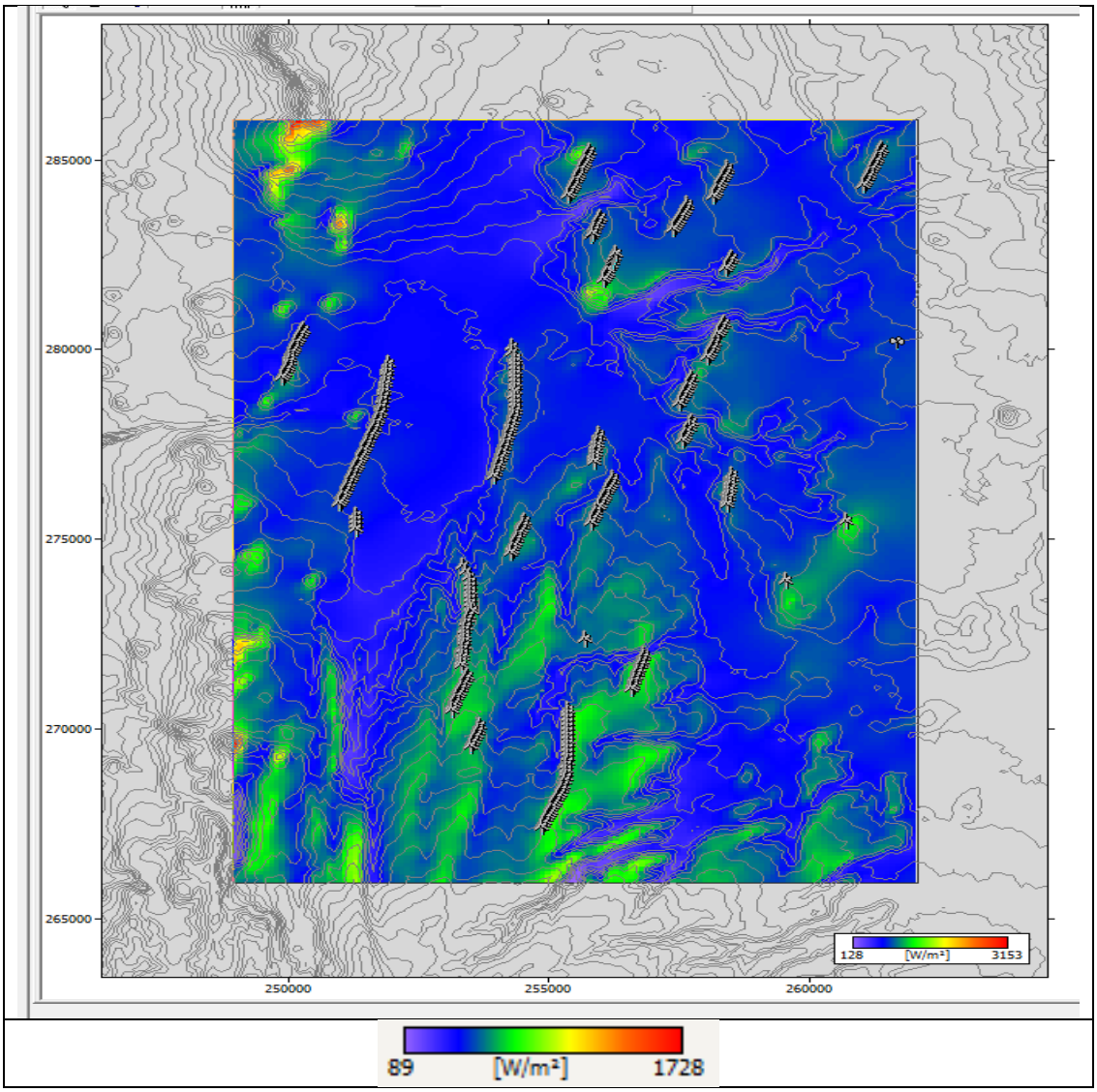

Figure 5.43: Power density Map at 45 m wind turbine hub heights using WRF simulated data at Sirima.

Maximum Value:	1728 W/m² at (250200, 286000)
Minimum Value:	89 W/m² at (255500, 266000)
Mean Value:	485 W/m²

Annual Energy Production (AEP)

Similar to the wind speed and power density resource maps, the figure 5.44 shows the analysis result for the site Annual energy production at 45 m hub height.

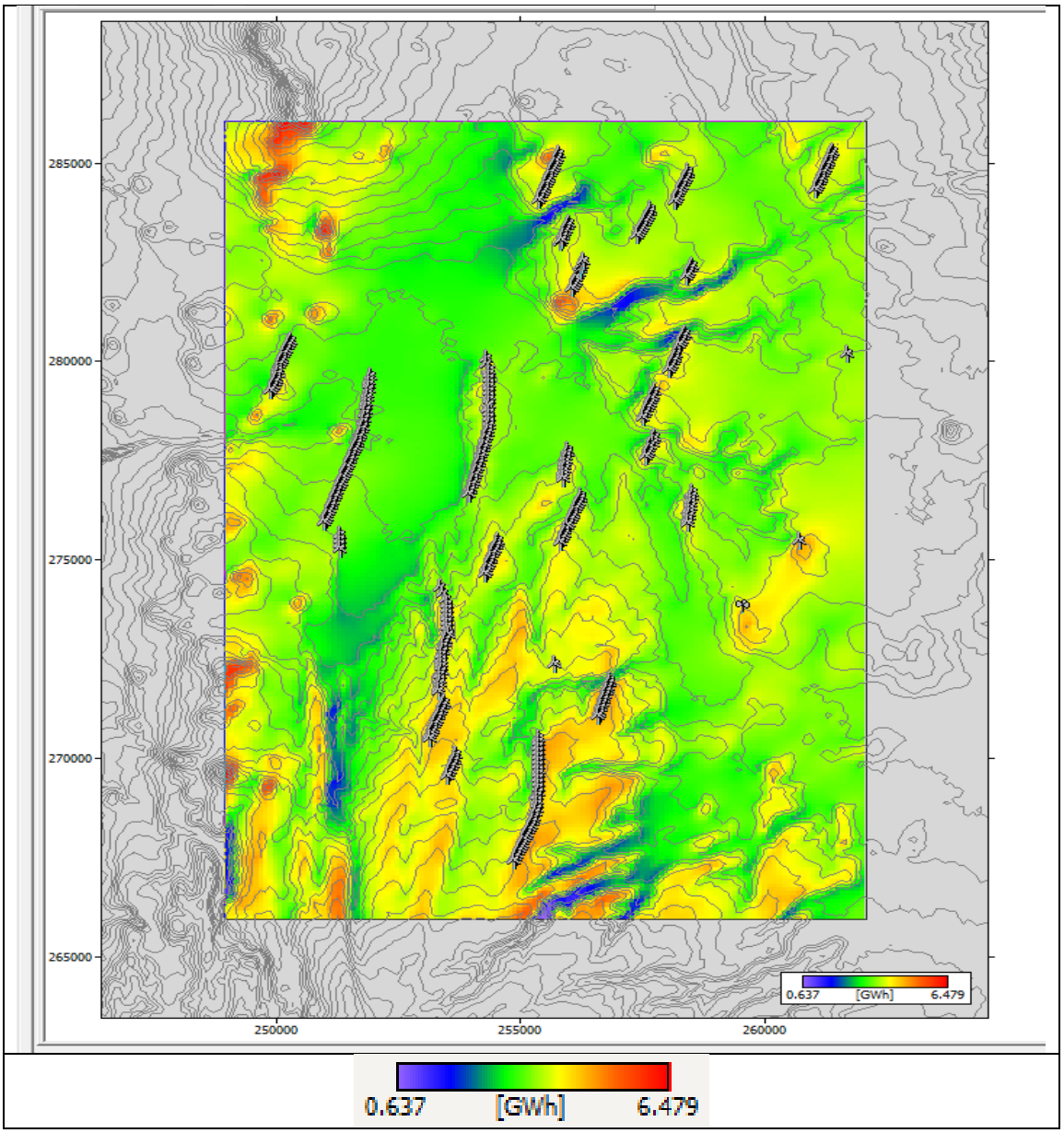

Figure 5.44: Annual Energy Production Map at 45 m wind turbine hub heights using WRF simulated data at Sirima.

Maximum Value:	6.479 GWh at (249000, 269600)
Minimum Value:	0.637 GWh at (255500, 266000)
Mean Value:	3.618 GWh

5.3.4 Accuracy of WRF-WAsP Simulations

Simulations of the mean wind speeds and wind power densities using WRF simulated data for three sites (Kalkumpei, Nyiru and Sirima) by WAsP 11 are presented in Table 5.16. Note that the values presented in table 5.16 are WAsP simulations after factoring in topography while values in tables 5.10, 5.12 and 5.14 are WRF simulated mean wind speeds.

Table 5.16: Score tables for WAsP 11 simulations at Lake Turkana, using WRF simulated winds at locations of the 3 masts. Top row contains the reference sites, left-hand column the predicted sites. Upper table: mean wind speeds and mean wind power densities. Lower table: percentage differences between predicted and measured wind speeds and power densities.

Site		Kalkumpei	Nyiru	Sirima	simulated
Kalkumpei	m/s	10.64	9.56	8.50	10.46
	W/m^2	843	624	435	777
Nyiru	m/s	11.26	10.38	9.30	10.58
	W/m^2	998	796	565	805
Sirima	m/s	11.54	10.65	9.71	9.57
	W/m^2	1084	862	643	602

Site		Kalkumpei	Nyiru	Sirima	simulated
Kalkumpei	m/s	-1.72	8.60	18.73	0
	W/m^2	-8.49	19.69	44.01	0
Nyiru	m/s	-6.42	1.89	12.09	0
	W/m^2	-23.97	1.11	29.81	0
Sirima	m/s	-20.58	-11.28	-1.46	0
	W/m^2	-80.06	-43.18	-6.81	0

When considering the overall mean wind speed presented in figures 5.26, 5.30, 5.33, 5.36, 5.39 and 5.42 and the statistical comparisons presented in table 5.16, WRF simulated wind dataset at Nyiru was the best representation of the 45 m wind climate to use in the WAsP model (in absence of actual wind data).

5.3.4.1 Evaluating WAsP mean wind speed using LIDAR data.

A simulation was designed to use the high resolution spatial data discussed in section 3.6 to validate WAsP and WRF-WAsP mean wind speed maps. WAsP was run for

15 days between 11th and 24th July 2009. Using the LIDAR data, 1139 virtual masts were designed within Lake Turkana wind farm. The virtual masts represent the locations of LIDAR wind speed data points that were used to validate simulated wind speeds from WAsP and WRF-WAsP. Figure 5.45 shows the Lake Turkana wind farm domain with the virtual wind turbine locations. The location of the LIDAR was 260743.2 Easting and 275307.7Northing.

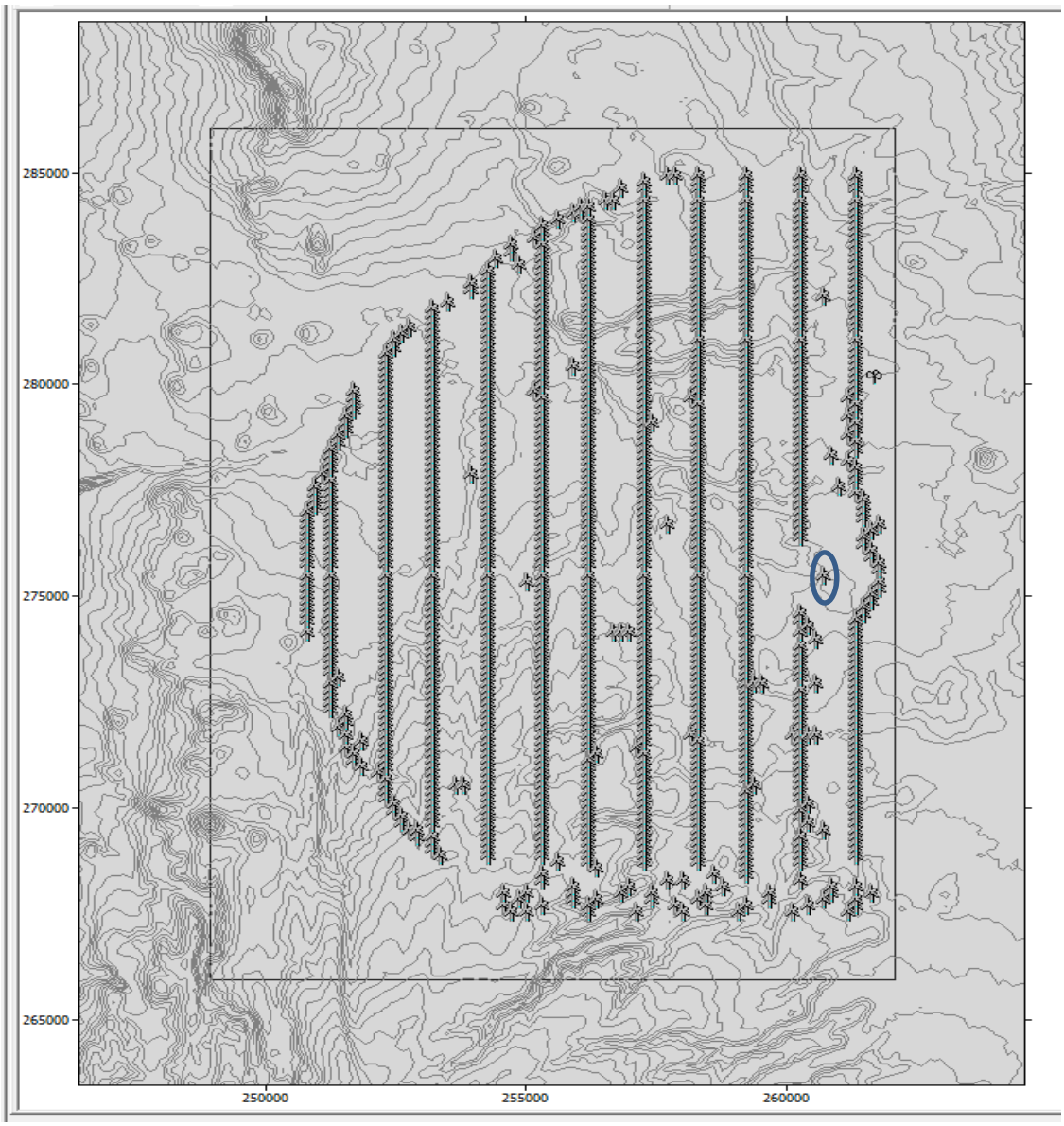

Figure 5.45: Location of the virtual masts and position of LIDAR (circled in blue).

The results for this evaluation exercise of WAsP mean wind speed map are given below.

Table 5.17: Error statistics between wind speed data generated by WAsP using observed data and LIDAR data. The first table contains ME results, the second contains RMSE results and the last contains IOA results.

ME

LIDAR - WAsP (Using Kalkumpei mast data)	-0.33 m/s
LIDAR - WAsP (Using Nyiru mast data)	0.16 m/s
LIDAR - WAsP (Using Sirima mast data)	0.63 m/s

RMSE

LIDAR - WAsP (Using Kalkumpei mast data)	1.06 m/s
LIDAR - WAsP (Using Nyiru mast data)	0.85 m/s
LIDAR - WAsP (Using Sirima mast data)	1.09 m/s

IOA

LIDAR - WAsP (Using Kalkumpei mast data)	0.46
LIDAR - WAsP (Using Nyiru mast data)	0.61
LIDAR - WAsP (Using Sirima mast data)	0.53

Evaluating WAsP mean wind speed map using LIDAR data shows that Nyiru station provides the best data to model mean wind speed over Lake Turkana wind farm domain with a mean difference of 0.16 m/s, RMSE of 0.85 m/s and IOA of 0.61 (table 5.17). Tables 5.9 and 5.16 show results from cross prediction using observed and WRF simulated data respectively. The results presented in these tables also indicate that observed data at Nyiru mast and WRF simulated data at Nyiru provide the best dataset for micro scale modelling using WAsP.

6. CHAPTER 6

This chapter provides conclusions from the study with special emphasis on LIDAR and wind resource assessment, WRF modelling, WAsP modelling and the combined WRF and WAsP modelling work. Recommendations are presented at the end of the chapter.

6.1 LIDAR and wind resource assessment

LIDAR was used to investigate the near surface wind field structure at the Lake Turkana wind farm site with the principal output being a 45 m terrain following mean wind speed map. Significant effort was directed towards verifying the accuracy of the LIDAR wind speeds using anemometer data at 3 mast location. Validation results showed an accuracy of less than 0.5 m/sec in the derived wind speed measurements. This outcome provided evidence that the selected range gates size and scanning strategy were appropriate for this region.

The processed data was presented as a series of 2D and 3D wind speed colour plots overlaid on a digital terrain model and presented in section 3.6.1. The analysis showed that the error margins of the instrument and the data post processing technique were within acceptable limits for wind resource assessment. These outputs can be used to make decisions initially regarding location of meteorological masts at the start of a wind resource assessment campaign and also the location of wind turbines. However, this terrain following mean wind speed map was used for verifying the outputs from WAsP model in this study as summarized in sections 6.3 and 6.4 below.

6.2 WRF modelling

The main aim for this section in this study was to assess if wind data from specific locations of the modelled region could be successfully used in the high-resolution industry-standard wind energy assessment model, WAsP, when no actual reliable wind data were available.

WRF model was run for one-year period (2009) at Lake Turkana region with three nested domains. The main domain had horizontal resolution of 18km and the two nested domains had 6km and 2km respectively. The wind farm was located within the third domain. Yonsei State University PBL scheme produced the best annual

statistics for Lake Turkana wind farm site because it incorporates a topographic correction (topo_wind=1). This correction improves surface wind biases using sub-grid variance and resolved topography to modify surface friction effect and enhanced flow at hill tops (Jiménez and Dudhia, 2012).

The annual mean error of 0.56 m/s computed at Sirima was a fairly big difference compared to 0.01 m/s and 0.16m/s at Kalkumpei and Nyiru respectively. This was partly attributed to the location of Sirima mast which was atop a very exposed ridgeline that can be subject to sporadic wind gusts and rapidly changing wind directions which can be difficult to model. Careful consideration should therefore be made when selecting the site to erect meteorological masts to avoid areas with exposed ridgelines, unless the whole region is covered with exposed ridgelines. New modelling approaches will have to be adopted in the latter case.

The results and validation analysis presented in sections 5.1.4 and 5.1.5 confirmed that WRF model can be used to generate wind data that may be applied directly in wind resource assessment at this complex topographic site. This outcome was consistent with the general conclusions by Emery et al., (2001).

6.3 WAsP modelling

The results presented in section 5.2 highlight some of the difficulties of modelling airflow in a complex terrain environment. Ruggedness index which is an objective measure of the extent of steep slopes in an area was not used as a measure of WAsP accuracy in this study because: Lake Turkana region is close to the equator thus the Coriolis force is very minimal and the wind direction is predominantly south-east. The RIX map (figure 5.24) also shows that the proposed turbine locations are in regions where RIX values are close to 0.

WAsP provides slightly different wind atlas maps when datasets from different masts are used. The mean wind speed over the wind farm domain was 10.72 m/s, 10.16 m/s and 10.19 m/s when observed data at Kalkumpei, Nyiru and Sirima was used respectively. Cross and self-prediction results indicate that Nyiru dataset was the most appropriate for WAsP modelling at this study site as discussed in section 5.2.2.

LIDAR data presented in section 3.6.1 provides a useful product for evaluating WAsP mean wind speed. This was achieved by creating virtual masts from the LIDAR data and comparing with data from WAsP model as discussed in section 5.3.4.1. Evaluating WAsP mean wind speed using LIDAR shows that Nyiru station provides the best data for WAsP modelling over Lake Turkana wind farm domain with a mean difference of 0.16 m/s, RMSE of 0.85 m/s and IOA of 0.61.

6.4 Combined mesoscale and microscale modelling

The overall aim of the combined mesoscale and microscale modelling work was to assess if wind data derived from the mesoscale model WRF, could be used as input to the microscale model WAsP to make reliable simulations of wind and energy for an area in complex terrain like the current study area. Wind data from WRF model was validated using observed data at 3 meteorological mast locations, the results are presented in section 5.1.4 and 5.1.5 and their conclusions in section 6.1.

It is relevant here to refer to conclusions made in the study by Bowen and Mortensen (1996), where it was suggested that accurate simulations using WAsP could be obtained provided that the following criteria are satisfied:

- Both the reference and predicted sites are subject to the same weather regime.
- The prevailing weather conditions are close to being neutrally stable.
- The terrain surrounding the reference and predicted sites is sufficiently gentle and smooth to ensure mostly attached flows.
- The reference data are reliable.

The use of mesoscale meteorological models to generate wind data can address some of the issues highlighted above, to make WAsP simulations more reliable. First, wind data can be obtained from appropriately located grid points so that the observed and predicted sites are subject to the same weather regimes. Another advantage using wind data from the prognostic model is that wind data can be obtained from sites of similar ‘ruggedness’ to the predicted site (or area).

The reliability of the reference data is a key component of a WAsP analysis. Obtaining wind data from a mesoscale meteorological model, that has limitations especially in complex terrain, could be argued as adding another level of uncertainty to the wind and energy simulations. However, it has been established that it is more

reliable to use this wind data than to use actual wind data from a site in a different climate or topographic environment (often some distance away from the potential wind farm site). The Karlsruhe Atmospheric Mesoscale Model (KAMM)/WAsP methodology follows a similar approach Petersen (1996) and Frank (2001)) when making wind and energy simulations.

WAsP computed domain mean wind speed using WRF simulated data at Kalkumpei, Nyiru and Sirima was 10.66 m/s, 9.86 m/s and 8.79 m/s respectively. The mean difference between these values and those presented in section 6.2 are 0.06 m/s, 0.3 m/s and 1.4 m/s respectively. However, cross and self-prediction results indicate that WRF simulated wind data at Nyiru was the most appropriate for WAsP modelling at this study site as shown in table 5.16.

This thesis has demonstrated that sophisticated computer models can be powerful tools for wind resource assessment. Awareness of model limitations and knowledge of airflow in complex terrain are also key requirements to consider when using models for resource assessment. The ability to obtain reliable wind data at sites where there are no actual wind measurements and use it to drive the higher resolution industry standard model, WAsP, could result in significant savings of both time and money for wind energy developers.

6.5 Recommendations

ALVPT software was used to retrieve wind speed and direction from the LIDAR data. Further studies to improve the performance of ALVPT software should be undertaken. Such improvements should enhance the use of LIDAR data in studying wind turbulence.

This study established that the winds are stronger at night to early morning. More work should be carried out to establish the relationship between wind speed at the wind farm and electricity demand in Kenya. This will ensure that the electricity that is generated is well utilised.

REFERENCES

Every reasonable effort has been made to acknowledge the owners of copyright material. I would be pleased to hear from any copyright owner who has been omitted or incorrectly acknowledged.

3TIER 2009. Bolivia Wind Atlas. Seattle, WA: 3TIER Environmental Forecast Group,.

Abild, J. 1994. Application of the wind atlas method to extremes of wind climatology.

Achberger, C., Ekström, M. and Bärring, L. 2002. Estimation of local near-surface wind conditions–a comparison of WASP and regression based techniques. *Meteorological Applications,* 9, 211-221.

Addison, J. F., Hunter, A., Bass, J. and Rebbeck, M. 2000. A Neural Network Version of the Measure Correlate Predict Algorithm for Estimating Wind Energy Yield. *13th International Congress on Condition Monitoring and Diagnostic Engineering,*. Houston, TX, 2000, .

Aguado, E., Burt, J. E., Rohli, R. V. and Schmidlin, T. W. 2007. *Understanding weather and climate,* Pearson Prentice Hall.

Albers, A. 2006. Evaluation of ZephIR. Deutsche WindGuard Consulting GmbH Report.

Anderson, Mike and Dugi K. A. 2004. A Review of MCP Techniques. RES Report 01327R00022.

Bailey, B. H. and Freedman, J. M. 2008. A Regional Assessment of the US Offshore Wind Energy Resource through the Use of Mesoscale Modeling. *Marine Technology Society Journal,* 42, 8-18.

Bailey, B. H., McDonald, S. L., Bernadett, D. W., Markus, M. J., and Elsholz, K. V .1997. Wind resource assessment handbook. *Albany-New York: AWS Scientific Inc*.

Barthelmie, R., Courtney, M., Højstrup, J. and Larsen, S. E. 1996. Meteorological aspects of offshore wind energy: Observations from the Vindeby wind farm. *Journal of Wind Engineering and Industrial Aerodynamics,* 62, 191-211.

Beaucage, P., Brower, M., Robinson, N., and Alonge, C. 2012. Overview of six commercial and research wake models for large offshore wind farms. *Proceedings of the European Wind Energy Associate (EWEA).*

Bechrakis, D. A., Deane, J. P. and McKeogh, E. J. 2004. Wind resource assessment of an area using short term data correlated to a long term data set. *Solar Energy,* 76, 725-732.

Berge, E., Gravdahl, A. R., Schelling, J., Tallhaug, L., and Undheim, O. 2006. Wind in complex terrain. A comparison of WAsP and two CFD-models. In *Proceedings from EWEC*.

Boccippio, D. J. 1995. A Diagnostic Analysis of the VVP Single-Doppler Retrieval Technique. *Journal of Atmospheric and Oceanic Technology,* 12, 230-248.

Botta, G., Castagna, R., Borghetti, M. and Mantegna, D. 1992. Wind analysis on complex terrain—The case of acqua spruzza. *Journal of Wind Engineering and Industrial Aerodynamics,* 39, 357-366.

Bowen, A. J. and Mortensen, N. G. 1996. Exploring the limits of WAsP: the Wind Atlas Analysis and Application Program. *1996 European Union Wind Energy Conference.* Gotenburg, Sweden.

Bowen, A. J. and Mortensen, N. G. 2004. *WAsP prediction errors due to site orography*.

Box, G. E., Jenkins, G. M. and Reinsel, G. C. 1994. *Time Series Analysis: Forecasting and Control,* Hoboken, New Jersey, USA, John Wiley and Sons.

Bradley, S., Antoniou, I., Von Hunerbein, S., De Noord, M. and Jorgensen, H. 2001. SODAR Calibration for Wind Energy Applications. Greater Manchester, UK.: University of Salford.

Bravo, M., Mira, T., Soler, M. and Cuxart, J. 2008. Intercomparison and evaluation of MM5 and Meso-NH mesoscale models in the stable boundary layer. *Boundary-Layer Meteorology,* 128, 77-101.

Brower, M. 2006. The Role of Wind Flow Modeling and Mapping. *AWEA and CanWEA Resource Assessment Workshop.* Syracuse, NY.

Brower, M., Zack, J., Bailey, B., Schwartz, M. and Elliott, D. 2004. 4.2 Mesoscale Modeling as a tool for Wind Resource Assessment and Mapping.

Burlando, M., Podestà, A., Villa, L., Ratto, C. F. and Cassulo, G. 2009. Preliminary estimate of the large-scale wind energy resource with few measurements available: The case of Montenegro. *Journal of Wind Engineering and Industrial Aerodynamics,* 97, 497-511.

Carvalho, D., Rocha, A., Gómez-Gesteira, M. and Santos, C. 2012. A sensitivity study of the WRF model in wind simulation for an area of high wind energy. *Environmental Modelling andamp; Software*, 33, 23-34.

Corbett, J. F., Ott, S., and Landberg, L. 2007. The new WAsP flow model: a fast linearized Mixed Spectral-Integration model applicable to complex terrain. In *European Wind Energy Conference and Exhibition*.

Corbett, J.-F., Ott, S. and Landberg, L. 2007. The new WAsP flow model: a fast, linearized Mixed Spectral-Integration model applicable to complex terrain. *2007 European Wind Energy Conference and Exhibition.*

CRC-CARE. 2010. Lake Turkana LIDAR Wind Field Assessment. Perth, Australia: CRC CARE.

Crook N.A., Didlake A., Sun J. and Zhang Y. 2005. Evaluating Various LIDAR-Based Wind Analysis Schemes Against Independent Observations. *2nd Symposium on LIDAR Atmospheric Applications.* San Diego, California.

Dey, C.H. 1998. *GRIB:* The WMO Format for the Storage of Weather Product Information and the Exchange of Weather Product Messages in Gridded Binary Form *as Used by NCEP Central Operations* (Vol. 388). NWS Office Note.

De Rooy, W. C. and Kok, K. 2004. A combined physical-statistical approach for the downscaling of model wind speed. *Weather and Forecasting*, 19, 485-495.

DEWI. 2010. Site-related Wind Potential Analysis and Energy Yield Assessment at the Site Lake Turkana, Kenya. Wilhelmshaven, Germany.: DEWI.

Djamai, M. and Merzouk, N. K. 2011. Wind farm feasibility study and site selection in Adrar, Algeria. *Energy Procedia* vol. 6, 136–142.

Dudhia, J. 1989. Numerical study of convection observed during the winter monsoon experiment using a mesoscale two-dimensional model. *Journal of the Atmospheric Sciences 46(20): 3077-3107.*

Elkinton, M. R. and McGowan, J. G. 2006. An Investigation of Wind-shear Models and Experimental Data Trends for Different Terrains. *Wind Engineering*, 30, 341-350.

Elliot, D. L., Holloday, C. G., Barchet, W. R., Foote, H. P. and Sandusky, W. F. 1986. Wind Energy Resource Atlas of the United States. Pacific Northwest Laboratory, Richland, Washington, National Renewable Energy Laboratory,

Golden, CO.: National Renewable Energy Laboratory, Golden, CO, Pacific Northwest Laboratory, Richland, Washington.

Emery, C., Tai, E. and Yarwood, G. 2001. Enhanced meteorological modeling and performance evaluation for two Texas ozone episodes. *prepared for the Texas Near Non-Attainment Areas through the Alamo Area Council of Governments", by ENVIRON International Corp, Novato, CA., http://www. tnrcc. state. tx. us/air/aqp/airquality_contracts. html# met01*.

Feuquay, L. F., Crescenti, G. H. and Celta, D. J. 2005. Validation Study of the Use of Wind Shear Exponents in Extrapolating Wind Speeds for Wind Resource Estimations. *13th Symposium on Meteorological Observations and Instrumentation.* Savannah, GA.

Finardi, S., Tinarelli, G., Faggian, P. and Brusasca, G. 1998. Evaluation of different wind field modeling techniques for wind energy applications over complex topography. *Journal of Wind Engineering and Industrial Aerodynamics*, 74, 283-294

Frank, H. and Landberg, L. 1997. Modelling the wind climate of Ireland. *Boundary-Layer Meteorology*, 85, 359-377.

Frank, H. P., Rathmann, N. G. O., Mortensen, N. G. and Landberg, L. 2001a. The numerical wind atlas, the KAMM/WAsP method. *Riso Tech. Rep. Riso-R-1252(EN).* Riso National Laboratory, Roskilde, Denmark.

Frank, H. P., Rathmann, O., Mortensen, N. G. and Landberg, L. 2001b. The numerical wind atlas-the KAMM/WAsP method.

Galperin, B., and Sukoriansky, S. 2010. Progress in turbulence parameterization for geophysical flows. In *The 3rd international workshop on Next-generation NWP models: bridging parameterization, explicit clouds, and large eddies. Seoul, Korea* (Vol. 5).

Gardner, P., Garrad, A., Jamieson, P., Snodin, H., Nicholls, G. and Tindal, A. 2004. Wind Energy - The Facts - Technology, vol. 1. European Wind Energy Association Report.

Giebel, G. and Sven-Erik G. 2004. Shear and stability in high met masts, and how WAsP treats it. In *Special topic conference: The science of making torque from wind*, pp. 356-363

Gustafson JR, W. I. and Leung, L. R. 2007. Regional downscaling for air quality assessment: A reasonable proposition? *Bulletin of the American Meteorological Society,* 88, 1215-1227.

Guzzi, R. and Justus, C. G. 1988. *Physical Climatology for Solar and Wind Energy: Miramare-Trieste, Italy, 21 Apr-16 May 1986,* World Scientific Publishing Company Incorporated.

Hanna, S. R. and Yang, R. 2001. Evaluations of mesoscale models' simulations of near-surface winds, temperature gradients, and mixing depths. *Journal of applied meteorology,* 40, 1095-1104.

Hannon S., Barr K., Novotny J., Oliver A., Bass J. and Anderson M. 2008. Large Scale Wind Resource Mapping Using A State-Of-The-Art 3D Scanning LIDAR. In *proceedings from European Wind Energy Conference and Exhibition*.

Holtslag, A. A. M. and Boville, B. A. 1993: Local versus non-local boundary layer diffusion in a global climate model, J. Climate, 6, 1825–1842.

Hong, S.-Y. 2007: Stable Boundary Layer Mixing in a Vertical Diffusion Scheme. The Korea Meteorological Society, fall conference, Seoul, Korea, Oct. 25-26.

Hong, S.-Y., and Pan H.-L. 1996: Nonlocal boundary layer vertical diffusion in a medium-range forecast model, Mon. Wea. Rev., 124, 2322–2339.

Hong, S.-Y., Noh, Y. and Dudhia, J. 2006. A New Vertical Diffusion Package with an Explicit Treatment of Entrainment Processes. *Monthly weather review 134(9): 2318-2341*.

Huffaker R. M., Jelalian A. V. and Thomson J. A. 1970. Laser-Doppler system for detection of aircraft trailing vortices. Proceedings of the IEEE 58, 322-326.

Hurley, P., Physick, W., Luhar, A. and Edwards, M. 2002. The Air Pollution Model (TAPM) Version 2. Part 2: Summary of some verification studies. *CSIRO Atmospheric Research Technical Paper,* 57.

Indeje, M. 2000. Predictions and Numerical Simulations of the regional climate of Equatorial Eastern Africa. PhD, North Carolina State University.

Jackson, P. and Hunt, J. 1975. Turbulent wind flow over a low hill. *Quarterly Journal of the Royal Meteorological Society,* 101, 929-955.

Jacobson, M. Z. 2005. Fundamentals of atmospheric modeling, Cambridge University Press.

Janjić, Z. 1990. The Step-Mountain Coordinate: Physical Package. *Monthly weather review 118(7): 1429-1443.*

Janjic, Z. 1996. The surface layer parameterization in the NCEP Eta Model. *World Meteorological Organization-publications-WMO TD: 4.16-14.17.*

Janjić, Z. 2002. Nonsingular implementation of the Mellor–Yamada level 2.5 scheme in the NCEP Meso model. *NCEP office note 437: 61*.

Jaynes, Daniel W., Jon G. McGowan, Anthony L. Rogers, and James F. Manwell.2007. Validation of Doppler Lidar for wind resource assessment applications. AWEA Windpower 2007 Conference, Los Angeles, CA.

Jensen, N. O., Petersen, E. L. and Troen, I. 1984. Extrapolation of mean wind statistics with special regard to wind energy applications, *World Meteorological Organization Geneva.*

Jiménez, P. A. and Dudhia, J. 2012. Improving the Representation of Resolved and Unresolved Topographic Effects on Surface Wind in the WRF Model. *Journal of Applied Meteorology and Climatology*, 51, 300-316.

Jiménez, P. A., González-Rouco, J. F., García-Bustamante, E., Navarro, J., Montávez, J. P., De Arellano, J. V.-G., Dudhia, J. and Muñoz-Roldan, A. 2010. Surface Wind Regionalization over Complex Terrain: Evaluation and Analysis of a High-Resolution WRF Simulation. *Journal of Applied Meteorology and Climatology,* 49, 268-287.

Kain, J. S. 1993. Convective parameterization for mesoscale models: The Kain-Fritsch scheme. *The representation of cumulus convection in numerical models, Meteor. Monogr,* 46, 165-170.

Kinuthia, J. H. and Asnani, G. C. 1982. A Newly Found Jet in North Kenya (Turkana Channel). *Mon. Wea. Rev*, 110, 1722–1728.

Kinuthia, J. H. 1992. Horizontal and Vertical Structure of the Lake Turkana Jet. *J. Appl. Meteor,* 31, 1248–1274.

Kirai, P. 2009. Energy systems: Vulnerability-Adaptation-Resilience (VAR).*Focus: sub-Saharan Africa, (Kenya) Helio International* .

Kline, J. 2002. Effects of Tubular Anemometer Towers on Wind Speed Measurements. *AWEA Windpower* Portland, OR.

Koscielny, A. J., Doviak, R. J. and Rabin, R. 1982. Statistical Considerations in the Estimation of Divergence From Single-Doppler Radar and Application to

Prestorm Boundary-Layer Observations. *Journal of applied meteorology*, 21, 197-210.

Kristensen, L. 1996. Cup Anemometer Behavior in Turbulent Environments. *Journal of Atmospheric and Oceanic Technology.,* vol. 15.

Kristensen, L. 1999. The Perennial Cup Anemometer. *Wind Energy,* vol. 2.

Kristensen, L., Rathmann, O. and Hansen, S. O. 2000. Extreme winds in Denmark. *Journal of Wind Engineering and Industrial Aerodynamics*, 87, 147-166.

Krishnamurthy, R., Choukulkar, A., Calhoun, R., Fine, J., Oliver, A., and Barr, K. S. 2013. Coherent Doppler lidar for wind farm characterization. *Wind Energy, 16*(2), 189-206.

Lalas, D. P. and Ratto, C. F. 1996. Modelling of atmospheric flow fields, World scientific.

Landberg, L. and Mortensen, N. 1993. A comparison of physical and statistical methods for estimating the wind resource at a site.

Landberg, L., L. Myllerup, Rathmann, O., Petersen, E. L., Jørgensen, B. H., Badger, J. and Mortensen, N. G. 2003. Wind resource estimation—an overview. *Wind Energy 6(3): 261-271.*

Lange, B. and Højstrup, J. 2001. Evaluation of the wind-resource estimation program WAsP for offshore applications. *Journal of Wind Engineering and Industrial Aerodynamics*, 89, 271-291.

Lee, S.-M. and Fernando, H. J. 2004. Evaluation of meteorological models MM5 and HOTMAC using PAFEX-I data. *Journal of applied meteorology,* 43, 1133-1148.

Lima, L. A. and Filho, C.R.B. 2012. Wind resource evaluation in São João does Cariri (SJC) - Paraiba, Brazil. *Renewable and* Sustainable Energy *Reviews* vol. 16, 474–480

Livingston, J. T. and Anderson, T. 2004. Wind Shear, Taller Turbines, and the Effects on Wind Farm Development Create a Need for Taller MET Towers. Windtower Composites Report.

Lockhart, T. and Bailey, B. 1998. The Maximum Type 40 Anemometer Calibration Project.: NRG Systems Report.

LTWP. 2013. Available: http://ltwp.co.ke/

Mahrer, Y., Segal, M. and Pielke, R. 1985. Mesoscale modelling of wind energy over non-homogeneous terrain. *Boundary-Layer Meteorology,* 31, 13-23.

Manwell, James F., Jon G. McGowan, and Anthony L. Rogers 2010. Wind energy explained: theory, design and application. *John Wiley and Sons Ltd*.

Mason, P. and Sykes, R. 1979. Flow over an isolated hill of moderate slope. *Quarterly Journal of the Royal Meteorological Society,* 105, 383-395.

McCaa, J. 2006. Understanding the Wind: Its Causes and Variability. *AWEA and CanWEA Resource Assessment Workshop.* Syracuse, NY.

Mellor, G. L. and T. Yamada. 1982. Development of a turbulence closure model for geophysical fluid problems. Reviews of Geophysics 20(4): 851-875.

Milborrow, D. 2002. Wind energy technology—the state of the art. *Proceedings of the Institution of Mechanical Engineers, Part A: Journal of Power and Energy,* 216, 23-30.

Mlawer, E. J., Taubman, S. J., Brown, P. D., Iacono, M. J. and Clough, S. A. 1997. Radiative transfer for inhomogeneous atmospheres: RRTM, a validated correlated-k model for the longwave. *Journal of Geophysical Research: Atmospheres (1984–2012),* 102**,** 16663-16682.

Moon, D. and Miler, R. 2005. Long-Term Reference Analysis - Statistics and Uncertainty from Length of Reference Data. *AWEA Windpower.* Denver, CO.

Mortensen, N. G. and Petersen, E. L. 1997. Influence of topographical input data on the accuracy of wind flow modelling in complex terrain. *EWEC-conference-Bookshop for Scientific Publications*, 317-320.

Mortensen, N. G. 2007. Getting started with WAsP 9. Risø-I-2571 (EN), Risoe National Laboratory, Technical University of Denmark, Roskilde (2007).

Mortensen, N. G. 2012. Planning and Development of Wind Farms: Wind Resource Assessment and Siting. Danmarks Tekniske Universitet, Risø Nationallaboratoriet for Bæredygtig Energi.

Muthuri, F. M., Ikumi, P. and Msafiri, F. 2009. Environmental and Social Impact Assessment Summary. Nairobi, Kenya: Lake Turkana Wind Power.

Neal, B. 2013. *ART Sodar Home Page.* [Online]. Available: http://www.sodar.com.

Niels G. Mortensen and Anthony, J. B. 1996. Exploring the limits of WASP : The Wind Atlas Analysis and Application Program. *1996 European Union Wind Energy Conference, 1996 Göte- borg, Sweden.*

Noh, Y., Cheon, W.G., Hong, S.-Y and Raasch, S. 2003: Improvement of the K-profile model for the planetary boundary layer based on large eddy simulation data. Bound.-Layer Meteor., 107, 401–427.

Oliver, A. 2006. Translating Data into Results: Analysis and Interpretation of Data. *AWEA and CanWEA Resource Assessment Workshop.* Syracuse, NY.

Oludhe, C. 2008. Assessment and Utilization of Wind Power in Kenya – A Review. *J.Kenya Meteorol. Soc.*, 2, 39–52.

Onat, N and Ersoz, S. 2011. Analysis of wind climate and wind energy potential of regions in Turkey. *Energy* vol. 36, 148–156.

Palaiologou, P., Kalabokidis, K., Haralambopoulos, D., Feidas, H and Polatidis, H. 2011. Wind characteristics and mapping for power production in the Island of Lesvos, Greece. *Computers and Geosciences* vol. 37, 962–972

Papadopoulos, K. H., Stefanatos, N. C., Paulsen, U. S. and Morfiadakis, E. 2001. Effects of Turbulence and Flow Inclination on the Performance of Cup Anemometers in the Field. *Boundary Layer Meteorology*, Vol. 101.

Pedersen, B., Hansen, K. S., Oye, S., Brinch, M. and Fabian, O. 1992. Some Experimental Investigations on the Influence of the Mounting Arrangements on the Accuracy of Cup-Anemometer Measurements. *Journal of Wind Engineering and Industrial Aerodynamics*, Vol. 39.

Pedersen, T. F and Uwe, S. P. 1999. Classification of Operational Characteristics of Commercial Cup-Anemometers. In *Proceedings from EWEC Conference*.

Pedersen, T. F. 2004. Power Curve Measurements Under Influence of Skew Airflow and Turbulence. Risø National Laboratory Report.

Pedersen, T. F., Gjerding, S., Ingham, P., Enevoldsen, P., Hansen, J. K. and Jørgensen, H. K. 2002. Wind Turbine Power Performance Verification in Complex Terrain and Wind Farms. Risø National Laboratory,: Technical University of Denmark.

Pereira, R., Guedes, R., and Santos, C. S. 2010. Comparing WAsP and CFD wind resource estimates for the" regular" user. In *Proceedings from EWEC*.

Perera, M. 1981. Shelter behind two-dimensional solid and porous fences. *Journal of Wind Engineering and Industrial Aerodynamics 8(1): 93-104.*

Periera, R., Guedes, R. and Santos, C. S. 2010. Comparing WAsP and CFD wind resource estimates for the" regular" user. *Proceedings from EWEC, 2010. Warsaw,* Poland

Petersen Erik L., Niels G. Mortensen., Lars Landberg., Jørgen Højstrup. and Helmut P. Frank. 1997. Wind Power Meteorology. Roskilde, Denmark.: Risø National Laboratory.

Petersen, E. L., Mortensen, N. G., Landberg, L., Højstrup, J. and Frank, H. P. 1998. Wind power meteorology. Part II: siting and models. *Wind Energy,* 1, 55-72.

Lindelöw-Marsden Petter. 2009. UpWind D1. Uncertainties in wind assessment with LIDAR. Roskilde, Denmark: Risø National Laboratory for Sustainable Energy, Technical University of Denmark.

Pleim, J. E. 2007. A combined local and nonlocal closure model for the atmospheric boundary layer. Part I: Model description and testing. *Journal of Applied Meteorology and Climatology 46(9): 1383-1395.*

Potter, C. W., Lew, D., McCaa, J., Cheng, S., Eichelberger, S. and Grimit, E. 2008. Creating the dataset for the western wind and solar integration study (USA). *Wind Engineering,* 32, 325-338.

Quarton, D. 2004. Wind Turbines – Part 121: Power Performance Measurements of Grid Connected Wind Turbines.: IEC 61400-12 Ed.1.

Ratto, C. 1996. An overview of mass-consistent models. *Modelling of Atmospheric Flow Fields. Singapore: World Scientific,* 379-400.

Reid, S. 1997. Modelling of channelled winds in high wind areas of New Zealand. *Weather Climate,* 17, 3-22.

Reid, S. J. and Turner, R. 2001. Correlation of real and model wind speeds in different terrains. *Weather and Forecasting,* 16, 620-627.

Rife, D. L., Davis, C. A., Liu, Y. and Warner, T. T. 2004. Predictability of low-level winds by mesoscale meteorological models. *Monthly weather review,* 132, 2553-2569.

RISØ. 2004. Summary of Cup Anemometer Classification According to IEC61400-121 Committee Draft.: Risø DTU.

Rogers, A. L., Walls, E., Henson, W. and Manwell, J. F. 2007. Addressing Ground Clutter Corruption of Sodar Measurements. *45th AIAA Aerospace Sciences Meeting and Exhibit (ASME Wind Energy Symposium).* Reno, NV.

Rogers, E., Black, T., Ferrier, B., Lin, Y., Parrish, D. and Dimego, G. 2001. Changes to the NCEP Meso Eta Analysis and Forecast System: Increase in resolution, new cloud microphysics, modified precipitation assimilation, modified 3DVAR analysis. *NWS Technical Procedures Bulletin,* 488**,** 15.

Romeo, R. and Magri, S. 1994. Wind energy evaluation for breakwater plants. *Wind Engineering,* 18, 199-206.

Schreck, S., Lundquist, J. and Shaw, W. 2008. U.S. Department of Energy Workshop Report—Research needs for wind resource characterization. Springfield, Virginia, USA: NREL/TP.

Seguro, J. and T. Lambert. 2000. Modern estimation of the parameters of the Weibull wind speed distribution for wind energy analysis. *Journal of Wind Engineering and Industrial Aerodynamics* 85(1): 75-84.

Skamarock, W., Klemp, J., Dudhia, J., Gill, D., Barker, D., Duda, M., Huang, X., Wang, W. and Powers, J. 2008. A description of the advanced research WRF version 3. NCAR Technical Note, NCAR/TN\ u2013475? STR, 123 pp.

Smith, D. A., Harris, M., Coffey, A. S., Mikkelsen, T., Jørgensen, H. E., Mann, J. and Danielian, R. 2006. Wind LIDAR evaluation at the Danish wind test site in Høvsøre. *Wind Energy*, 9, 87-93.

Standard, I. 2005. IEC 61400-12-1. *Wind turbines–Part 12-1: Power performance measurements of electricity producing wind turbines*.

Stensrud, D. J. 2007. *Parameterization schemes: keys to understanding numerical weather prediction models*, Cambridge University Press.

Stohl, A., Baumann, K., Wotawa, G., Langer, M., Neininger, B., Piringer, M. and Formayer, H. 1997. Diagnostic downscaling of large-scale wind fields to compute local-scale trajectories. *Journal of applied meteorology*, 36, 931-942.

Suárez, J. C., Gardiner, B. A. and Quine, C. P. 1999. A comparison of three methods for predicting wind speeds in complex forested terrain. *Meteorological Applications*, 6, 329-342.

Sukoriansky, S., Galperin, B. and Perov, V. 2005. Application of a new spectral theory of stably stratified turbulence to the atmospheric boundary layer over sea ice. *Boundary-Layer Meteorology*, *117*(2), 231-257.

Sukoriansky, S., Galperin, B. and Perov, V. 2006. A quasi-normal scale elimination model of turbulence and its application to stably stratified flows. *Nonlinear Processes in Geophysics*, 13**,** 9-22.

Sumner, J., Watters, C. S. and Masson, C. 2010. CFD in wind energy: the virtual, multiscale wind tunnel. *Energies*, 3**,** 989-1013.

Sumner, J., Watters, C. S., and Masson, C.2010. CFD in wind energy: the virtual, multiscale wind tunnel. *Energies*, *3*(5), 989-1013.

Taylor, P., Walmsley, J. and Salmon, J. 1983. A simple model of neutrally stratified boundary-layer flow over real terrain incorporating wavenumber-dependent scaling. *Boundary-Layer Meteorology*, 26, 169-189.

Theuri, D., and Hamlin, T. 2008. Solar and wind energy resource assessment: Kenya country report. *SWERA Project*.

Troen, I. and Lundtang Petersen, E. 1989. European wind atlas.

Troen, I. and Mahrt, L. 1986. A simple model of the atmospheric boundary layer; sensitivity to surface evaporation. *Boundary-Layer Meteorology*, 37**,** 129-148.

UCAR. 2012. *WRF-ARW Online Tutorial* [Online]. Available: http://www.mmm.ucar.edu/wrf/OnLineTutorial/index.htm 2013].

VanLuvanee, D., Rogers, T., Randall, G., Williamson, A. and Miller, T. 2009. Comparison of WASP, CFD, NWP and analytical methods for estimating site wide wind speeds. *Proceedings from AWEA Windpower*.

VanLuvanee, D., Rogers, T., Randall, G., Williamson, A., and Miller, T. 2009. Comparison of WAsP, MS-Micro/3, CFD, NWP, and analytical methods for estimating site-wide wind speeds. In *Presentation from AWEA Wind Resource Assessment Workshop*.

Vestas. 2016. Available at https://www.vestas.com/

Wagner, Rozenn, Ioannis Antoniou, Søren M. Pedersen, Michael S. Courtney, and Hans E. Jørgensen. 2009. The influence of the wind speed profile on wind turbine performance measurements. *Wind Energy 12, 348-362.*

Walford, C. A. 2006. *Wind turbine reliability: understanding and minimizing wind turbine operation and maintenance costs*, United States. Department of Energy.

Walls E., Rogers, A. L. and Manwell, J. F. 2006. Long Island, MA: SODAR-Based Wind Resource Assessment. *Renewable Energy Research Laboratory Report.* Amherst, MA.: University of Massachusetts.

Walmsley, J. L., Salmon, J. and Taylor, P. 1982. On the application of a model of boundary-layer flow over low hills to real terrain. *Boundary-Layer Meteorology*, 23, 17-46.

Walmsley, J., Taylor, P. and Keith, T. 1986. A simple model of neutrally stratified boundary-layer flow over complex terrain with surface roughness modulations (MS3DJH/3R). *Boundary-Layer Meteorology*, 36, 157-186.

WASP. 2013. *WAsP 10.2. Wind Turbine Generators* [Online]. Available: www.wasp.dk.

Wei Wang, C. B., Michael Duda, Jimy Dudhia, Dave Gill, Michael Kavulich, Kelly Keene, Hui-Chuan Lin, John Michalakes, Syed Rizvi and Xin Zhang. 2012. Weather Research and Forecasting ARW Version 3 Modeling System User's Guide National Centre for Atmospheric Research (NCEP).

Westermann, D. 2003. Investigation and Classification of the Anemometer Thies First Class.: Deutsche WindGuard Wind Tunnel Services.

Wharton, S. and Lundquist, J. K. 2010. Atmospheric stability impacts on power curves of tall wind turbines—an analysis of a west coast north american wind farm. *Lawrence Livermore National Laboratory*.

Willmott, C. J. 1982. Some comments on the evaluation of model performance. *Bulletin of the American Meteorological Society*, 63, 1309-1313.

Wood, N. 1995. The onset of separation in neutral, turbulent flow over hills. *Boundary-Layer Meteorology*, 76, 137-164.

Žagar, N., Žagar, M., Cedilnik, J., Gregorič, G. and Rakovec, J. 2006. Validation of mesoscale low-level winds obtained by dynamical downscaling of ERA40 over complex terrain. *Tellus A*, 58, 445-455.